

# DICE: Entropy-Regularized Equilibrium Selection for Stable Multi-Agent LLM Coordination

**Yi Xie** \*

YIX@ARIZONA.EDU

*Department of Electrical & Computer Engineering  
University of Arizona  
Tucson, AZ 85721-0104, USA*

**Zhanke Zhou** \*

CSZKZHOU@COMP.HKBU.EDU.HK

*Department of Computer Science  
Hong Kong Baptist University  
Kowloon Tong, Hong Kong SAR*

**Chentao Cao**

CSCTCAO@COMP.HKBU.EDU.HK

*Department of Computer Science  
Hong Kong Baptist University  
Kowloon Tong, Hong Kong SAR*

**Bo Liu**

BOLIU@ARIZONA.EDU

*Department of Electrical & Computer Engineering  
University of Arizona  
Tucson, AZ 85721-0104, USA*

**Bo Han**

BHANML@COMP.HKBU.EDU.HK

*Department of Computer Science  
Hong Kong Baptist University  
Kowloon Tong, Hong Kong SAR*

## Abstract

Multi-agent large language model (LLM) systems often fail to reliably outperform a single strong model equipped with best-of- $N$  sampling. We argue that a core source of this instability is *ill-posed equilibrium selection*: current systems specify what information agents share, but not which coordination convention should be selected. We formalize a broad class of such systems as discounted incomplete-information Markov games and show that two common pathologies, oscillation between competing conventions and drift across them, can both induce unstable learning and linear Bayesian regret. To obtain a well-posed target, we introduce the Heterogeneous Quantal Response Equilibrium (HQRE), an entropy-regularized equilibrium concept with agent- and state-dependent temperatures. Under a monotonicity condition, HQRE is unique, admits linearly convergent mirror updates, and yields bounded Bayesian regret; the same condition yields rollout-measurable stability diagnostics. We instantiate this objective in two algorithms: DICE-PC, which coordinates frozen models through prompt-control actions, and DICE-FT, which performs parameter-efficient mirror fine-tuning. Across eleven benchmarks in four domains, DICE improves accuracy-cost trade-offs over strong within-class baselines; on reasoning and planning tasks, DICE-PC improves by 4.3 percentage points on average and DICE-FT by 8.5 points.

**Keywords:** multi-agent large language models, equilibrium selection, entropy regularization, quantal response equilibrium, incomplete-information Markov games

---

\*. These authors contributed equally to this work.

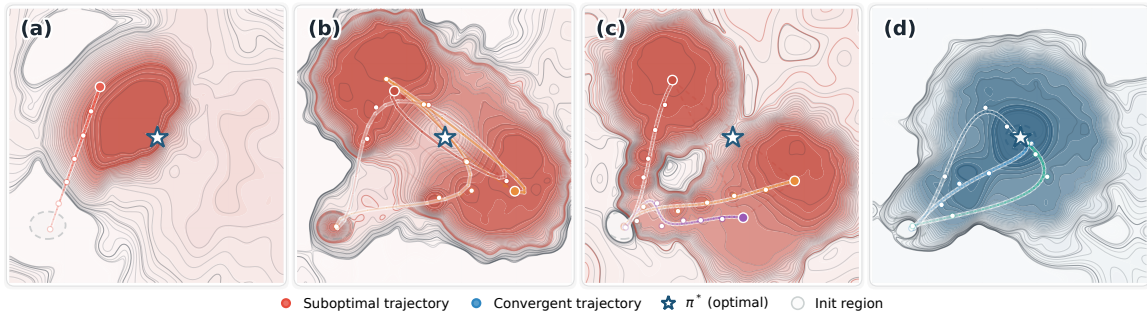


Figure 1: **Loss landscapes under different coordination paradigms.** More agents create more possible ways to coordinate. Without an explicit selection rule, the system can saturate at a single-agent ceiling (a), oscillate between competing conventions (b), or drift across conventions during learning (c). DICE turns the implicit choice of convention into an explicit one, collapsing the landscape to a single basin (d). Shading encodes loss (darker = lower); the dashed ellipse marks the shared initialization region and the star marks the reference policy  $\pi^*$ . Landscapes are schematic; the underlying phenomena are formalized in Section 3.

## 1 Introduction

Multi-agent LLM systems promise greater capability by distributing work across specialized roles such as planning, solving, critiquing, and verification (Liu et al., 2024b; Hong et al., 2024). While adding more agents expands parallel exploration, it also increases system complexity, particularly in multi-agent coordination. In practice, small changes in prompts, sampling, or context truncation can push the same system into completely different joint behaviors. One agent may follow a divide-and-conquer protocol, while another acts under a debate-and-merge protocol. A coordination convention is a consistent method of coordination in which no agent benefits from unilaterally deviating. Each convention is reasonable on its own, but mixing them results in incoherent behavior and severe system instability.

This instability helps explain a recurring empirical finding: multi-agent designs often fail to reliably outperform a single strong model equipped with best-of- $N$  sampling and lightweight verification (Kim et al., 2025; Cemri et al., 2025). The issue is not only what information agents exchange, but whether the system specifies a stable rule for choosing among multiple self-consistent ways of coordinating (Liu et al., 2024a; Shi et al., 2025). Current architectures usually address the first question through shared transcripts, judges, summarizers, or routing heuristics. They rarely address the second.

Our central claim is that *ill-posed equilibrium selection* is a core source of instability in multi-agent LLM systems. Existing methods typically address what information becomes public among agents, but they do not address which coordination convention should be selected, or why that convention should remain stable under perturbations. We therefore separate two concerns that are usually conflated: *information structure*, which governs what agents can observe, and *coordination mechanism*, which governs how a particular convention is selected and maintained. To study both within a single framework, we model a broad class of multi-agent architectures as a discounted incomplete-information Markov game

(IIMG) with a shared public stream and private agent histories. Figure 1 illustrates how this distinction plays out across common coordination paradigms.

A single strong model with best-of- $N$  sampling (panel a) induces an effectively unimodal landscape: selection is stable, but performance saturates at a ceiling set by the capacity of one agent. Adding multiple agents through message passing or debate (panel b) raises this ceiling by pooling capacity, yet the resulting landscape typically contains competing basins, so learning oscillates between conventions rather than committing to either. Letting multiple agents learn together without an explicit selection rule (panel c) introduces a further failure mode: the realized convention can drift across training, so the system never settles. Both oscillation and drift yield linear Bayesian regret.

These failures share a common root cause. The underlying game admits several self-consistent joint strategies, and nothing in the system selects which one should be realized. HQRE regularization (panel d) resolves this by implementing an explicit equilibrium-selection mechanism, yielding a single dominant basin and restoring convergence toward a selected convention. Panels (a) through (c) thus illustrate three increasingly severe coordination failures, while panel (d) shows that a single regularization mechanism, which we introduce next, resolves all three by providing a unique equilibrium target.

We call this mechanism the *Heterogeneous Quantal Response Equilibrium* (HQRE): an entropy-regularized equilibrium concept with agent- and state-dependent temperatures. The resulting method, DICE (**D**iscounted **I**ncomplete-information **C**oordination via **E**ntropy), performs entropy-regularized equilibrium selection within the IIMG framework. Unlike a generic exploration bonus, the regularization here plays a structural role: it makes the coordination game well-posed, so that equilibrium selection admits a unique solution rather than a set of competing ones.

Under a monotonicity condition in which regularization curvature dominates cross-agent coupling, HQRE is unique and explicit mirror updates converge linearly, yielding Bayesian regret that is uniformly bounded in the horizon; we defer the precise statements and the supporting smoothness assumptions to Section 4. Because the monotonicity condition can be conservative at LLM scale, we treat it primarily as a design principle. It motivates the regularization structure and yields rollout-measurable stability diagnostics that we track throughout our evaluation.

We instantiate the HQRE objective in two complementary deployment regimes. DICE-PC learns distributions over bounded prompt-control actions to coordinate frozen execution models, preserving pretrained generalization while stabilizing equilibrium selection. DICE-FT performs parameter-efficient mirror fine-tuning under differentiated token-type regularization, providing additional gains on coordination-heavy tasks at the cost of greater optimization difficulty. We evaluate both on eleven benchmarks spanning reasoning, planning, active information gathering, and multi-agent coordination, with stability diagnostics reported alongside accuracy and token cost.

The main contributions of this paper are summarized as follows:

- **Formalization.** We formalize multi-agent LLM coordination as a discounted IIMG, explicitly separating information structure from coordination mechanism, and identify well-posed equilibrium selection as a critical but previously unaddressed design dimension.

- **Failure-mode analysis.** Within the IIMG framework, we prove that debate-style defensive mixing and equilibrium multiplicity can each produce linear Bayesian regret, identifying ill-posed equilibrium selection as the common root cause and establishing that richer communication alone is neither necessary nor sufficient for stable coordination.
- **Regularized equilibrium theory.** We introduce HQRE as an entropy-regularized equilibrium concept with the following guarantees under a monotonicity condition: (i) provable uniqueness of the equilibrium, (ii) linear convergence of explicit KL-mirror updates under standard field-Lipschitz and local-quadratic assumptions, (iii) uniformly bounded Bayesian regret, and (iv) rollout-measurable stability diagnostics derived from the theory.
- **Algorithms and evaluation.** We instantiate the HQRE objective as DICE-PC and DICE-FT. Validation on eleven benchmarks across four domains demonstrates improved accuracy–cost trade-offs and reduced instability relative to single-model, debate-style, and ensembling baselines under matched deployment constraints. DICE-PC achieves +4.3 pp average improvement over prompt-control baselines and DICE-FT achieves +8.5 pp over fine-tuning baselines across six reasoning and planning benchmarks (Section 6).

Beyond the specific algorithms, this work introduces three methodological contributions to multi-agent system that are reusable beyond the LLM coordination setting. First, the IIMG formalization provides a reusable modeling tool: any multi-agent system with private information and a shared public stream can be embedded in this framework (Lemma 2), enabling diagnosis of coordination failures through the coupling constant  $L_c$  and the monotonicity margin. Second, the inexact mirror recurrence (Corollary\* 1) is a general-purpose bridge theorem for connecting exact variational-inequality convergence to practical deep-learning optimization with clipping, sampling, and function approximation—applicable whenever mirror descent is used with implementable surrogates. Third, the four-component error decomposition (Proposition 18) establishes a diagnostic methodology: by isolating clipping, sampling, representation, and optimization errors, it provides a template for error attribution in any approximate policy-optimization pipeline.

**Paper organization.** The remainder of the paper is organized as follows. Section 2 surveys related work. Section 3 formalizes the IIMG framework and identifies failure modes of unregularized coordination. Section 4 introduces HQRE and establishes uniqueness, convergence, and regret guarantees. Section 5 presents the DICE-PC and DICE-FT algorithms. Section 6 provides experimental evaluation, and Section 8 concludes.

**Relation to the conference version.** This manuscript is a substantially extended version of our previous work published at *ICML 2025* (Xie et al., 2025). The conference version introduced ECON and used Bayesian Nash equilibrium (BNE) as a principled target for belief-driven multi-agent LLM coordination. The present manuscript identifies a limitation of that unregularized target: BNE existence alone does not make coordination well posed when multiple self-consistent equilibria coexist. The main extensions are summarized in Section 7, including (1) a discounted incomplete-information Markov game formulation with explicit protocol embedding and failure-mode analysis of ill-posed BNE selection, (2) a new entropy-regularized HQRE theory with uniqueness, KL-mirror convergence, zero-temperature connection to BNE, and bounded-regret guarantees, and (3) two deployable algorithms, DICE-PC and DICE-FT, supported by an inexact mirror recurrence, a field-error decomposition, and broader experimental validation across 11 benchmarks in 4 domains.

## 2 Related Work

**Single-model reasoning.** Single-model reasoning methods improve exploration within a single policy but cannot address instability arising from coexisting coordination conventions. Chain-of-thought prompting (Wei et al., 2022) and zero-shot reasoning instructions (Kojima et al., 2022) elicit intermediate computations, while self-consistency (Wang et al., 2023) and tree-based exploration methods (Yao et al., 2023) improve robustness by aggregating or searching over multiple candidate traces. A complementary line of work automates or schedules prompts to match the task structure, including least-to-most prompting (Zhou et al., 2022), complexity-aware prompting (Fu et al., 2022), automatic chain-of-thought discovery (Zhang et al., 2023), contrastive prompting (Chia et al., 2023), inception prompting (Li et al., 2023b), and tool-augmented prompting (Zhou et al., 2025a; Lu et al., 2023). These approaches are limited to improving exploration or verification within a single model.

**Multi-agent coordination protocols.** Multi-agent LLM coordination protocols increase communication bandwidth but typically lack a formal equilibrium-selection target that guarantees stability. Debate and message-passing frameworks (Du et al., 2023; Li et al., 2023a) aim to improve solutions via critique and refinement. System-oriented agent frameworks coordinate multiple LLMs with tools, memory, and communication, such as MetaGPT (Hong et al., 2024), AutoGen (Wu et al., 2024), and Lumos (Yin et al., 2024). Other protocols facilitate information exchange or consensus building across agents (Yin et al., 2023; Lan et al., 2024; Yuan et al., 2024). Recent evaluations, however, report that multi-agent systems do not reliably outperform strong single-model baselines and can be sensitive to prompts and sampling (Kim et al., 2025; Cemri et al., 2025). Our work is aligned with these findings and focuses on a specific missing design dimension: making equilibrium selection well-posed rather than increasing communication volume. The scaling analysis of Kim et al. (2025) is particularly relevant: their finding that multi-agent systems often fail to outperform single-model baselines at larger scales aligns with our coordination-vs-capacity regime analysis (Section 6.7), and our IIMG framework provides a formal explanation through the coupling constant  $L_c$ . Similarly, the failure patterns cataloged by Cemri et al. (2025), including inconsistent outputs under prompt perturbation, sensitivity to agent ordering, and degradation under scaling, correspond to the equilibrium multiplicity and defensive mixing failures formalized in Sections 3.3-3.4.

**Aggregation and adjudication.** Explicit aggregation and adjudication mechanisms specify how outputs are combined but do not provide convergence or uniqueness guarantees for the resulting joint policy. For example, ChatEval uses referee agents for structured evaluations (Chan et al., 2024), and RECONCILE aggregates a round-table discussion with confidence-weighted consensus (Chen et al., 2024). These systems specify *what information is shared* and how outputs are combined, but typically do not provide a formal selection target that guarantees stability under perturbations. In contrast, we formulate a unified incomplete-information Markov game view and introduce an entropy-regularized equilibrium concept. This concept turns equilibrium selection into a well-posed fixed-point problem with uniqueness and convergence guarantees under verifiable coupling conditions.

**Multi-agent RL formalisms.** Standard multi-agent RL formalisms typically address scalability and credit assignment but not equilibrium selection. From a reinforcement learning

Table 1: Qualitative comparison of coordination approaches.

Approach	Equilibrium guarantee	Convergence	Communication
Debate / MAD	None	Oscillation risk	Full transcript
Ensemble / SC	None (aggregation only)	N/A (no learning)	Output voting
CTDE (QMIX, etc.)	Nash (set-valued)	Empirical	Latent mixing
<b>DICE (ours)</b>	<b>Unique HQRE</b>	<b>Linear</b>	Public stream

perspective, decentralized partially observable models such as DEC-POMDPs (Bernstein et al., 2002) and Markov games under centralized training with decentralized execution (CTDE) are standard formalisms for cooperative multi-agent control (Lowe et al., 2017; Lanctot et al., 2017; Gronauer and Diepold, 2022; Xiao et al., 2023). Value decomposition and monotone mixing networks (Sunehag et al., 2017; Rashid et al., 2020; Wang et al., 2020; Graves et al., 2023) provide scalable CTDE recipes by aligning individual action-values with a global objective. Our algorithms use monotone critics and mixing consistent with these CTDE principles, while our main contribution targets a different bottleneck that is salient in open-ended LLM coordination: equilibrium multiplicity and selection instability.

**Regularized game theory.** Our equilibrium concept builds on regularized game theory and first-order methods for monotone variational inequalities. Quantal Response Equilibrium (QRE) models bounded rationality via logit responses (McKelvey and Palfrey, 1995, 1998), and classical conditions for existence and uniqueness under (strong) monotonicity trace back to early game-theoretic analyses (Rosen, 1965). Mirror-descent-style methods for monotone problems yield convergence guarantees in appropriate Bregman geometries (Nemirovski et al., 2009), and entropy regularization connects policy optimization to maximum-entropy control and inference views (Sutton and Barto, 2018; Levine, 2018). We extend these principles to a heterogeneous entropy-regularized equilibrium for discounted incomplete-information Markov games with shared public streams, and leverage the resulting uniqueness and KL-mirror convergence to obtain stability diagnostics and bounded Bayesian regret guarantees.

**Distinction from single-agent entropy regularization.** Before proceeding to the formal framework, we clarify a potential source of confusion. A natural question is how HQRE relates to single-agent maximum-entropy methods, which also add entropy to the objective. Single-agent maximum-entropy RL (e.g., SAC (Haarnoja et al., 2018)) uses entropy regularization primarily for exploration and robustness within a single decision-maker. In contrast, the entropy term in HQRE serves an equilibrium-selection role: it converts set-valued multi-agent best responses into a unique fixed point, a function that has no analogue in the single-agent setting where the optimal policy is generically unique.

### 3 Coordination Framework and Bayesian Regret under Incomplete Information

We treat multi-agent LLM coordination as an equilibrium phenomenon in an incomplete-information game. We use “equilibrium” in formal and theoretical passages (Sections 3–5) and “coordination convention” in informal and motivational passages (introduction, experiment discussion, conclusion); both refer to a self-consistent joint policy from which no agent

Table 2: Summary of results in Section 3.

Result	Guarantee	Representative condition
IIMG formulation (§3.1)	Models coordination as private histories + shared public stream	(A1)–(A5)
Explicit-communication protocols (§3.1)	Covers shared-chat, blackboard, coordinator-mediated, and no-exchange regimes	Public commitment of coordination-relevant information
BNE existence (§3.2)	Existence of a behavioral BNE in the discounted IIMG	(A1)–(A4)
Rate-dependent Bayesian regret (§3.2)	If $\mathbb{E}[\Delta_k] \leq C_\Delta k^{-\alpha}$ , then $\text{Regret}(T) \leq \frac{2NR_{\max}C_\Delta}{(1-\gamma)^2} \sum_{k=1}^T k^{-\alpha}$	Performance difference + TV bound
Multiplicity $\Rightarrow$ linear regret (§3.3)	Unstable selection can yield $\text{Regret}(T) = \Omega(T)$	Two equilibria + persistent mis-selection
Debate-style dynamics $\Rightarrow$ linear regret (§3.4)	Persistent defensive mixing implies $\text{Regret}_{\text{MAD}}(T) = \Omega(T)$	Defensive mixing + nondegenerate gap

benefits by unilaterally deviating. The public stream  $y^t$  captures all publicly committed coordination-relevant information, ranging from rich shared chat and judge-feedback protocols to communication-light designs. This viewpoint separates the *information structure* of a protocol from the *mechanism that yields stability*: explicit information exchange may be present or absent; stable coordination requires a well-posed equilibrium selection mechanism.

### 3.1 IIMG model and explicit-communication protocols

There are  $N$  agents indexed by  $\mathcal{N} = \{1, \dots, N\}$ . Before the formal definition, the key modeling idea is as follows: agents share a public stream  $y^t$  (e.g., shared chat or judge feedback) and maintain private histories  $h_i^t$  (e.g., scratchpads or retrieved documents). A discounted IIMG is specified by the following components (we explain each in turn):

$$\langle \mathcal{N}, \mathcal{S}, \mathcal{A}, \mathcal{O}, \mathcal{Y}, \mathcal{P}, \Omega, G, (\phi_i)_{i \in \mathcal{N}}, \gamma, \mu_0 \rangle.$$

Here,  $\mathcal{S}$ ,  $\mathcal{A}$ ,  $\gamma$ , and  $\mu_0$  are standard Markov-game components familiar from stochastic games and Dec-POMDPs (Amato et al., 2019; Konidaris and Barto, 2009; Konidaris, 2016). The key additions for incomplete-information coordination are the public-stream space  $\mathcal{Y}$ , the public-stream map  $G$ , the private-observation kernel  $\Omega$ , and the reward decomposition  $\phi_i$ . In the table below, standard components are listed first, followed by the IIMG-specific ones.

#### Standard Markov-game components

$\mathcal{N}$	Agent set $\{1, \dots, N\}$	$\mathcal{S}$	Latent state space
$\mathcal{A} = \prod_i \mathcal{A}_i$	Joint action space	$\mathcal{O} = \prod_i \mathcal{O}_i$	Joint private-obs space
$\mathcal{P}$	Transition kernel $\mathcal{S} \times \mathcal{A} \rightarrow \Delta(\mathcal{S})$	$\gamma$	Discount factor $\in (0, 1)$
$\mu_0$	Initial state distribution		

#### Novel IIMG-specific components

$\mathcal{Y}$	Public-stream space	$G$	Public-stream map $\mathcal{A} \rightarrow \mathcal{Y}$
$\Omega$	Observation kernel $\mathcal{S} \times \mathcal{A} \rightarrow \Delta(\mathcal{O})$	$\phi_i$	Agent $i$ 's reward component

The function  $G$  determines what becomes common knowledge among agents; varying  $G$  captures a spectrum from no communication ( $G$  constant) to full transparency ( $G$  bijective). Agent  $i$  receives instantaneous reward

$$R_i(s, \mathbf{a}) := \phi_i(s, G(\mathbf{a})),$$

with discount factor  $\gamma \in (0, 1)$  and initial state  $s^0 \sim \mu_0$ . At each time  $t \geq 0$ , agents simultaneously choose a (possibly structured) macro-action  $\mathbf{a}^t$ , producing the public stream token  $y^t = G(\mathbf{a}^t)$ . The state then transitions to  $s^{t+1} \sim \mathcal{P}(\cdot | s^t, \mathbf{a}^t)$ , and each agent receives a private observation  $o_i^{t+1} \sim \Omega(\cdot | s^{t+1}, \mathbf{a}^t)$ . This action-only  $G$  is a convenient normal form; state-dependent or within-round sequencing effects can be represented by augmenting  $\mathcal{S}$  and refining the time index.

**Interpretation in MA-LLM coordination.** In MA-LLM systems, the latent state  $s^t$  aggregates the task instance, environment/tool state, and any hidden ground truth needed to define rewards. An action  $a_i^t$  corresponds to the agent’s round- $t$  committed act under the protocol (e.g., a publicly posted message, a one-shot candidate, a tool call, or a bounded decoding/prompt-control choice). The public stream token  $y^t$  records the protocol’s publicly committed record that becomes common knowledge (e.g., shared transcript segments, judge feedback, or a coordinator’s aggregated outcome), while the private observation  $o_i^t$  captures agent-local information not revealed in  $y^t$  (private scratchpad, retrieved documents, tool traces, etc.). The discount  $\gamma$  also models attenuation of far-future influence under context limits and truncation by downweighting long-range effects.

**Definition 1** (Explicit-communication protocol). *A multi-agent coordination architecture is an explicit-communication protocol if there exists a finite public-stream space  $\mathcal{Y}$  and a publicly observed process  $\{y^t\}_{t \geq 0}$  such that each agent  $i$  can be modeled by a behavioral policy  $\pi_i(\cdot | h_i^t, t)$  with information state*

$$h_i^t = (o_i^0, a_i^0, y^0, r_i^0, \dots, a_i^{t-1}, y^{t-1}, r_i^{t-1}, o_i^t), \quad h_i^0 = (o_i^0),$$

and any private message available only to agent  $i$  is treated as part of  $o_i^t$ . The public stream is the only coordination-relevant information shared across agents; no agent observes another agent’s private history beyond what is revealed in  $\{y^u\}_{u \leq t}$ .

In words, agent  $i$ ’s information state at time  $t$  groups four types of data: private observations  $(o_i^0, \dots, o_i^t)$ , own actions  $(a_i^0, \dots, a_i^{t-1})$ , public-stream tokens  $(y^0, \dots, y^{t-1})$ , and received rewards  $(r_i^0, \dots, r_i^{t-1})$ .

**Lemma 2** (Protocol embedding). *Any explicit communication protocol in Definition 1 can be represented as a discounted IIMG by augmenting the state and observation kernels so that, for any joint behavioral policy  $\pi$ , the induced trajectory distribution over  $(s^t, y^t, \mathbf{o}^t, \mathbf{a}^t)_{t \geq 0}$  and each discounted return  $U_i(\pi)$  are preserved. Consequently, equilibrium notions and Bayesian regret computed from Eq. (1)–Eq. (2) are invariant under this embedding.*

A constructive embedding is provided in the Appendix. Intuitively, the embedding augments the state to track the protocol’s internal bookkeeping, so any trajectory distribution under the protocol is faithfully reproduced in the IIMG.

**DICE within the explicit-communication framework.** DICE instantiates Definition 1 with a minimal public stream that records the coordinator’s context, together with the aggregated outcome. DICE’s equilibrium selection mechanism, not communication volume, is what provides stability.

**Behavioral policies.** A (possibly nonstationary) behavioral policy  $\pi_i$  maps information states to action distributions,  $\pi_i(\cdot \mid h_i^t, t) \in \Delta(\mathcal{A}_i)$ . We write  $\boldsymbol{\pi} = (\pi_1, \dots, \pi_N)$  and  $\Pi = \prod_{i=1}^N \Pi_i$ .

**Returns and Bayesian regret.** Given  $\boldsymbol{\pi}$ , agent  $i$ ’s discounted return and social welfare (the sum of all agents’ returns) are

$$U_i(\boldsymbol{\pi}) = \mathbb{E}_{\boldsymbol{\pi}} \left[ \sum_{t=0}^{\infty} \gamma^t R_i(s^t, \mathbf{a}^t) \right], \quad W(\boldsymbol{\pi}) = \sum_{i=1}^N U_i(\boldsymbol{\pi}). \quad (1)$$

We measure performance over *learning iterations*  $k = 1, 2, \dots$  (distinct from environment time  $t$ ) via Bayesian regret relative to a reference joint policy  $\boldsymbol{\pi}^*$ :

$$\text{Regret}(T) := \mathbb{E} \left[ \sum_{k=1}^T (W(\boldsymbol{\pi}^*) - W(\boldsymbol{\pi}^k)) \right]. \quad (2)$$

**Occupancies and policy geometry.** To translate convergence in policy space into welfare bounds, we need a sensitivity lemma that relates policy changes to occupancy changes. We now introduce the necessary occupancy measures. The discounted state occupancy is

$$d^{\boldsymbol{\pi}}(s) := (1 - \gamma) \sum_{t \geq 0} \gamma^t \Pr_{\boldsymbol{\pi}}(s^t = s).$$

Let  $h^t = (h_1^t, \dots, h_N^t)$  denote the joint history. The discounted joint history occupancy is

$$\mathbf{H}_{\text{disc}}^{\boldsymbol{\pi}}(h^t, t) := (1 - \gamma) \gamma^t \text{Law}(h^t \mid \boldsymbol{\pi}).$$

We measure worst-case deviations of joint action distributions using the joint-policy TV metric, denoted  $\rho_{\Pi}$  to distinguish it from both the occupancy measure  $d^{\boldsymbol{\pi}}$  and the reward components  $\phi_i$ :

$$\rho_{\Pi}(\boldsymbol{\pi}, \boldsymbol{\pi}') := \sup_{(h^t, t)} \text{TV} \left( \otimes_{i=1}^N \pi_i(\cdot \mid h_i^t, t), \otimes_{i=1}^N \pi'_i(\cdot \mid h_i^t, t) \right). \quad (3)$$

Occupancy sensitivity holds with  $C_{\text{occ}} = \frac{2\gamma}{1-\gamma}$  (by a standard simulation lemma; a derivation is included in the Appendix):

$$\|d^{\boldsymbol{\pi}} - d^{\tilde{\boldsymbol{\pi}}}\|_1 \leq C_{\text{occ}} \rho_{\Pi}(\boldsymbol{\pi}, \tilde{\boldsymbol{\pi}}).$$

**Standing assumptions.** We invoke the following standard conditions only when required. Each theorem statement specifies which assumptions are needed.

(A1) Finite spaces:  $\mathcal{S}$ , each  $\mathcal{A}_i$ , and each  $\mathcal{O}_i$  are finite.

(A2) Bounded rewards:  $|\phi_i| \leq R_{\text{max}}$  for all  $i$ , and a policy-independent  $\mu_0$ .

- (A3) Measurable behavioral policies (measurable in countable coordinates, i.e., the policy is a well-defined function of the history).
- (A4) Perfect recall (behavioral strategies are w.l.o.g. under truncation/discounting).
- (A5) Limited feedback: at time  $t$ , agent  $i$  observes only  $(o_i^t, y^t, r_i^t)$  and not other agents' actions.

Assumptions (A1)–(A4) are standard in the Dec-POMDP and stochastic-game literature; (A5) is specific to this work and captures the information asymmetry inherent in MA-LLM coordination, where agents share information only through the public stream. (A1) ensures that the best-response map is well-defined on a compact domain; (A2) guarantees bounded returns; (A3)–(A4) provide the measurability needed for behavioral strategies.

### 3.2 Unregularized equilibria and regret control

With the IIMG framework and standing assumptions in place, we now characterize the regret consequences of operating without an equilibrium-selection mechanism. Before introducing regularization, we establish that unregularized games admit equilibria (Theorem 4) but provide no mechanism to select among them: the game does not specify *which* equilibrium open-ended learning will select. This gap is the root cause of the instability identified in the introduction, and it alone is sufficient for regret to accumulate, even when the underlying game admits equilibria with good welfare.

**Theorem 3** (Compactness and continuity of the policy space). *Under (A1)–(A2), the joint behavioral policy space  $\Pi$  is nonempty, convex, compact, and metrizable under the product topology. Moreover, each payoff  $U_i : \Pi \rightarrow \mathbb{R}$  defined in Eq. (1) is continuous.*

Proof is deferred to Appendix A.2. Compactness ensures that best-response sequences have convergent subsequences; continuity ensures that limits of approximate equilibria are exact equilibria. Both properties are reused in the existence proof for the regularized equilibrium.

**Bayesian Nash equilibrium (BNE).** A joint policy  $\pi^*$  is a BNE if no agent can improve its return by unilateral deviation:

$$\pi_i^* \in \arg \max_{\pi_i \in \Pi_i} U_i(\pi_i, \pi_{-i}^*), \quad \forall i \in \mathcal{N}.$$

**Theorem 4** (Existence of BNE). *Under assumptions (A1)–(A4), the discounted IIMG admits a behavioral BNE.*

The proof uses finite-horizon truncations and compactness; details are deferred to Appendix A.3. Existence alone does not tell us which equilibrium learning will select; the next subsections show that multiplicity of BNE is the core obstacle.

**Regret transfer from convergence to a fixed equilibrium.** Fix a reference BNE  $\pi^*$  and define the occupancy-averaged deviation

$$\bar{\Delta}_k := \mathbb{E}_{(h^t, t) \sim H_{\text{disc}}^{\pi^*}} \left[ \text{TV}(\pi^k(\cdot | h^t, t), \pi^*(\cdot | h^t, t)) \right].$$

Intuitively,  $\bar{\Delta}_k$  measures how far the current policy is from the reference equilibrium, averaged over visited states. The following corollary shows that the rate at which  $\bar{\Delta}_k$  decays directly controls regret.

**Corollary 5** (Rate-dependent Bayesian regret). *If  $\mathbb{E}[\bar{\Delta}_k] \leq C_\Delta k^{-\alpha}$  for some  $C_\Delta > 0$  and  $\alpha > 0$ , then for all  $T \geq 1$ ,*

$$\text{Regret}(T) \leq \frac{2NR_{\max}C_\Delta}{(1-\gamma)^2} \sum_{k=1}^T k^{-\alpha}.$$

*In particular, for  $\alpha = \frac{1}{2}$  this yields  $\text{Regret}(T) = O(\frac{N\sqrt{T}}{(1-\gamma)^2})$ .*

The bound follows from a performance-difference argument combined with TV control; details are deferred to Appendix A.6. Corollary 5 is informative only when learning converges to a *single* equilibrium so that  $\bar{\Delta}_k \rightarrow 0$  for some fixed  $\boldsymbol{\pi}^*$ . The next two subsections show that this condition can fail through two distinct mechanisms, selection instability and persistent defensive mixing, regardless of how rich the public stream is.

### 3.3 Linear regret under equilibrium multiplicity

When a game admits multiple equilibria with different welfare, learning that does not settle on a single mode incurs a welfare gap whenever it selects a lower-welfare equilibrium. If this mis-selection persists with non-vanishing probability, regret can accumulate linearly, even when every iterate is itself an equilibrium.

**Proposition 6** (Equilibrium multiplicity with persistent mis-selection can induce linear Bayesian regret). *Assume the unregularized game admits two equilibria  $\boldsymbol{\pi}^{(1)}$  and  $\boldsymbol{\pi}^{(2)}$  such that  $W(\boldsymbol{\pi}^{(1)}) - W(\boldsymbol{\pi}^{(2)}) = \Delta_W > 0$ . Let  $\{\boldsymbol{\pi}^k\}_{k \geq 1}$  be the iterates produced by a learning procedure and suppose  $\boldsymbol{\pi}^k \in \{\boldsymbol{\pi}^{(1)}, \boldsymbol{\pi}^{(2)}\}$  for all  $k$ . If there exist  $p_0 > 0$  and  $k_0$  such that for all  $k \geq k_0$ ,*

$$\Pr(\boldsymbol{\pi}^k = \boldsymbol{\pi}^{(2)}) \geq p_0,$$

*then the Bayesian regret relative to  $\boldsymbol{\pi}^{(1)}$  is linear:*

$$\text{Regret}(T) \geq p_0 \Delta_W (T - k_0 + 1) = \Omega(\Delta_W T).$$

*More generally, the same conclusion (up to constants) holds if  $\Pr(W(\boldsymbol{\pi}^k) \leq W(\boldsymbol{\pi}^{(1)}) - \Delta_W/2) \geq p_0$  for all  $k \geq k_0$ .*

Proof is deferred to Appendix A.7. The assumption that iterates lie exactly in  $\{\boldsymbol{\pi}^{(1)}, \boldsymbol{\pi}^{(2)}\}$  is illustrative to the reader; the general statement (final two lines of the proposition) is the practically relevant claim, as the general condition applies whenever learning persistently visits a low-welfare region with bounded-away probability. Proposition 6 is diagnostic: it formalizes how the empirically observed persistent mis-selection in multi-agent LLM systems (Section 6.2.3) translates to linear regret, motivating explicit equilibrium selection.

### 3.4 Debate-style dynamics and persistent regret

Even rich explicit communication cannot prevent persistent welfare gaps when strategic uncertainty forces agents into defensive randomization, and regret accumulates linearly.

**Mechanism and link to selection.** Debate-style protocols often induce an adversarial evaluation loop (e.g., through judge selection or counter-argument pressure), so agents hedge against being exploited by maintaining randomized defenses. As a concrete illustration, consider a two-agent debate where agent 1 proposes a solution and agent 2 critiques it. If agent 1 commits to a deterministic strategy, agent 2 can craft a targeted counter-argument; anticipating this, agent 1 randomizes over alternative proposals, and agent 2 likewise randomizes its critique style. The result is a mixed equilibrium where both agents hedge rather than committing to the welfare-maximizing coordinated strategy. In the IIMG view, best-response behavior remains effectively set-valued near saddle-like regions. Because both agents hedge, learning can stabilize in defensive mixing rather than committing to a high-welfare equilibrium, yielding a non-vanishing per-iteration welfare gap.

**Lemma 7** (Persistent suboptimality under defensive mixing). *Consider a debate-style multi-agent setting and fix an agent  $i$ . Let  $s_k$  denote the (random) environment state encountered at learning iteration  $k$  (e.g., the initial state of the  $k$ -th episode). Under persistent mixing and nondegenerate action-value gaps (Appendix A.8), there exist  $\delta_{\min} > 0$  and  $k_0$  such that for all  $k \geq k_0$ ,*

$$\mathbb{E} \left[ \max_{a_i} Q_i^*(s_k, a_i, a_{-i}^k) - Q_i^*(s_k, a_i^k, a_{-i}^k) \right] \geq \delta_{\min}.$$

Here  $Q_i^*(s, a_i, a_{-i})$  is agent  $i$ 's action-value function under the opponents' current policy.

Proof is deferred to Appendix A.8.

**Corollary 8** (Linear Bayesian regret for debate-style dynamics). *Under the conditions of Lemma 7 and standard  $O(1/\sqrt{k})$  estimation errors, debate-style dynamics incur linear Bayesian regret:*

$$\text{Regret}_{\text{MAD}}(T) = \Omega(T).$$

Proof is deferred to Appendix A.8. Like Proposition 6, this result is diagnostic: it formalizes the regret consequence of empirically observed defensive mixing (Figure 2a). Sections 3.3 and 3.4 establish that ill-posed equilibrium selection is the common root cause of both failure modes. Section 4 addresses this through entropy regularization.

**Implication.** *Sublinear Bayesian regret requires convergence to a single equilibrium. Equilibrium multiplicity and debate-induced defensive mixing each prevent convergence, leading to  $\Omega(T)$  regret.*

## 4 Regularized Equilibrium Theory: HQRE Uniqueness and Convergence

The essential results in this section are: Theorem 12 (HQRE uniqueness under strong monotonicity, plus linear convergence of explicit KL-mirror steps under additional regularity), and Corollary 14 (bounded Bayesian regret from the linear-rate guarantee). Lemma 13 (zero-temperature limit connecting HQRE to unregularized BNE) is useful context but not required for the algorithm sections. The hierarchical extension (Section 4.2) can be consulted selectively. The key methodological advance in this section is the monotonicity criterion itself: it provides a single verifiable condition that simultaneously guarantees uniqueness and convergence, replacing the ad hoc stability checks prevalent in multi-agent LLM practice.

Table 3: Summary of HQRE guarantees in Sec. 4.

Result	Guarantee	Representative condition
HQRE existence (§4.1)	Existence of HQRE in discounted IIMG	$\alpha_{\min} > 0$
Regularization gap bound (§4.1)	$J_i^\alpha(\boldsymbol{\pi}) - U_i(\boldsymbol{\pi})$ is uniformly bounded	Entropy bound on $\Delta(\mathcal{A}_i)$
HQRE uniqueness (§4.1)	Unique HQRE in the strongly monotone regime	$\alpha_{\min} > L_c$
Explicit KL-mirror linear convergence (§4.1)	Linear convergence of explicit mirror steps in KL geometry	$\alpha_{\min} > L_c$ plus field Lipschitzness and local quadratic KL geometry
Zero-temperature limit (§4.1)	HQRE $\rightarrow$ unregularized equilibria as $\alpha \downarrow 0$	$\alpha_{\max} \downarrow 0$
Bounded Bayesian regret (§4.1)	Linear KL convergence implies Bayesian regret bounded uniformly in $T$	$\alpha_{\min} > L_c$
Hierarchical scalability (§4.2)	Unique Local-Global HQRE with structure-dependent stability margin	$\mu_{\text{hier}} > 0$

#### 4.1 HQRE: existence, uniqueness, and convergence

We introduce an entropy-regularized equilibrium concept that converts set-valued best responses into single-valued maps, yielding uniqueness and convergence guarantees. We regularize each agent’s objective by adding an entropy bonus weighted by a temperature parameter  $\alpha_{i,t}$ . Let  $\mathcal{H}(p) := -\sum_a p(a) \log p(a)$  denote Shannon entropy and fix a heterogeneous temperature schedule  $\boldsymbol{\alpha} = \{\alpha_{i,t}(h_i^t)\}$ . The entropy-regularized objective is

$$J_i^\alpha(\boldsymbol{\pi}) := \mathbb{E}_\pi \left[ \sum_{t \geq 0} \gamma^t (R_i(s^t, \mathbf{a}^t) + \alpha_{i,t}(h_i^t) \mathcal{H}(\pi_i(\cdot | h_i^t, t))) \right]. \quad (4)$$

Write  $\alpha_{\min} := \inf_{i,t,h_i^t} \alpha_{i,t}(h_i^t)$  and  $\alpha_{\max} := \sup_{i,t,h_i^t} \alpha_{i,t}(h_i^t)$ . These extremes bound the range of regularization strength across all agents, states, and times.

**Lemma 9** (Pointwise regularization gap). *For any joint policy  $\boldsymbol{\pi} \in \Pi$  and any agent  $i$ ,*

$$0 \leq J_i^\alpha(\boldsymbol{\pi}) - U_i(\boldsymbol{\pi}) \leq \frac{\alpha_{\max} \log |\mathcal{A}_i|}{1 - \gamma}.$$

Consequently,

$$0 \leq \sum_{i=1}^N J_i^\alpha(\boldsymbol{\pi}) - W(\boldsymbol{\pi}) \leq \frac{\alpha_{\max}}{1 - \gamma} \sum_{i=1}^N \log |\mathcal{A}_i|.$$

The bound follows directly from  $\mathcal{H}(\pi_i(\cdot | h_i^t, t)) \leq \log |\mathcal{A}_i|$ ; a proof is deferred to the Appendix. Given  $\boldsymbol{\pi}$ , let  $Q_i^\pi(h_i^t, a_i, t) := \mathbb{E}_\pi [\sum_{s \geq t} \gamma^{s-t} R_i(s^s, \mathbf{a}^s) | h_i^t, a_i^t = a_i]$  denote agent  $i$ ’s action-value function under  $\boldsymbol{\pi}$ . The logit best response at each information state is defined by

$$(\mathcal{B}_i^\alpha(\boldsymbol{\pi}))(a_i | h_i^t, t) := \frac{\exp(Q_i^\pi(h_i^t, a_i, t)/\alpha_{i,t}(h_i^t))}{\sum_{a'_i} \exp(Q_i^\pi(h_i^t, a'_i, t)/\alpha_{i,t}(h_i^t))}. \quad (5)$$

Let  $\mathcal{B}^\alpha(\boldsymbol{\pi}) := (\mathcal{B}_1^\alpha(\boldsymbol{\pi}), \dots, \mathcal{B}_N^\alpha(\boldsymbol{\pi}))$ . A *heterogeneous quantal response equilibrium (HQRE)* is a fixed point  $\boldsymbol{\pi}^* = \mathcal{B}^\alpha(\boldsymbol{\pi}^*)$ . At an HQRE, every agent plays a softmax distribution over actions weighted by their expected value, and all agents' value estimates are mutually consistent. The temperature controls how sharply each agent concentrates on high-value actions: lower temperatures yield near-deterministic play, while higher temperatures maintain exploratory mixing. The key property is, unlike unregularized best responses, the logit map is single-valued and continuous, enabling the uniqueness and convergence results as follows.

**Theorem 10** (Existence of HQRE). *Under (A1)–(A4) and  $\alpha_{\min} > 0$ , an HQRE exists.*

The proof applies Schauder's fixed-point theorem using compactness of  $\Pi$  and continuity of  $\mathcal{B}^\alpha$ ; details are deferred to Appendix B.4. Existence guarantees that HQRE is a meaningful solution concept; the next theorem addresses uniqueness. The following result shows that if the temperature is large enough to dominate the worst-case cross-agent Q-value sensitivity  $C_Q$ , the logit map is a contraction and the HQRE is unique. The threshold scales with  $N$  because this criterion treats all agent interactions uniformly. Formally:

**Theorem 11** (Contraction criterion). *For any  $\boldsymbol{\pi}, \tilde{\boldsymbol{\pi}} \in \Pi$ ,*

$$\rho_\Pi(\mathcal{B}^\alpha(\boldsymbol{\pi}), \mathcal{B}^\alpha(\tilde{\boldsymbol{\pi}})) \leq \frac{NC_Q}{2\alpha_{\min}} \rho_\Pi(\boldsymbol{\pi}, \tilde{\boldsymbol{\pi}}),$$

where  $C_Q \leq \frac{(2-\gamma)R_{\max}}{(1-\gamma)^2}$  bounds the sensitivity of agent  $i$ 's Q-values to opponents' policy changes in TV distance (see Lemma 33 for the formal statement). Hence, if  $\alpha_{\min} > \frac{NC_Q}{2}$ , the HQRE is unique and the synchronous iteration  $\boldsymbol{\pi}^{k+1} = \mathcal{B}^\alpha(\boldsymbol{\pi}^k)$  converges geometrically.

Proof is deferred to Appendix B.5. Theorem 12 below provides a sharper criterion that is used in all subsequent results. Theorem 11 provides a clean sufficient condition but can be loose, because the contraction condition treats all cross-agent interactions uniformly (hence the factor of  $N$ ). We now present a sharper monotonicity criterion that accounts for the actual strength of coupling between agents. In loosely coupled games, monotonicity imposes a much weaker requirement on the temperature.

**Weighted KL geometry.** Intuitively, we weight each information state by how often it is visited under the target policy. This means that convergence guarantees focus on states that matter for performance, rather than worst-case states that may never be reached. Let  $\{w_i(h_i^t, t)\}$  be positive weights with  $\sum_{(h_i^t, t)} w_i(h_i^t, t) = 1$  and define the weighted block norm

$$\|\boldsymbol{\pi} - \boldsymbol{\pi}'\|_{1,2;w}^2 := \sum_{i=1}^N \sum_{(h_i^t, t)} w_i(h_i^t, t) \|\pi_i(\cdot | h_i^t, t) - \pi'_i(\cdot | h_i^t, t)\|_1^2,$$

and the weighted KL–Bregman divergence  $D_\Psi$  as follows:

$$\Psi(\boldsymbol{\pi}) := \sum_{i=1}^N \sum_{(h_i^t, t)} w_i(h_i^t, t) \alpha_{i,t}(h_i^t) \sum_{a_i \in \mathcal{A}_i} \pi_i(a_i | h_i^t, t) \log \pi_i(a_i | h_i^t, t), \quad (6)$$

$$\begin{aligned} D_\Psi(\boldsymbol{\pi}, \boldsymbol{\pi}') &:= \Psi(\boldsymbol{\pi}) - \Psi(\boldsymbol{\pi}') - \langle \nabla \Psi(\boldsymbol{\pi}'), \boldsymbol{\pi} - \boldsymbol{\pi}' \rangle \\ &= \sum_{i=1}^N \sum_{(h_i^t, t)} w_i(h_i^t, t) \alpha_{i,t}(h_i^t) \text{KL}(\pi_i(\cdot | h_i^t, t) \parallel \pi'_i(\cdot | h_i^t, t)). \end{aligned} \quad (7)$$

In words,  $D_\Psi$  is a temperature- and occupancy-weighted KL divergence between joint policies. We define  $L_c$  as the tightest constant such that the unregularized operator is  $L_c$ -hypomonotone in this geometry, measuring the worst-case cross-agent coupling:

$$-\sum_{i=1}^N \langle \nabla_{\pi_i} U_i(\boldsymbol{\pi}) - \nabla_{\pi_i} U_i(\boldsymbol{\pi}'), \pi_i - \pi'_i \rangle \geq -L_c \|\boldsymbol{\pi} - \boldsymbol{\pi}'\|_{1,2;w}^2, \quad \forall \boldsymbol{\pi}, \boldsymbol{\pi}' \in \Pi. \quad (8)$$

When  $L_c = 0$  the game is fully cooperative; larger  $L_c$  indicates stronger strategic coupling. A computable upper bound is in Appendix B.6; Section 6.2.1 illustrates the computation for a concrete  $2 \times 2$  game. Then, we have

$$F_{\text{reg}}(\boldsymbol{\pi}) := (-\nabla_{\pi_1} J_1^\alpha(\boldsymbol{\pi}), \dots, -\nabla_{\pi_N} J_N^\alpha(\boldsymbol{\pi})). \quad (9)$$

**Theorem 12** (Monotonicity criterion: uniqueness and linear convergence). *Let  $\mu := \alpha_{\min} - L_c$ . For all  $\boldsymbol{\pi}, \boldsymbol{\pi}' \in \Pi$ ,*

$$\langle F_{\text{reg}}(\boldsymbol{\pi}) - F_{\text{reg}}(\boldsymbol{\pi}'), \boldsymbol{\pi} - \boldsymbol{\pi}' \rangle \geq \mu \|\boldsymbol{\pi} - \boldsymbol{\pi}'\|_{1,2;w}^2.$$

*If  $\mu > 0$ , the HQRE is unique. Assume in addition that:*

- (i)  $F_{\text{reg}}$  is  $L_F$ -Lipschitz in  $\|\cdot\|_{1,2;w}$ ;
- (ii) the weighted KL geometry admits a local quadratic upper bound on a neighborhood containing  $\boldsymbol{\pi}^*$  and the iterates, namely

$$\frac{\alpha_{\min}}{2} \|\boldsymbol{\pi} - \boldsymbol{\pi}'\|_{1,2;w}^2 \leq D_\Psi(\boldsymbol{\pi}, \boldsymbol{\pi}') \leq \frac{L_\Psi}{2} \|\boldsymbol{\pi} - \boldsymbol{\pi}'\|_{1,2;w}^2.$$

*A sufficient condition for (ii) is that the iterate region stays in the  $\nu_{\min}$ -interior of each local simplex, in which case one may take  $L_\Psi = \alpha_{\max}/\nu_{\min}$ ; see Appendix C.4.*

*Consider the explicit mirror step*

$$\boldsymbol{\pi}^{k+1} = \arg \min_{\tilde{\boldsymbol{\pi}} \in \Pi} \left\{ \langle F_{\text{reg}}(\boldsymbol{\pi}^k), \tilde{\boldsymbol{\pi}} - \boldsymbol{\pi}^k \rangle + \frac{1}{\eta} D_\Psi(\tilde{\boldsymbol{\pi}}, \boldsymbol{\pi}^k) \right\}. \quad (10)$$

*If*

$$0 < \eta \leq \min \left\{ \frac{\mu \alpha_{\min}^2}{L_F^2 L_\Psi}, \frac{\alpha_{\min}}{L_F} \right\},$$

*then*

$$D_\Psi(\boldsymbol{\pi}^*, \boldsymbol{\pi}^{k+1}) \leq \rho D_\Psi(\boldsymbol{\pi}^*, \boldsymbol{\pi}^k), \quad \rho := 1 - \eta \frac{\mu}{L_\Psi} \in (0, 1). \quad (11)$$

The uniqueness claim uses only strong monotonicity of  $F_{\text{reg}}$ . The linear-rate claim adds the standard field-Lipschitz and local-quadratic assumptions needed for explicit mirror descent in KL geometry. The proof is deferred to Appendix B.6 and Appendix C.4.

*Remark.* The additional assumptions for the linear-rate part are not implied by monotonicity alone. In particular, the upper quadratic control of  $D_\Psi$  is local for entropy / KL mirror maps and requires an iterate region that stays away from the boundary of the simplex. Practically, our DICE-FT implementation enforces this regime through positive temperatures, KL trust regions, and step rejection; see Remark 49.

**Lemma 13** (Zero-temperature limit). *Let  $\alpha^{(n)}$  be temperature schedules<sup>1</sup> with  $\alpha_{\max}^{(n)} := \sup_{i,t,h_i^t} \alpha_{i,t}^{(n)}(h_i^t) \downarrow 0$ , and let  $\pi^{(n)}$  be an HQRE under  $\alpha^{(n)}$ . Any accumulation point of  $\{\pi^{(n)}\}$  is a BNE of the unregularized game.*

Proof is deferred to Appendix B.7.

**Corollary 14** (Bounded Bayesian regret under linear KL convergence). *Fix a unique HQRE  $\pi^*$  under  $\alpha$  in the regime  $\alpha_{\min} > L_c$ , and define (note that  $\bar{\Delta}_k$  is now measured relative to the unique HQRE rather than an arbitrary BNE as in Corollary 5)*

$$\bar{\Delta}_k := \mathbb{E}_{(h^t, t) \sim \mathcal{H}_{\text{disc}}^{\pi^*}} \left[ \text{TV}(\pi^k(\cdot | h^t, t), \pi^*(\cdot | h^t, t)) \right].$$

*Suppose an algorithm produces iterates  $\{\pi^k\}_{k \geq 1}$  such that  $\mathbb{E}[D_\Psi(\pi^*, \pi^k)] \leq C_0 \rho^k$  for some  $C_0 > 0$  and  $\rho \in (0, 1)$ . Then there exists a constant  $C_{\text{Pins}}$  (depending only on the block weights and action spaces) such that  $\mathbb{E}[\bar{\Delta}_k] \leq C_{\text{Pins}} \sqrt{C_0} \rho^{k/2}$ , and the Bayesian regret relative to  $\pi^*$  is bounded uniformly in  $T$ :*

$$\text{Regret}(T) \leq \frac{2NR_{\max}C_{\text{Pins}}\sqrt{C_0}}{(1-\gamma)^2} \sum_{k=1}^T \rho^{k/2} \leq \frac{2NR_{\max}C_{\text{Pins}}\sqrt{C_0}}{(1-\gamma)^2} \cdot \frac{\sqrt{\rho}}{1-\sqrt{\rho}}.$$

The Pinsker-type control and the bound follow from Corollary 5 and are deferred to the Appendix.<sup>2</sup> Together, Theorem 12 and Corollary 14 close the regret gap identified in Section 3: regularization provides a unique target, fast convergence toward it, and bounded regret along the way.

**Main result.** *Entropy regularization converts set-valued best responses into a single-valued logit map, yielding an explicit equilibrium-selection mechanism. In the strongly monotone regime  $\alpha_{\min} > L_c$ , the selected HQRE is unique (Theorem 12); under the additional field-Lipschitz and local-quadratic assumptions stated there, explicit KL-mirror updates converge linearly (Eq. 11), and Bayesian regret is bounded uniformly in the horizon  $T$  (Corollary 14).*

## 4.2 Hierarchical coordination via Local–Global HQRE

The contraction threshold in Theorem 11 scales with  $N$  and can be conservative for large agent populations. A Local–Global hierarchy groups agents into clusters, each internally coordinated via a local HQRE, with a global controller selecting between clusters, yielding stability margins governed by structural coupling rather than the raw agent count. Let  $\mathcal{C} = \{C_1, \dots, C_K\}$  be a partition of agents into  $K$  clusters. Let  $z^t$  denote a finite public context variable that is measurable with respect to the public stream  $\{y^u\}_{u \leq t}$ , and write  $\mathcal{Z}$  for its range. Within each cluster, a local coordinator aggregates context-conditional values

$$\bar{Q}_{\text{loc},c}(z, \mathbf{a}_{C_c}, t) := \sum_{i \in C_c} w_i^{(c)}(z) \bar{Q}_i^\pi(z, a_i, t) + b_c(z), \quad (12)$$

1. The superscript  $(n)$  indexes the sequence of temperature schedules, not exponentiation.  
 2. The constant  $C_{\text{Pins}}$  scales as  $O(\sqrt{\sum_i |\mathcal{A}_i|/w_{\min}})$ , where  $w_{\min} := \min_{i, (h_i^t, t)} w_i(h_i^t, t)$ ; the bound remains non-vacuous when action spaces are moderate and occupancy weights are bounded away from zero.

where  $\bar{Q}_i^\pi(z, a_i, t) := \mathbb{E}[Q_i^\pi(h_i^t, a_i, t) \mid z^t = z]$ . A global coordinator combines cluster values through a gating policy  $g: \mathcal{Z} \rightarrow \Delta^K$ :

$$Q_{\text{tot}}(z, \mathbf{a}, t) := \sum_{c=1}^K g_c(z) \bar{Q}_{\text{loc},c}(z, \mathbf{a}_{C_c}, t) + b_0(z). \quad (13)$$

We regularize execution agents with  $\alpha$  and the global coordinator with temperature  $\tau_g > 0$ . Formal definitions and the composite KL geometry are provided in Appendix B.8.

**Theorem 15** (Hierarchical existence). *Under (A1)–(A2),  $\alpha_{\min} > 0$ , and  $\tau_g > 0$ , a Local–Global HQRE exists.*

Proof is deferred to Appendix B.9.

**Proposition 16** (Structural coupling bound). *The hierarchical coupling constant can be bounded as*

$$L_{\text{hier}} \leq W_{\max}^{\text{loc}} C_Q + C_{\text{occ}} (W_{\max}^{\text{loc}} L_g^{\text{dist}} R_{\max} + L_w^{\text{dist}} R_{\max}),$$

where  $W_{\max}^{\text{loc}}$  bounds local mixing weights and  $C_{\text{occ}}, C_Q$  are as in Sec. 3.1.

Proof is deferred to Appendix B.10.

Let  $L_c^{(c)}$  denote the within-cluster coupling constant and define local margins  $\mu_c := \alpha_{\min} - L_c^{(c)}$  and gate margin  $\mu_g := \tau_g$ . The hierarchical stability margin is

$$\mu_{\text{hier}} := \min_{c \in \{1, \dots, K\}} \mu_c + \mu_g - L_{\text{hier}}. \quad (14)$$

**Theorem 17** (Hierarchical uniqueness and linear convergence). *If  $\mu_{\text{hier}} > 0$ , then the Local–Global HQRE is unique. Moreover, assume the hierarchical field is Lipschitz in the composite block norm and that the composite KL geometry admits a local quadratic upper bound on the iterate region, with constant  $L_{\Psi}^{\text{hier}}$ . Then blockwise explicit mirror steps converge linearly in  $D_{\Psi}^{\text{hier}}$  with rate*

$$\rho_{\text{hier}} = 1 - \eta_{\text{hier}} \frac{\mu_{\text{hier}}}{L_{\Psi}^{\text{hier}}} \in (0, 1)$$

for sufficiently small  $\eta_{\text{hier}}$ .

The composite geometry and proof are deferred to Appendix B.11 and Appendix C.5. As in the flat case, uniqueness uses strong monotonicity alone, while the linear-rate claim requires the hierarchical analogues of field Lipschitzness and local quadratic KL geometry. Section 5 instantiates these results as DICE-PC and DICE-FT.

## 5 Algorithms: DICE-PC and DICE-FT

This section presents two algorithms that bridge the gap between the exact KL-mirror theory above and practical LLM-scale optimization, targeting the entropy-regularized HQRE objective of Sec. 4 under different deployment constraints. Throughout,  $\boldsymbol{\pi} = (\pi_1, \dots, \pi_N)$  denotes the joint policy and  $\pi_i$  denotes agent  $i$ 's individual policy. *DICE-PC* coordinates frozen execution LLMs by learning distributions over prompt-control actions, while *DICE-FT* fine-tunes token-level policies via clipped KL-prox mirror updates that approximate the

policy-space KL-mirror dynamics of Theorem 12. Both are implemented as coordinator-mediated instances of Definition 1. Readers primarily interested in experimental results may proceed directly to Section 6.

The essential results in this section are: Corollary\* 1 (inexact KL-mirror recurrence for DICE-FT), Proposition 18 (one-step field-error budget), and the two algorithms (Algorithms 1–2). The error decomposition, empirical diagnostics, and sensitivity discussion provide supporting evidence and can be consulted selectively.

At each environment step  $t$ , a Coordinator publishes a context message  $m^t$  and aggregates one-shot candidates into the public outcome  $y^t$ . We take the public stream token to be the augmented record  $\tilde{y}^t = (m^t, y^t)$ , so execution agents share only  $\{\tilde{y}^u\}_{u \leq t}$  and never observe each other's private trajectories. DICE-PC applies the finite-action HQRE response induced by Eq. (5) on learned candidate sets, whereas DICE-FT approximates policy-space KL-prox mirror steps in the entropic geometry induced by the HQRE objective Eq. (4). The HQRE temperature enters as an explicit entropy weight, while a KL trust region controls the approximation error from parameterization and finite-sample estimation.

**Remark (Theory–algorithm gap for DICE-FT).** The exact convergence guarantee of Theorem 12 applies to explicit mirror steps driven by the exact regularized field  $F_{\text{reg}}(\boldsymbol{\pi}^k)$ . DICE-FT replaces that field with an implementable surrogate

$$\widehat{F}^k = F_{\text{reg}}(\boldsymbol{\pi}^k) + e^k, \quad e^k = e_{\text{clip}}^k + e_{\text{samp}}^k + e_{\text{repr}}^k + e_{\text{opt}}^k,$$

where the four terms correspond respectively to clipping, finite-sample estimation, representation or critic approximation, and the residual gap between the actual finite-step parameter update and the idealized policy-space mirror step. The correct object to bound is therefore not a KL distance to the best-response map  $\mathcal{B}^\alpha$  but the dual-norm size of the field perturbation  $e^k$ , which can then be propagated through an inexact mirror recurrence.

**Corollary\* 1** (Inexact KL-mirror recurrence for DICE-FT). *Assume the conditions of Theorem 12 hold and let  $\boldsymbol{\pi}^*$  denote the unique HQRE. Model one DICE-FT update as inducing an iterate satisfying*

$$\boldsymbol{\pi}^{k+1} = \arg \min_{\tilde{\boldsymbol{\pi}} \in \Pi} \left\{ \langle F_{\text{reg}}(\boldsymbol{\pi}^k) + e^k, \tilde{\boldsymbol{\pi}} - \boldsymbol{\pi}^k \rangle + \frac{1}{\eta} D_\Psi(\tilde{\boldsymbol{\pi}}, \boldsymbol{\pi}^k) \right\}. \quad (15)$$

If

$$0 < \eta \leq \min \left\{ \frac{\mu \alpha_{\min}^2}{L_F^2 L_\Psi}, \frac{\alpha_{\min}}{L_F}, \frac{\alpha_{\min} \mu}{4L_F^2} \right\}, \quad \mu := \alpha_{\min} - L_c,$$

then

$$D_\Psi(\boldsymbol{\pi}^*, \boldsymbol{\pi}^{k+1}) \leq \rho D_\Psi(\boldsymbol{\pi}^*, \boldsymbol{\pi}^k) + C_{\text{err}} \|e^k\|_*^2, \quad (16)$$

where

$$\rho := 1 - \eta \frac{\mu}{L_\Psi} \in (0, 1), \quad C_{\text{err}} := \frac{\eta}{\mu} + \frac{\eta^2}{\alpha_{\min}}.$$

Consequently, if  $\mathbb{E}[\|e^k\|_*^2 \mid \mathcal{F}_k] \leq \bar{\mathcal{E}}_k$ , then

$$\mathbb{E}[D_\Psi(\boldsymbol{\pi}^*, \boldsymbol{\pi}^k)] \leq \rho^k D_\Psi(\boldsymbol{\pi}^*, \boldsymbol{\pi}^0) + C_{\text{err}} \sum_{j=0}^{k-1} \rho^{k-1-j} \mathbb{E}[\bar{\mathcal{E}}_j].$$

If in addition  $\sup_k \mathbb{E}[\bar{\mathcal{E}}_k] \leq \bar{\mathcal{E}}$ , then

$$\limsup_{k \rightarrow \infty} \mathbb{E}[D_\Psi(\boldsymbol{\pi}^*, \boldsymbol{\pi}^k)] \leq \frac{C_{\text{err}}}{1 - \rho} \bar{\mathcal{E}}.$$

The proof is deferred to Appendix C.4. The key point is that the practical algorithm is analyzed through a field-error recurrence in dual norm rather than through any triangle inequality in KL space.

**Proposition 18** (One-step field-error budget for DICE-FT). *Write the implementable field error in Eq. (15) as  $e^k = e_{\text{clip}}^k + e_{\text{samp}}^k + e_{\text{repr}}^k + e_{\text{opt}}^k$ . Assume:*

1. (Bounded update features) the per-sample score / update feature satisfies  $\|s(\tau)\|_* \leq G_{\text{max}}$  almost surely.
2. (Clip-overshoot moment) defining

$$\Delta_{\text{clip}}^k := \mathbb{E}\left[(\hat{r}(\tau) - \text{clip}_\varepsilon(\hat{r}(\tau)))^2 \mid \mathcal{F}_k\right],$$

we have  $\mathbb{E}[\|e_{\text{clip}}^k\|_*^2 \mid \mathcal{F}_k] \leq G_{\text{max}}^2 \Delta_{\text{clip}}^k$ .

3. (Finite-sample estimation)  $\mathbb{E}[\|e_{\text{samp}}^k\|_*^2 \mid \mathcal{F}_k] \leq \sigma_g^2 / G$ .
4. (Monotone-mixer transfer) the representation / critic approximation error obeys

$$\mathbb{E}[\|e_{\text{repr}}^k\|_*^2 \mid \mathcal{F}_k] \leq C_{\text{mix}}^2 (L_{\text{repr}}^k)^2,$$

where  $L_{\text{repr}}^k$  is a measurable per-agent value-approximation proxy and  $C_{\text{mix}}$  is the local transfer constant induced by the nonnegative mixer in Eq. (18); see Appendix C.10.

5. (Optimization / parameterization residual)

$$\mathbb{E}[\|e_{\text{opt}}^k\|_*^2 \mid \mathcal{F}_k] \leq (L_{\text{opt}}^k)^2,$$

where  $L_{\text{opt}}^k$  is any measurable proxy for the residual gap between the actual finite-step neural update and the idealized policy-space mirror step.

Then

$$\mathbb{E}[\|e^k\|_*^2 \mid \mathcal{F}_k] \leq 4\left(G_{\text{max}}^2 \Delta_{\text{clip}}^k + \frac{\sigma_g^2}{G} + C_{\text{mix}}^2 (L_{\text{repr}}^k)^2 + (L_{\text{opt}}^k)^2\right). \quad (17)$$

If, in addition,  $\Delta_{\text{clip}}^k \leq p_{\text{clip}}^k c_{\text{ov}}^2 \varepsilon^2$  for some overshoot constant  $c_{\text{ov}}$ , then the clipping contribution is  $O(p_{\text{clip}}^k \varepsilon^2)$ .

*Proof sketch.* Decompose  $e^k$  in dual norm using  $\|a + b + c + d\|_*^2 \leq 4(\|a\|_*^2 + \dots + \|d\|_*^2)$  and bound each component via the stated assumptions. Full derivation in Appendix C.9.  $\square$

Combining Corollary\* 1 and Proposition 18 yields the practical DICE-FT recurrence with error budget  $\mathcal{E}_k$  given by the right-hand side of Eq. (17).

**Empirical error diagnostics.** We therefore track the measurable components entering Eq. (17): the clip-overshoot moment  $\Delta_{\text{clip}}^k$ , the sampling term  $\sigma_g^2 / G$ , and two approximation proxies  $L_{\text{repr}}^k$  and  $L_{\text{opt}}^k$ . These diagnostics support the qualitative prediction of the inexact recurrence without collapsing the theory to a single post-hoc scalar. The field-error budget predicts that halving  $G$  from 8 to 4 roughly doubles the sampling contribution, consistent with the observed performance degradation at  $G=4$  in our ablations (Appendix C.6).

Table 4: Architectural Comparison: DICE-PC vs. DICE-FT.

Feature	DICE-PC (Prompt-Control)	DICE-FT (Fine-Tuning)
<b>Action Space</b>	Finite sets $\mathcal{U}$ (Prompt-based)	Full vocab $\mathcal{V}$ (Token-based)
<b>Learned Comps.</b>	Belief / Controller / Critic / Mixer	LoRA Policy / Critic / Mixer
<b>LLM Weights</b>	<b>Frozen</b> (No gradient)	<b>Fine-tuned</b> (Gradient updates)
<b>Equilibrium</b>	Targets HQRE (Sec. 4.1) entropy-regularized fixed point	
<b>Updates</b>	Logit best response on $\mathcal{U}_{i,t}$	Clipped KL-prox mirror update
<b>Deployment</b>	Lightweight inference overlay	Standalone fine-tuned model

**Sensitivity to group size.** Proposition 18 isolates the only explicit  $G$ -dependence in the sampling term  $\sigma_g^2/G$ . This predicts diminishing returns from increasing  $G$  once sampling noise is no longer the dominant term in the error budget. Our group-size ablations are consistent with this pattern and identify  $G=8$  as the best cost–accuracy trade-off in our setting; see Appendix C.6.

We control these gaps empirically through the KL diagnostics defined below ( $\widehat{\text{KL}}_{\text{old}}$  and  $\widehat{\text{KL}}_{\text{ref}}$ ), which serve as the rollout-measurable stability proxies described in the introduction. Section 6 reports these diagnostics alongside end-task performance.

### 5.1 Shared components: beliefs, critics, and value aggregation

Both algorithms share three components: (i) a belief encoder that compresses histories, (ii) a monotone mixer that aggregates per-agent values, and (iii) a soft baseline for variance reduction. We define each in turn.

**Beliefs and public context.** Agents in the IIMG of Sec. 3.1 condition on information states  $h_i^t$  that include private observations and the public stream. Because  $h_i^t$  grows with the interaction horizon, we compress it into a fixed-dimensional belief embedding  $b_i^t = B_i(h_i^t; \theta^B) \in \mathbb{R}^{d_B}$  via a learned encoder that consumes the agent’s private history (including the public stream text  $\tilde{y}^{\leq t}$ ). Architectural details are given in Appendix C.8.

In addition, we compute a public context feature  $z^t = Z(\tilde{y}^{\leq t})$  that is measurable with respect to  $\sigma(\{\tilde{y}^u\}_{u \leq t})$ . The feature  $z^t$  is used only by centralized training components (critics and mixers); at deployment, agents require only  $b_i^t$  and  $\tilde{y}^{\leq t}$ .

**Monotone mixing.** To connect to the Local–Global theory in Sec. 4.2, we maintain per-agent action-values and aggregate them through a monotone mixer,

$$Q_{\text{tot}}(z^t, \mathbf{a}^t, t) = f_{\text{mix}}\left(z^t, \{Q_i(b_i^t, a_i^t, t)\}_{i=1}^N; \phi_{\text{mix}}\right), \quad \frac{\partial f_{\text{mix}}}{\partial Q_i} \geq 0 \quad \forall i, \quad (18)$$

which is the flat ( $K=1$ ) instance of the hierarchical aggregation in Eq. (13).

**HQRE-shaped policies and soft baselines.** Given action-values and a temperature schedule  $\alpha > 0$ , the HQRE logit best response has the form

$$\pi_i^{\text{soft}}(a_i | b_i^t, t) \propto \exp\left(Q_i(b_i^t, a_i, t)/\alpha_{i,t}\right),$$

matching Eq. (5) with the information state  $h_i^t$  replaced by its belief embedding  $b_i^t$ .

When the action set is finite, the corresponding soft baseline at a belief state is

$$V_i^{\text{soft}}(b_i^t, t) := \alpha_{i,t} \log \sum_{a_i \in \mathcal{A}_i} \exp\left(\frac{1}{\alpha_{i,t}} Q_i(b_i^t, a_i, t)\right),$$

and the entropy-regularized advantage for a sampled action is  $Q_i - V_i^{\text{soft}}$ . DICE-PC uses this baseline exactly on a finite candidate set, while DICE-FT learns a soft baseline head as a tractable approximation of the same log-sum-exp normalizer over the token vocabulary.

**KL-prox mirror updates in practice (DICE-FT).** For DICE-FT, the idealized policy-space iteration in Theorem 12 is the explicit mirror step Eq. (10) driven by the exact field  $F_{\text{reg}}(\pi^k)$ . In practice we replace this field with a clipped stochastic surrogate computed from token log-probabilities and enforce a KL trust region to a frozen snapshot policy  $\pi^{\text{old}}$  (the current policy frozen at the start of each update iteration). This makes the update implementable with standard deep learning primitives: rollouts store token log-probabilities under  $\pi^{\text{old}}$ , the current policy computes new log-probabilities on the same tokens, importance ratios and KL are computed directly, and early stopping enforces a per-update KL target.

## 5.2 DICE-PC: prompt-control coordination

DICE-PC coordinates frozen execution LLMs by learning distributions over prompt-control actions rather than exchanging intermediate deliberation trajectories.

At each environment step  $t$ , the Coordinator publishes a context  $m^t$  and each execution agent generates a one-shot candidate; the Coordinator then aggregates candidates into the public outcome  $y^t$  via a benchmark-dependent rule (best-of- $N$  for reasoning, majority vote for planning, critic scoring for active reasoning, concatenation for interactive tasks). Each execution agent selects a bounded prompt-control action  $u_i^t \in \mathcal{U}$ , parameterizing decode-time behavior of a frozen LLM (temperature, nucleus threshold, repetition penalty, tool-access flag). Since  $\mathcal{U}$  is high-dimensional, DICE-PC performs policy improvement on a small finite candidate set  $\mathcal{U}_{i,t} \subset \mathcal{U}$  induced by a controller  $\mu_i(b_i^t; \theta_i^u)$  with quantization and anchors, preserving the logit best-response structure of Eq. (5).

**Sampling and rewards.** Given  $b_i^t$  and  $\mathcal{U}_{i,t}$ , the agent evaluates  $Q_i(b_i^t, u, t)$  for  $u \in \mathcal{U}_{i,t}$ , forms the HQRE logit best response

$$\pi_i(u \mid b_i^t, t) := \frac{\exp(Q_i(b_i^t, u, t)/\alpha_{i,t})}{\sum_{u' \in \mathcal{U}_{i,t}} \exp(Q_i(b_i^t, u', t)/\alpha_{i,t})}, \quad u \in \mathcal{U}_{i,t},$$

samples  $u_i^t \sim \pi_i(\cdot \mid b_i^t, t)$ , and decodes a one-shot candidate with the frozen LLM under  $u_i^t$ . Rewards are bounded per-agent scalars  $r_i^t$  with  $|r_i^t| \leq R_{\text{max}}$ , consistent with assumption (A2); their task-specific decomposition is described in Sec. 6.

**Critic updates and policy improvement.** When learning is enabled, we update critics and the mixer by regression on replayed transitions. For one-turn tasks ( $H=1$ ), we regress  $Q_i(b_i^0, u_i^0, 0)$  to the observed return  $r_i^0$  (with optional normalization); for multi-step tasks we use a discounted return-to-go or TD target. Policy improvement is then implicit: at each visited belief state, sampling uses the updated logit best response  $\pi_i(\cdot \mid b_i^t, t)$  induced by  $Q_i$  and  $\alpha_{i,t}$ , which directly instantiates the regularized best-response map  $\mathcal{B}_i^\alpha$  of Eq. (5).

---

**Algorithm 1** DICE-PC: prompt-control coordination via HQRE logit best response

---

**Require:** Frozen execution LLMs  $\{\text{LLM}_i\}$ ; Coordinator; replay buffer  $\mathcal{D}$ ; encoder / controller / critic / mixer parameters

```

1: for episode / query do
2:   for  $t = 0, 1, \dots, H - 1$  do
3:     Coordinator produces context  $m^t$ ; broadcast to all agents
4:     for each execution agent  $i$  (in parallel) do
5:       Update  $h_i^t$ ; compute belief  $b_i^t = B_i(h_i^t)$ ; form candidate set  $\mathcal{U}_{i,t}$  around  $\mu_i(b_i^t)$ 
6:       Evaluate  $Q_i(b_i^t, u, t)$  for  $u \in \mathcal{U}_{i,t}$ ; sample  $u_i^t \sim \pi_i(\cdot | b_i^t, t)$ 
7:       Decode frozen LLM $_i$  under control  $u_i^t$  to obtain candidate  $z_i^t$ 
8:     end for
9:     Coordinator aggregates candidates into the outcome  $y^t$ ; public stream token is  $\tilde{y}^t = (m^t, y^t)$ 
10:    Compute rewards  $\{r_i^t\}$ ; store  $(h^t, \mathbf{u}^t, \tilde{y}^t, \mathbf{r}^t)$  in  $\mathcal{D}$ 
11:    if learning enabled then
12:      Update critics  $\{Q_i\}$  and mixer  $f_{\text{mix}}$  by regression on minibatches from  $\mathcal{D}$ 
13:      Update belief / controller encoders by backprop through the critic losses
14:    end if
15:  end for
16: end for

```

---

We keep  $\alpha_{i,t}$  bounded away from zero to ensure well-posed selection; the zero-temperature limit (Lemma 13) remains a theoretical connection to the unregularized game, not an algorithmic target. Algorithm 1 summarizes the procedure.

### 5.3 DICE-FT: HQRE-oriented mirror fine-tuning

While DICE-PC coordinates frozen models through prompt control, DICE-FT directly adjusts the models’ token-level generation probabilities. It does so using clipped KL-prox mirror updates toward the HQRE fixed point. The remainder of this subsection describes four components in order: (1) the heterogeneous temperature instantiation, (2) critic targets and advantage computation, (3) the clipped actor loss with entropy regularization, and (4) KL diagnostics for stability monitoring. Readers primarily interested in experimental results may skip to Section 6 after reading the summary box at the end of this section.

Each environment step  $t$  corresponds to one agent output (e.g., a complete response). Within that step, the agent makes  $L_i$  sequential token decisions indexed by  $\ell = 0, \dots, L_i - 1$ . The HQRE temperature  $\alpha_{i,t,\ell}$ , extending the environment-step temperature  $\alpha_{i,t}$  to a per-token granularity, applies at each token position within each step, consistent with the IIMG modeling in Sec. 3.1.

**Trainable components and stored quantities.** For each agent  $i$  we train an actor  $\pi_{\theta_i}(\cdot | b_i^t, \ell)$  (implemented with parameter-efficient adapters such as LoRA), a token-action critic  $Q_{\psi_i}(b_i^t, x, \ell)$  evaluated only on sampled tokens, and a soft baseline head  $V_{\nu_i}^{\text{soft}}(z^t, b_i^t, \ell)$ .

We also train a shared monotone mixer as a nonnegative linear map,

$$Q_{\text{tot}}(z^t, \mathbf{x}_{\ell+1}, \ell) = \sum_{i=1}^N w_i^{\text{mix}}(z^t) Q_i(b_i^t, x_{i,\ell+1}, \ell) + b^{\text{mix}}(z^t), \quad w_i^{\text{mix}}(z) \geq 0, \quad (19)$$

which matches the flat instance of the hierarchical aggregation in Eq. (13).

At each update iteration, we roll out a frozen snapshot policy  $\pi^{\text{old}}$  and store, for every sampled token, its log-probability under  $\pi^{\text{old}}$ , under the current policy, and under a fixed reference policy  $\pi_{\text{ref}}$ . These stored log-probabilities make the importance ratios, entropy terms, and KL diagnostics directly computable.

**Heterogeneous temperatures.** We instantiate the agent- and state-dependent temperature  $\alpha_{i,t}(h_i^t)$  of Eq. (4) as a two-level position-dependent schedule  $\alpha_{i,t,\ell} \in \{\alpha_{\text{lo}}, \alpha_{\text{hi}}\}$ . The level switches based on whether the predictive entropy of a frozen reference model at the current prefix exceeds a threshold  $h_0$ . This schedule uses only information available at generation time; the minimum temperature  $\alpha_{\text{min}} = \alpha_{\text{lo}} > 0$  satisfies the theory’s requirement. Full specification of the threshold and two-level values is in Appendix C.8.

**Training objective overview.** The training objective combines three components in a compositional pipeline: (1) critic regression losses that estimate per-token action values from rollout returns; (2) advantages that weight these estimates by the mixer coefficients and add a group-relative control variate for variance reduction; and (3) a clipped actor loss that performs the approximate KL-mirror step using the computed advantages and an explicit entropy bonus matching the HQRE temperature. Each component feeds into the next, and we describe them in order below.

For a sampled rollout  $g$  with agent output length  $L_i^{(g)}$ , we define a per-token scalar regression target by distributing the terminal return across tokens,

$$G_{i,\ell}^{(g)} := \frac{r_i^{(g)}}{\max\{L_i^{(g)}, 1\}}, \quad \ell = 0, \dots, L_i^{(g)} - 1,$$

and mask tokens beyond a maximum generation budget to avoid unstable gradients from truncated outputs. This uniform allocation is intentionally simple: it avoids the need for per-token reward models but may under-weight early tokens that determine the solution structure. We leave token-level credit assignment to future work.

**Component 1: Critic regression losses.** We train per-agent critics  $Q_{\psi_i}$  and soft baselines  $V_{\nu_i}^{\text{soft}}$  by standard squared-error regression on the per-token return targets  $G_{i,\ell}^{(g)}$ ; the mixer is trained jointly through its dependence on the same targets. The explicit loss equations are given in Appendix C.8.

**Component 2: Advantage computation.** The weighted entropy-regularized advantage for each sampled token is

$$A_i^{(w)}(z^t, b_i^t, x_{i,\ell+1}, \ell) := w_i^{\text{mix}}(z^t) \left( Q_{\psi_i}(b_i^t, x_{i,\ell+1}, \ell) - V_{\nu_i}^{\text{soft}}(z^t, b_i^t, \ell) \right). \quad (20)$$

**Group-relative control variates.** We augment advantages with a group-relative control variate ( $\lambda_{\text{grp}}=0.5$ ) computed from  $G$  rollouts via leave-one-out standardization:

$$\tilde{A}_i^{(g,\ell)} := A_i^{(w)}(z^{(g)}, b_i^{(g)}, x_{i,\ell+1}^{(g)}, \ell) + \lambda_{\text{grp}} \widehat{A}_{\text{grp}}^{(g)}. \quad (21)$$

The critic-based advantage in Eq. (20) remains the primary signal; the group-relative term serves only for variance reduction (full derivation in Appendix C.8).

**Component 3: Clipped actor loss.** The actor update follows a PPO-style clipped surrogate, augmented with the HQRE entropy term. Let  $\rho_i^{(g,\ell)}$  be the importance ratio between the current policy and the frozen snapshot policy at the sampled token,

$$\rho_i^{(g,\ell)} = \exp\left(\log \pi_{\theta_i}(x_{i,\ell+1}^{(g)} | b_i^{(g)}, \ell) - \log \pi_{\theta_i^{\text{old}}}(x_{i,\ell+1}^{(g)} | b_i^{(g)}, \ell)\right).$$

We update each actor by maximizing the clipped near-prox surrogate with an explicit entropy weight matching the HQRE temperature,

$$\begin{aligned} \mathcal{L}_i^{\text{actor}}(\theta_i) = & \mathbb{E}_{g,\ell} \left[ \min(\rho_i^{(g,\ell)} \tilde{A}_i^{(g,\ell)}, \text{clip}(\rho_i^{(g,\ell)}, 1-\varepsilon_\ell, 1+\varepsilon_\ell) \tilde{A}_i^{(g,\ell)}) \right] \\ & + \mathbb{E}_{g,\ell} \left[ \alpha_{i,t,\ell} \mathcal{H}(\pi_{\theta_i}(\cdot | b_i^{(g)}, \ell)) \right], \end{aligned} \quad (22)$$

where  $\varepsilon_\ell$  can be position-dependent (in our experiments,  $\varepsilon_\ell = 0.2$  for all positions).

**KL diagnostics as stability proxies.** We control the approximation error through two KL diagnostics:  $\widehat{\text{KL}}_{\text{old}}$  (per-update snapshot KL triggering early stopping) and  $\widehat{\text{KL}}_{\text{ref}}$  (cumulative drift from the pretrained model, with rejected updates exceeding budget  $\beta_{\text{KL}}$ ). In experiments,  $\widehat{\text{KL}}_{\text{old}} > 0.05$  reliably signals overshooting and  $\widehat{\text{KL}}_{\text{ref}} > 0.3$  signals drift risking exit from the stable convergence regime; we recommend these as conservative thresholds. These serve as empirical proxies for the monotonicity margin  $\alpha_{\text{min}} - L_c$  (Theorem 12).

**Deployment.** At deployment, the centralized critic and mixer are discarded, and each agent runs its fine-tuned policy using only its private history and the public stream. DICE-PC can additionally be applied as a lightweight inference overlay on top of DICE-FT to further stabilize selection without modifying fine-tuned weights.

Algorithm 2 summarizes the training procedure.

***Algorithm summary.** DICE-PC learns distributions over bounded prompt-control actions to coordinate frozen LLMs, while DICE-FT fine-tunes token-level policies via clipped KL-prox mirror updates. Both target the HQRE fixed point using monotone critics, heterogeneous temperatures, and KL diagnostics that serve as practical stability proxies.*

## 6 Experiments

This section evaluates DICE-PC and DICE-FT against single-model, debate-style, and ensembling baselines. We organize experiments to mirror the causal chain underlying DICE: mechanism validation of HQRE-based equilibrium selection and its deployable diagnostics (Sections 6.2–6.3), end-task evaluation across eleven benchmarks in four domains under bounded public-stream budgets (Sections 6.4–6.5), and communication efficiency and sensitivity analysis (Sections 6.6–6.7). Table 5 maps each claim to its supporting experiment.

---

**Algorithm 2** DICE-FT: token-level KL-prox mirror fine-tuning with a monotone critic

---

**Require:** Training prompts; reference policy  $\pi_{\text{ref}}$ ; actor / belief / critic / mixer parameters; group size  $G$ ; schedules  $\{\alpha_{i,t,\ell}, \varepsilon_\ell\}$ ; KL targets and budgets

- 1: **for** update iteration  $k = 1, 2, \dots$  **do**
- 2:   Freeze current actors as  $\pi^{\text{old}}$
- 3:   Sample a minibatch of prompts; for each prompt sample  $G$  joint rollouts under  $\pi^{\text{old}}$
- 4:   For each rollout, store sampled tokens and log-probabilities under  $\pi^{\text{old}}$  and  $\pi_{\text{ref}}$ ; compute rewards and group returns
- 5:   Compute  $\hat{A}_{\text{grp}}$  by leave-one-out standardization; build per-token targets  $G_{i,\ell}$  with masking
- 6:   // *Critic update*: Update critics  $\{Q_{\psi_i}, V_{\nu_i}^{\text{soft}}\}$  and mixer by minimizing  $\sum_i (\mathcal{L}_{Q_i} + \mathcal{L}_{V_i})$
- 7:   // *Advantage computation*: Compute per-token advantages  $\tilde{A}_i^{(g,\ell)}$  via Eq. (21) and temperatures  $\alpha_{i,t,\ell}$
- 8:   // *Actor update with early stopping*: Update actors by maximizing Eq. (22) with early stopping when  $\overline{\text{KL}}_{\text{old}}$  exceeds target
- 9:   // *KL safeguard*: If  $\overline{\text{KL}}_{\text{ref}}$  exceeds budget, reject the update and optionally increase  $G$  for high-variance prompts in the next iteration
- 10: **end for**

---

## 6.1 Overview and Experimental Protocol

All experiments share a common protocol to ensure fair comparison. Unless explicitly noted, each DICE instance uses one Coordinator and three Executors under the coordinator-mediated protocol described in Section 5. The Coordinator broadcasts a single global strategy message per round (capped at 70 tokens), Executors generate one-shot candidates independently, and the Coordinator aggregates candidates into the public outcome. This design fixes the public-stream footprint per step.

We evaluate two deployment variants throughout. *DICE-PC* keeps Executor LLM weights frozen and learns only a lightweight decision layer comprising belief encoders, value networks, mixers, and prompt-control heads using HQRE-shaped mirror updates. *DICE-FT* additionally fine-tunes Executors via parameter-efficient adapters under the same HQRE mirror objective. Both variants employ the heterogeneous temperature schedule and differentiated training constraints described in Section 5.3.

We evaluate on four domains: (1) reasoning (AIME24/25, MATH-500 (Hendrycks et al., 2021), ZebraLogic (Lin et al., 2025), AutoLogic (Zhu et al., 2025)); (2) constrained planning (PlanBench (Valmeekam et al., 2023), TravelPlanner); (3) active reasoning requiring iterative information gathering (ARBench) (Zhou et al., 2025b); and (4) multi-agent coordination (LLM-COORDINATION-BENCH (Agashe et al., 2023)). This selection covers both one-step episodes and multi-turn interactive settings where discounting and incomplete information play central roles. The per-agent reward  $r_i^t$  is computed from benchmark outputs as follows: AIME and MATH-500 use binary correctness (1 if the final answer matches the ground truth, 0 otherwise); ZebraLogic and AutoLogic use binary correctness of the logical assignment; PlanBench uses binary plan validity; TravelPlanner uses the fraction of hard constraints satisfied; ARBench uses the benchmark’s native scoring function; Overcooked-AI uses the

environment’s shaped reward; and Hanabi uses the game score normalized to  $[0, 1]$ . Our primary configurations use Qwen3-4B and Qwen3-8B as Executors, with Qwen3-32B and GPT-4-Turbo as scale references.<sup>3</sup> We use open-source model families (Qwen, LLaMA) as primary backbones and include closed-source references where public numbers are available, marking them clearly in all tables. Because closed-source models use different evaluation pipelines (prompt formats, sampling strategies, tool access), their entries serve as contextual reference points rather than controlled comparisons.

Baselines fall into three categories: prompt-only inference methods (zero-/few-shot CoT, Self-Consistency, ToT, debate variants), single-agent fine-tuning (PPO/GRPO/DAPO-style updates), and multi-agent fine-tuning under matched parameter budgets. We group results by method class in all tables to enable fair within-class comparisons that isolate coordination effects from backbone differences.

### 6.1.1 TRAINING DETAILS

DICE-PC trains belief encoders, value networks, mixers, and prompt-control heads using Adam (learning rate  $3 \times 10^{-4}$ ,  $\beta_1=0.9$ ,  $\beta_2=0.999$ ) with a replay buffer of 10K transitions and minibatch size 256. DICE-FT uses the same optimizer with learning rate  $1 \times 10^{-5}$  for LoRA adapters (rank 16,  $\alpha_{\text{LoRA}}=32$ ) and  $3 \times 10^{-4}$  for critic and mixer heads. The default group size is  $G=8$  rollouts per prompt, the clip parameter is  $\varepsilon_\ell=0.2$ , and the heterogeneous temperature schedule uses  $\alpha_{\text{hi}}=0.1$ ,  $\alpha_{\text{lo}}=0.01$ , with entropy threshold  $h_0=1.5$  nats. Training runs for 200 iterations on reasoning benchmarks and 500 iterations on interactive benchmarks, with ABR-based early stopping (the Average Best-Response gap, defined in Section 6.3.2; threshold 0.1, used uniformly across all benchmarks without per-task tuning). All experiments were conducted on  $4 \times \text{A100-80GB}$  GPUs. Approximate wall-clock training times (GPU-hours) by benchmark class: TEXT-HANABI (decision layer only),  $\sim 2$ ; reasoning benchmarks (AIME, MATH-500, ZebraLogic, AutoLogic),  $\sim 6$  for DICE-PC and  $\sim 18$  for DICE-FT; planning (PlanBench, TravelPlanner),  $\sim 8$  for DICE-PC and  $\sim 22$  for DICE-FT; active reasoning (ARBench),  $\sim 10$  for DICE-PC; interactive (Overcooked-AI, Hanabi, CollabEscape/Capture),  $\sim 12$  for DICE-PC and  $\sim 24$  for DICE-FT.

### 6.1.2 MONOTONICITY VERIFICATION AT SCALE

The theoretical guarantees of Theorem 12 require the monotonicity condition  $\alpha_{\min} > L_c$ . We verify this condition directly only in the TEXT-HANABI experiments (Section 6.2.3), where the lightweight decision layer makes online estimation of  $L_c$  tractable. For the large-scale reasoning and planning benchmarks (Tables 6–8), estimating  $L_c$  would require computing second-order cross-agent gradient information through the full LLM, which is computationally prohibitive at current scale. Instead, we rely on the KL diagnostics  $\widehat{\text{KL}}_{\text{old}}$  and  $\widehat{\text{KL}}_{\text{ref}}$  as indirect stability proxies: controlled KL drift is necessary but not sufficient for the monotonicity condition to hold, so the diagnostics provide evidence of stability without formally certifying uniqueness. Developing scalable, data-driven estimators for  $L_c$  at LLM scale is an important open problem (Section 8).

---

3. We append “-Inst” for instruct-tuned variants and “-Base” for base (unaligned) checkpoints. “Qwen3-A3B” denotes the 30B MoE variant with 3B active parameters.

Table 5: Experiment-to-claim map. Each theoretical claim is paired with the section and key evidence that supports it.

Claim	Section	Key evidence
HQRE temperature selects among multiple equilibria	6.2.1	Fig. 2
Uniqueness margins predict stability under incomplete information	6.2.3	Fig. 3
Debate locks into defensive mixing with linear regret	6.2.3	Fig. 4(a, c)
HQRE achieves bounded Bayesian regret	6.2.3	Fig. 4(b, c)
Practical updates follow KL-mirror geometry	6.3	Fig. 5
ABR provides a reliable stopping criterion	6.3	Fig. 6
Hierarchical decomposition improves scalability margins	6.3.3	Fig. 7
End-task gains under bounded public streams	6.4–6.5	Tables 6, 8; Fig. 8; Tables 9–12
Communication efficiency under deployment budgets	6.6	Tables 9, 11

For reproducibility, we report both performance and communication cost across all tasks. Token accounting includes total generated tokens from all agents, message rounds per episode, and per-turn token rates where applicable. Training uses standard data sets with contamination audits to ensure no evaluation instances appear in training data. We report  $\text{pass}@K$  and  $\text{avg}@K$  metrics with benchmark-specific sampling counts, averaging over five random seeds unless stated otherwise.

For interactive coordination environments with native multi-agent interfaces, we follow the benchmark’s turn-taking or simultaneous-action protocol and treat the environment-visible trajectory log as the public stream. TEXT-HANABI is used for mechanism diagnostics under a two-agent interface; its details are specified in Section 6.2.2.

### 6.1.3 REPRODUCIBILITY

All hyperparameters are specified above (optimizer, learning rates, LoRA rank and  $\alpha$ , group size  $G$ , clip parameter  $\varepsilon$ , temperature schedule, and early-stopping threshold). We report means over 5 random seeds (seeds 0–4) for all DICE entries and include standard deviations where they exceed 0.5%. Each seed controls the random number generator for decision-layer weight initialization (or LoRA adapter initialization for DICE-FT), training data shuffling, and rollout sampling. Anonymous code, configuration files, and evaluation scripts are included in the supplementary material for review.

## 6.2 Mechanism Validation: Equilibrium Selection

We validate HQRE-based equilibrium selection in a closed-form coordination game and then test whether theory-derived uniqueness margins remain predictive under partial observability, long horizons, and function approximation.

### 6.2.1 CLOSED-FORM VERIFICATION IN A MINIMAL COORDINATION GAME

Consider a symmetric  $2 \times 2$  coordination game parameterized by  $\varepsilon \in (0, 1)$ , with payoffs  $u(L, L) = 1$ ,  $u(R, R) = 1 - \varepsilon$ , and  $u(L, R) = u(R, L) = 0$ . We set  $\varepsilon = 0.3$  (so  $u(R, R) = 0.7$ ). The game admits two pure Nash equilibria and one unstable mixed equilibrium. Under symmetric HQRE, the logit response becomes a contraction when  $\alpha$  exceeds a conservative sufficient bound of  $(2 - \varepsilon)/4 \approx 0.425$ , obtained from Theorem 11’s contraction criterion applied to this game. We numerically compute all fixed points across temperatures to characterize the actual phase transition.

Figure 2 confirms a sharp transition from three equilibria to a unique equilibrium at  $\alpha^* \approx 0.261$ , well below the conservative bound. As  $\alpha$  increases, the selected HQRE moves toward greater mixing and welfare decreases as entropy rises, illustrating the regularization–performance trade-off. In the opposite limit  $\alpha \rightarrow 0$ , HQRE strategies approach pure Nash equilibria, consistent with Lemma 13. The closed-form analysis confirms that HQRE temperature controls equilibrium multiplicity in principle; we next test whether these predictions persist under partial observability, long horizons, and function approximation.

### 6.2.2 TEXT-HANABI SETUP

TEXT-HANABI is a two-agent Dec-POMDP with  $\gamma = 0.99$  and horizon  $T = 200$ . Both agents are frozen QWEN3-4B language models. To isolate equilibrium-selection effects from backbone changes, learning is restricted to a lightweight decision layer (approximately 12M parameters per agent) that selects high-level actions and bounded decoding controls. The decision layer consists of a two-layer Transformer belief encoder (4 heads, hidden dimension 256), an MLP value head (two hidden layers of 512 units), and a linear action controller, together with the belief and value components used by the HQRE updates. We follow the benchmark’s native interaction protocol and treat the environment-visible trajectory as the public stream for the IIMG abstraction. Token accounting, temperature schedules, and stopping rules follow the default experimental setup described in Section 6.1.

### 6.2.3 UNIQUENESS MARGINS IN TEXT-HANABI

We test whether the uniqueness margin from Theorem 12 remains predictive in a structured cooperative game with partial observability and long horizons. To isolate equilibrium-selection effects from backbone changes, both agents are frozen and learning is restricted to the decision layer and critics. We compare three learning dynamics: unregularized best-response learning, debate-style message passing (MAD protocol with three rounds per step), and HQRE-based coordination (both homogeneous and heterogeneous temperatures).

Our central diagnostic is the estimated uniqueness margin  $\mu_k = \alpha_{\min, k} - \widehat{L}_{c, k}$  (Section 4.1), where  $\widehat{L}_{c, k}$  is an online estimate of the coupling constant. When  $\mu_k > 0$ , Theorem 12 predicts a unique HQRE and linear-rate convergence of KL–mirror updates.

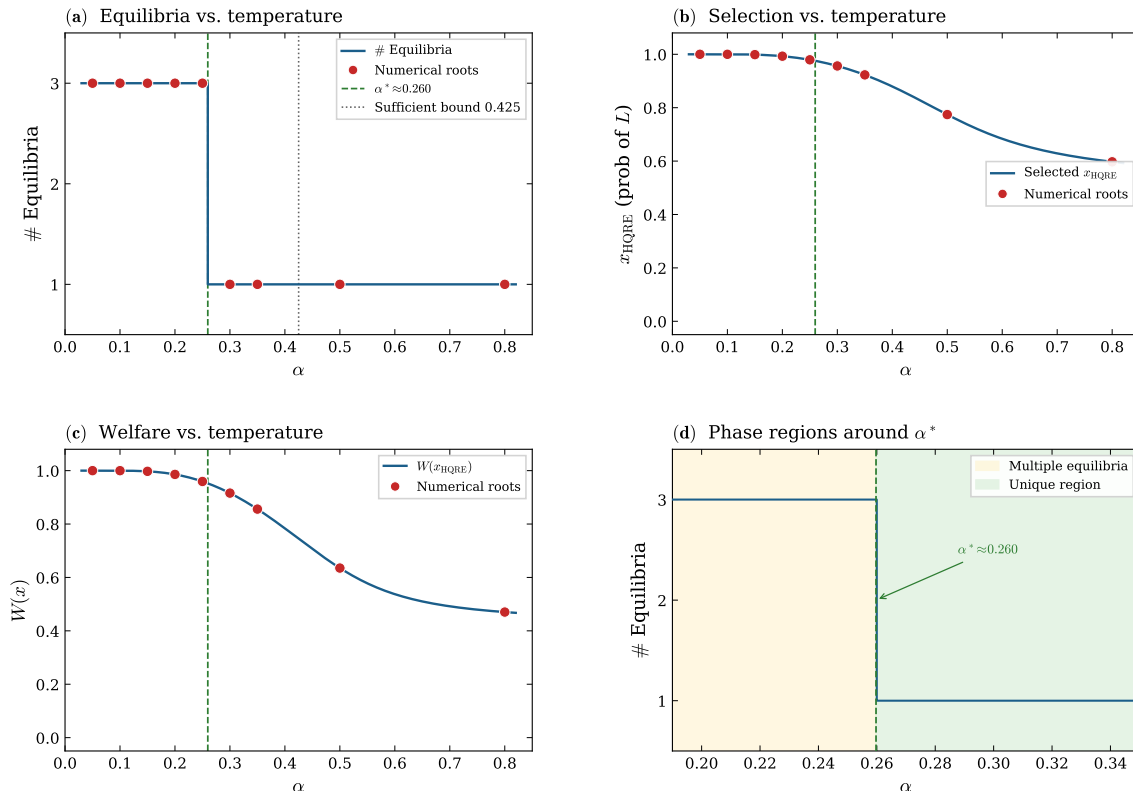


Figure 2: HQRE in a  $2 \times 2$  coordination game ( $\varepsilon = 0.3$ ). (a) Number of equilibria versus temperature  $\alpha$  shows a phase change from three equilibria to a unique equilibrium; the empirical boundary occurs at  $\alpha^* \approx 0.261$  (green dashed), tighter than the sufficient bound 0.425 (gray dotted). (b) Selected symmetric equilibrium  $x_{\text{HQRE}}$  decreases with  $\alpha$  due to increased mixing. (c) Welfare  $W(x)$  declines correspondingly as entropy rises. (d) Phase diagram marking multiple-equilibria (yellow) and unique (green) regions around  $\alpha^*$ .

Figure 3 shows that the margin becomes positive after roughly 20 iterations and stabilizes at  $0.074 \pm 0.005$ , providing an explicit stability certificate for the learned policy. Unregularized best-response learning plateaus with oscillatory behavior characteristic of equilibrium switching (Proposition 6). In contrast, HQRE-based learning exhibits exponential decay of the optimality-gap proxy. By iteration 80, the gap ratio exceeds  $20\times$  and the probability of maintaining a positive margin reaches 1.0 across seeds.

#### 6.2.4 DEBATE DYNAMICS AND REGRET ACCUMULATION

The uniqueness-margin analysis explains *why* unregularized learning fails (equilibrium multiplicity), but the theoretical framework also predicts a distinct failure mode for debate: persistent defensive mixing that maintains a positive welfare-gap floor even after convergence (Lemma 7). To test both predictions simultaneously and verify the bounded-regret guarantee of Corollary 14, we measure three additional diagnostics in the same TEXT-HANABI setup.

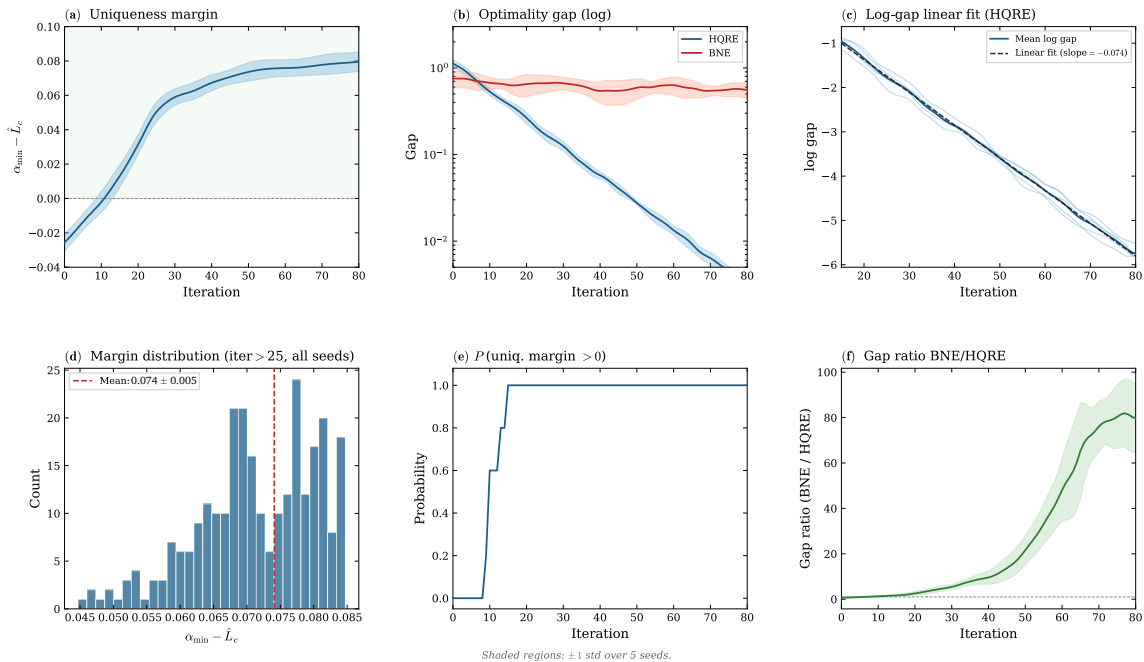


Figure 3: Uniqueness margin and linear-rate convergence in TEXT-HANABI. **(a)** The uniqueness margin  $\alpha_{\min} - \hat{L}_c$  becomes positive and stabilizes. **(b)** Optimality gap: HQRE decays exponentially, whereas BNE plateaus. **(c)** A linear fit in log-space is consistent with the predicted linear convergence regime of explicit KL-mirror theory. **(d)** Distribution of the margin after convergence. **(e)** The probability of a positive margin approaches 1.0. **(f)** The gap ratio exceeds  $20\times$  by iteration 80. Shaded regions indicate  $\pm 1$  std over 5 seeds.

Figure 4(a) confirms that debate-style dynamics maintain elevated mixing entropy ( $\bar{\mathcal{H}} > 0.6$ ) throughout training, consistent with persistent defensive mixing. This stands in contrast to unregularized BNE, whose entropy oscillates due to equilibrium switching, and to HQRE, whose entropy decays monotonically toward the unique equilibrium level. The distinction is operationally meaningful: debate agents *converge* (to a mixed strategy), but to the wrong target, whereas BNE agents *fail to converge* at all.

Figure 4(b–c) translates these mixing patterns into welfare and regret. The debate welfare gap stabilizes at a positive floor  $\delta_{\min} \approx 0.14$ , yielding linear cumulative regret; unregularized BNE accumulates regret at a similar average rate despite its oscillatory trajectory. Under HQRE, the welfare gap decays exponentially and the average Bayesian regret  $\text{Regret}(T)/T$  converges to zero, confirming the  $O(1)$  cumulative regret bound of Corollary 14. Together with the uniqueness-margin results, these diagnostics provide empirical support for the three negative results (single-model capacity ceiling via Figure 3(a), debate defensive mixing via panel (a), and multiplicity-induced drift via Figure 3) and the positive HQRE convergence and regret guarantees.

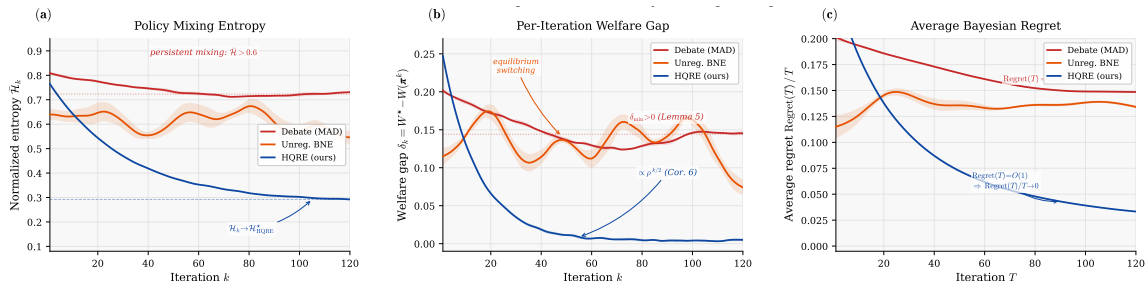


Figure 4: Defensive mixing persistence and Bayesian regret diagnostics in TEXT-HANABI. (a) Normalized policy mixing entropy  $\bar{\mathcal{H}}_k$  averaged over visited information states. Debate maintains  $\bar{\mathcal{H}} > 0.6$  throughout training (persistent defensive mixing, consistent with Lemma 7), while HQRE decays monotonically to the unique equilibrium entropy level  $\mathcal{H}_{\text{HQRE}}^*$ . (b) Per-iteration welfare gap  $\delta_k = W^* - W(\pi^k)$ . Debate exhibits a positive floor  $\delta_{\min} > 0$ ; unregularized BNE shows recurrent drift spikes from equilibrium switching; HQRE decays at rate  $\rho^{k/2}$  consistent with Corollary 14. (c) Average Bayesian regret  $\text{Regret}(T)/T$ . Debate and unregularized BNE converge to positive constants (linear cumulative regret), confirming Proposition 6 and Corollary 8. HQRE converges to zero (bounded cumulative regret, Corollary 14). Shaded regions:  $\pm 1$  std over 5 seeds.

### 6.3 Convergence Diagnostics and Deployment Criteria

Beyond uniqueness, deployment requires diagnostics that are measurable without access to best responses and robust under function approximation. We validate three practical questions under the TEXT-HANABI setup: whether practical updates follow KL-mirror geometry, how to determine convergence for early stopping, and whether a Local-Global hierarchy improves stability margins as interaction structure becomes more complex.

#### 6.3.1 MIRROR-GEOMETRY FIDELITY

For each iteration in TEXT-HANABI, we compute the mirror-descent improvement lower bound from measured KL step sizes and per-token temperatures, and compare it to realized improvements from held-out rollouts. If practical updates approximate the ideal KL-mirror step, realized improvements should match or exceed the theoretical lower bounds.

Figure 5 confirms that improvement-to-bound ratios concentrate near 1.0 across seeds, with update directions maintaining high cosine similarity to the logit best response and small KL divergence from the exact mirror step. These diagnostics indicate that the implementation remains faithful to the KL-mirror geometry that underlies our convergence guarantees, despite partial observability and function approximation.

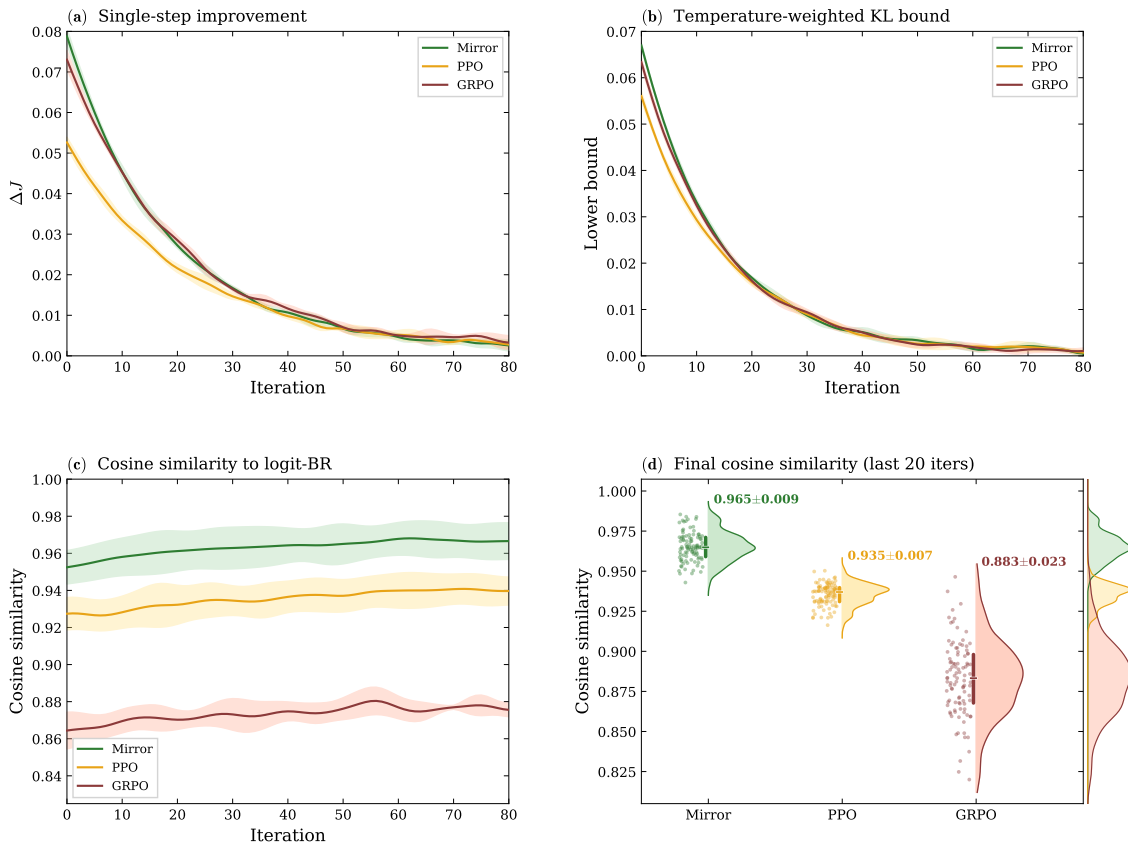


Figure 5: Practical algorithms approximate mirror geometry in TEXT-HANABI. (a–b) Single-step improvements match the theoretical lower bounds. (c) Ratios concentrate near 1.0. (d) High cosine similarity to logit best response. Shaded regions:  $\pm 1$  std over 5 seeds.

### 6.3.2 AVERAGE BEST-RESPONSE GAP AS A STOPPING CRITERION

Large-scale training requires a convergence signal measurable without exact best responses and stable enough for early stopping. The *Average Best-Response gap* (ABR) is defined as

$$\text{ABR}_k := \frac{1}{|\mathcal{B}_k|} \sum_{(h,t) \in \mathcal{B}_k} \max_{a_i} \widehat{Q}_i(h, a_i, t) - \widehat{Q}_i(h, a_i^k, t),$$

where  $\mathcal{B}_k$  is the set of information-state-timestep pairs visited in the replay buffer at iteration  $k$ ,  $\widehat{Q}_i$  is the learned critic, and  $a_i^k$  is the action taken by the current policy. Under the conditions that the critic regression has converged (critic loss below  $10^{-3}$ ) and the replay buffer covers at least 80% of reachable information states, ABR upper-bounds the true optimality gap up to constants.

Figure 6 shows that ABR consistently upper-bounds the optimality gap while remaining reasonably tight, with tightness ratios concentrating in the range 0.7–0.9 across methods and seeds. A simple threshold rule ( $\text{ABR} < 0.1$ ) reliably identifies converged policies. We therefore adopt ABR-based early stopping in all subsequent large-scale experiments.

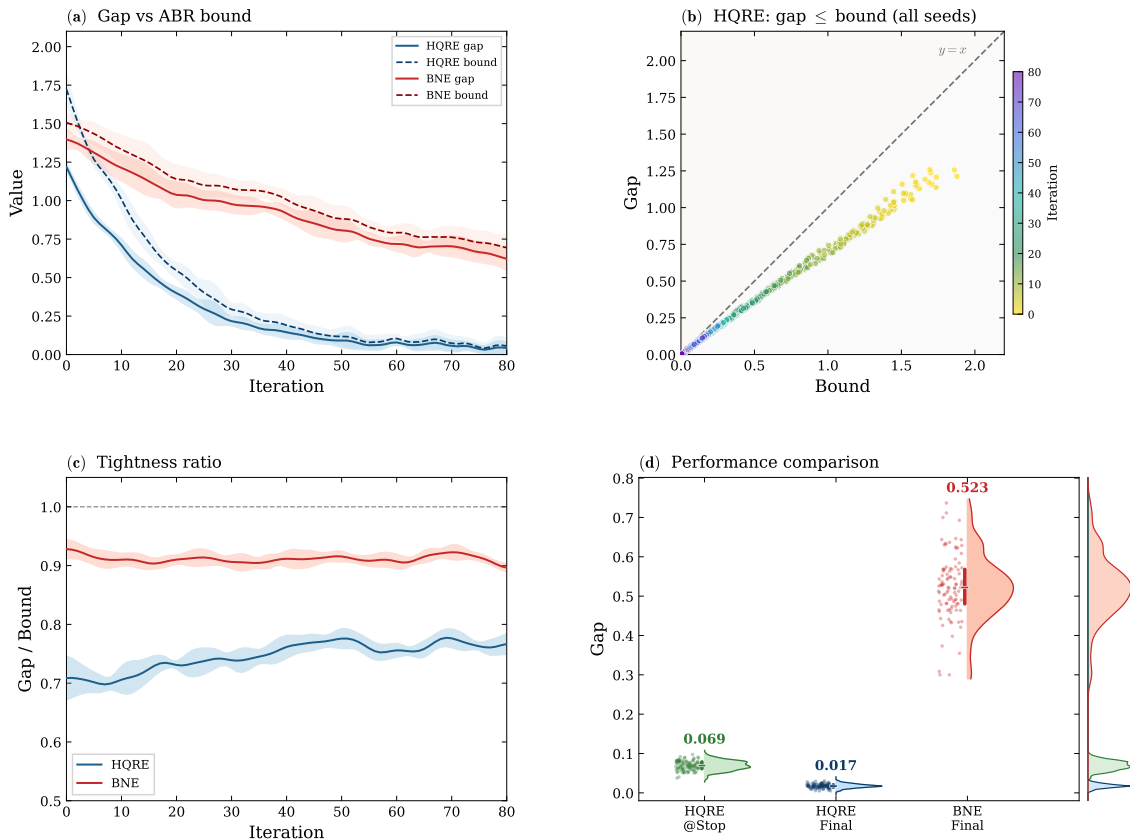


Figure 6: ABR as a convergence metric. **(a)** ABR upper-bounds the optimality gap and is tight in practice. **(b)** Uniform validity (points below the diagonal). **(c)** Tightness ratios concentrate near 0.7–0.9 depending on the method. **(d)** Early-stopping with the rule  $ABR < 0.1$  yields policies close to final convergence.

### 6.3.3 HIERARCHICAL DECOMPOSITION FOR SCALABILITY

The uniqueness condition in Theorem 12 can be conservative when treated as structure-agnostic, as the contraction threshold scales with agent count. Section 4.2 predicts that introducing a Local–Global hierarchy yields stability margins governed by structural coupling rather than raw agent count. We test this prediction by instantiating a two-level hierarchical HQRE variant in TEXT-HANABI. The hierarchical policy consists of a global controller that selects macro-intents via a softmax gate, and local heads that handle concrete arguments and decoding parameters for each intent type. We match total trainable parameters and environment interactions to a flat baseline and use the same ABR-based early-stopping.

Figure 7 shows that the hierarchical variant converges faster and reaches a substantially lower final optimality gap (0.01 versus 0.07) compared to the flat baseline under matched budgets. The global margin remains positive with probability one throughout training, consistent with the unique-equilibrium guarantee of the hierarchical theory. The gap ratio

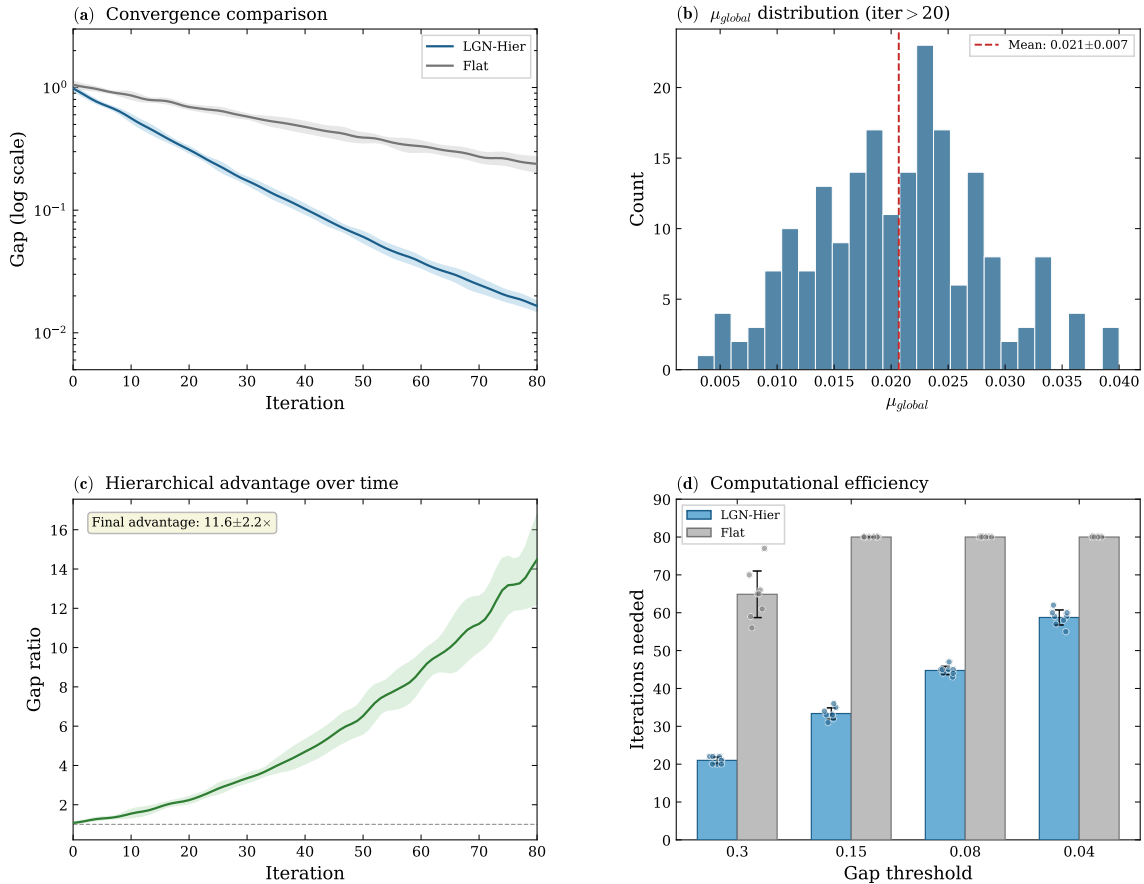


Figure 7: Hierarchical scaling in TEXT-HANABI. **(a)** Faster convergence for Local–Global HQRE versus a flat baseline. **(b)** Distribution of the global uniqueness margin. **(c)** Gap ratio showing up to 10× improvement from hierarchical decomposition. **(d)** Iterations needed to reach varying gap thresholds. Shaded regions:  $\pm 1$  std over 5 seeds.

between methods reaches ten-fold by convergence, confirming that structural decomposition improves coordination learning beyond flat architectures.

### 6.4 Reasoning and Planning Tasks

We evaluate whether these mechanism-level properties translate into end-task gains. In one-step episodes ( $H = 1$ ), a single public-stream token  $\tilde{y}^0 = (m^0, y^0)$  encodes the Coordinator context and final output. In this regime, DICE improves coordination mainly via equilibrium selection under a fixed public-stream budget.

#### 6.4.1 GENERAL REASONING AND PLANNING

Table 6 reports results across mathematical reasoning (AIME24/25, MATH-500), logical reasoning (ZebraLogic, AutoLogic), and planning (PlanBench), with methods grouped by

Table 6: Performance on general reasoning and planning benchmarks. Prompt-control baselines use instruct-tuned models (Qwen3-Inst); fine-tuning baselines use base models (Qwen3-Base). Entries marked  $\diamond$  are taken from publicly reported results (papers or official leaderboards) where available, or from our reimplementations using official released code under our evaluation protocol; unmarked entries are our own runs. Closed-source entries serve as uncontrolled reference points; see text for caveats. Best result per column is **bold**; second-best is underlined. All DICE entries report mean over 5 seeds; standard deviations are  $< 0.5\%$  on all benchmarks and are omitted for space. DICE-PC (3 $\times$ 4B) generates approximately 4.2K total tokens per problem on AIME24 (across 3 agents  $\times$   $G=8$  rollouts); single-model CoT baselines generate approximately 1.1K tokens per problem.

Method	Size	General Reasoning (%)				Planning (%)	
		AIME24	AIME25	MATH-500	ZebraLogic	AutoLogic	PlanBench
<i>Prompt-control baselines (inference-time, instruct LMs)</i>							
Qwen3-Inst (Zero-shot CoT) $\diamond$	4B	60.7	49.7	74.0	68.0	63.5	29.5
Qwen3-Inst (Few-shot CoT) $\diamond$	4B	80.0	71.1	96.8	87.7	83.0	40.1
Qwen3-Inst (SC@64) $\diamond$	4B	75.4	65.6	88.2	82.1	78.1	36.3
Qwen3-Inst (ToT) $\diamond$	4B	75.1	65.5	87.9	81.9	77.8	37.0
Qwen3-Inst (ReAct) $\diamond$	4B	78.4	68.0	90.1	84.2	80.6	37.9
Qwen3-Inst (SC@64) $\diamond$	14B	83.1	73.4	97.9	90.3	87.1	39.7
Qwen3-Inst Debate (prompt) $\diamond$	3 $\times$ 4B	65.8	57.6	94.1	83.7	84.2	37.2
Qwen3-Inst Debate+Judge (prompt) $\diamond$	3 $\times$ 4B	68.9	60.7	95.3	85.9	85.5	38.1
Qwen3-Inst Role-play (prompt) $\diamond$	3 $\times$ 4B	67.3	59.1	94.7	84.6	84.8	37.8
<i>Single-agent fine-tuning baselines (base LMs)</i>							
Qwen3-Base-PPO $\diamond$	8B	36.8	26.3	90.1	34.0	79.9	32.6
Qwen3-Base-GRPO	8B	39.1	27.9	90.7	35.4	80.3	33.1
Qwen3-Base-DAPO	8B	41.3	30.1	91.5	36.7	80.9	33.5
Qwen3-Base-GRPO $\diamond$	14B	45.2	34.1	92.2	38.7	81.4	34.8
Qwen3-Base-DAPO $\diamond$	14B	47.7	36.0	92.7	40.2	82.1	35.6
<i>Multi-agent fine-tuning baselines</i>							
Qwen3-Base Debate (FT) $\diamond$	3 $\times$ 4B	63.9	55.3	94.6	81.7	84.6	37.5
Qwen3-Base Debate+Judge (FT) $\diamond$	3 $\times$ 4B	66.8	58.2	95.2	83.8	85.3	38.4
Qwen3-Base Role-play (FT) $\diamond$	3 $\times$ 4B	65.1	56.7	95.0	82.6	85.0	37.9
Qwen3-Base Debate (FT)	3 $\times$ 8B	68.7	59.1	95.2	84.1	85.1	38.3
Qwen3-Base Debate+Judge (FT)	3 $\times$ 8B	71.1	61.7	95.9	86.3	85.9	39.1
Qwen3-Base Role-play (FT)	3 $\times$ 8B	69.9	60.5	95.7	85.1	85.5	38.7
<i>Reference: base, thinking, and closed-source models</i>							
Qwen3-Base	14B	31.7	23.3	90.1	33.1	79.1	29.7
Qwen3-Base	32B	31.0	20.2	88.6	29.2	78.5	34.3
Qwen2.5-Base	72B	18.9	15.0	83.6	26.6	76.7	33.7
GPT-4o-mini	–	8.1	8.8	78.2	20.1	62.5	34.7
Qwen3-A3B	30B	80.4	70.9	98.0	89.5	88.1	39.1
QwQ	32B	79.5	69.5	98.0	76.8	86.3	37.9
Qwen3 (thinking)	32B	81.4	72.9	97.2	88.8	87.3	40.3
DeepSeek-R1 Distill	70B	70.0	56.3	94.5	71.3	83.5	<b>99.1</b>
OpenAI o3-mini	–	79.6	74.8	98.0	88.9	86.3	41.2
Qwen3-235B-A22B $\diamond$	235B	84.9	76.1	98.8	91.7	88.9	42.5
OpenAI o3 $\diamond$	–	<u>85.8</u>	<u>76.3</u>	<u>98.9</u>	<u>92.1</u>	<u>89.0</u>	42.1
<i>DICE (ours)</i>							
Llama 3.1-Base (DICE-PC)	3 $\times$ 8B	70.3	63.4	86.1	80.7	83.9	37.1
Qwen3-Base (DICE-PC)	3 $\times$ 4B	<b>86.3</b>	<b>76.7</b>	<b>99.1</b>	<b>93.1</b>	<b>89.1</b>	<u>42.7</u>
Qwen3-Base (DICE-FT) $\diamond$	3 $\times$ 4B	84.7	74.2	98.6	91.1	88.3	41.9

Table 7: Disentangling coordination quality from multi-rollout selection on general reasoning and planning benchmarks.  $G=1$  reports single-rollout accuracy without cross-rollout selection;  $G=8+\text{select}$  follows the default DICE-PC inference protocol.

Method	Mode	Avg.	AIME24	AIME25	MATH-500	ZebraLogic	AutoLogic	PlanBench
Single-model (Qwen3-Inst few-shot CoT)	$G=1$	76.4	80.0	71.1	96.8	87.7	83.0	40.1
Single-model best-of- $N$ (token-matched)	select	77.9	82.4	72.6	97.6	89.1	84.6	40.9
3-agent fixed-control	$G=1$	78.5	82.8	73.5	98.1	89.6	86.2	40.8
3-agent fixed-control	$G=8+\text{select}$	79.4	84.0	74.5	98.5	90.6	87.0	41.5
DICE-PC	$G=1$	79.8	84.4	75.0	98.7	91.4	87.7	41.3
DICE-PC	$G=8+\text{select}$	<b>81.2</b>	<b>86.3</b>	<b>76.7</b>	<b>99.1</b>	<b>93.1</b>	<b>89.1</b>	<b>42.7</b>

class. Within the prompt-control class, DICE-PC achieves the best or tied-best accuracy on most benchmarks without modifying Executor weights, demonstrating that coordination gains can arise from equilibrium selection over bounded control actions rather than backbone updates. We caution that closed-source comparisons are not controlled. DICE-PC uses  $G=8$  rollouts per prompt and selects the best aggregated outcome, providing a pass@ $K$ -like advantage over single-pass evaluations such as the publicly reported o3 numbers. Closed-source models may also use undocumented strategies (internal verification, tool-augmented pipelines) that are not reflected in the comparison. Apparent advantages of DICE over these baselines should therefore be interpreted with caution.

To disentangle coordination quality from multi-rollout selection, Table 7 reports both single-rollout ( $G=1$ ) and selected ( $G=8+\text{select}$ ) performance for DICE-PC and matched controls. The key comparison is between DICE-PC and the 3-agent fixed-control baseline at  $G=1$ , which isolates the effect of learned HQRE-shaped coordination from the effect of multi-sample selection. The single-model best-of- $N$  row provides a token-matched search control. DICE-PC retains a clear advantage in single-rollout mode (+1.3 pp average over the fixed-control baseline at  $G=1$ ), confirming that coordination gains persist after removing multi-rollout selection. Increasing  $G$  from 1 to 8 yields a smaller additional gain (+1.4 pp).

Within the fine-tuning class, DICE-FT consistently outperforms single-agent (PPO, GRPO, DAPO) baselines at comparable or larger scales and remains competitive with multi-agent fine-tuning baselines that use greater total capacity. Notably, DICE-PC slightly outperforms DICE-FT at the same Executor backbone on several reasoning tasks. We attribute this to two factors: the optimization difficulty of jointly updating control components and token policies under HQRE constraints, and the fact that DICE-PC better preserves pretrained generalization by keeping the backbone frozen. This pattern reverses on coordination-heavy benchmarks (Section 6.5.2), where DICE-FT’s parameter adaptation provides additional gains.

#### 6.4.2 CONSTRAINT-HEAVY PLANNING ON TRAVELPLANNER

TravelPlanner stresses constraint satisfaction in a combinatorial plan space where a single violated hard constraint invalidates an otherwise plausible plan. Table 8 reports results in both two-stage (delivery plus planning) and sole-planning settings.

In the two-stage setting, DICE with GPT-4-Turbo maintains perfect delivery rate and improves final pass rate relative to debate-style coordination and multi-agent fine-tuning

Table 8: TravelPlanner results (condensed): Delivery Rate and Final Pass Rate, the two most informative summary metrics. Best result per column within each setting is **bold**; DICE rows are highlighted. Full per-constraint breakdowns (Commonsense and Hard Constraint micro/macro pass rates) are provided in Appendix Table 16.

	Validation (#180)		Test (#1,000)	
	Delivery Rate	Final PR	Delivery Rate	Final PR
Greedy Search	100	0	100	0
<i>Two-stage</i>				
GPT-4-Turbo	89.4	0.6	93.1	0.6
GPT-o3	92.8	1.4	95.6	1.9
Debate (GPT-4) @3round	95.2	2.3	97.8	3.7
MA-FT (Qwen3-32B)	97.2	3.1	98.6	4.3
MA-Debate (Qwen3-235B)	96.7	3.8	98.9	5.7
DICE (GPT-4)	<b>100</b>	<b>7.2</b>	<b>100</b>	<b>9.3</b>
DICE-PC (Qwen3-32B)	98.3	3.9	99.1	5.4
DICE-FT (Qwen3-32B)	<b>100</b>	5.6	<b>100</b>	7.1
<i>Sole-planning</i>				
Direct <sub>GPT-4-Turbo</sub>	<b>100</b>	4.4	<b>100</b>	4.4
Direct <sub>GPT-o3</sub>	<b>100</b>	6.1	<b>100</b>	5.8
Debate (GPT-4) @3round	97.7	6.7	98.2	7.1
MA-FT (Qwen3-32B)	<b>100</b>	9.1	<b>100</b>	9.7
MA-Debate (Qwen3-235B)	99.4	10.1	99.8	11.3
DICE-PC (GPT-4)	<b>100</b>	<b>12.9</b>	<b>100</b>	<b>15.2</b>
DICE-PC (Qwen3-32B)	<b>100</b>	8.9	<b>100</b>	10.3
DICE-FT (Qwen3-32B)	<b>100</b>	10.6	<b>100</b>	12.7

baselines. The gains are especially pronounced on hard constraints. DICE variants with Qwen3-32B similarly improve over comparable baselines. In the sole-planning setting, DICE again improves final pass rate, and DICE-FT approaches GPT-4-level planning quality when paired with larger open models. These improvements are consistent with the uniqueness analysis in Sections 6.2.1–6.2.3: when HQRE stabilizes equilibrium selection, executors converge to a single coherent plan rather than oscillating between incompatible alternatives.

## 6.5 Active and Interactive Tasks

We next consider multi-turn interactive episodes ( $H > 1$ ), where the public stream evolves across steps and coordination requires stable belief updating and long-horizon decision making under incomplete information.

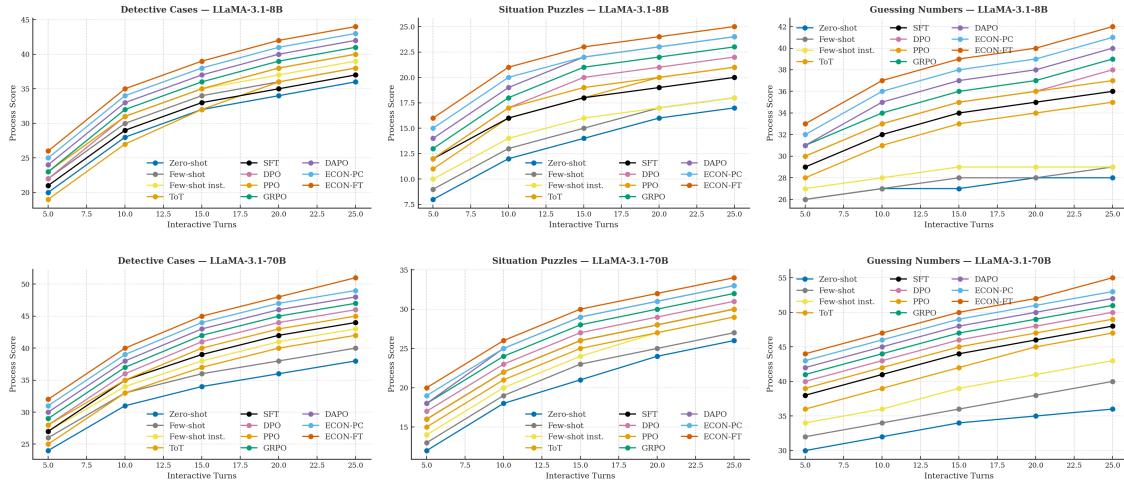


Figure 8: Active reasoning trajectories on ARBench. DICE variants reach high accuracy ( $> 90\%$  on Detective Cases,  $> 80\%$  on Situation Puzzles) in fewer turns (20–25 vs. 35–40) than single-model CoT and debate baselines, while using similar total token budgets per episode. Shaded regions:  $\pm 1$  std over 5 seeds.

### 6.5.1 ACTIVE REASONING DYNAMICS ON ARBENCH

Active reasoning tasks require iterative information gathering and hypothesis refinement, directly stress-testing stable long-horizon decision making under partial information. We evaluate on ARBench comprising Detective Cases, Situation Puzzles, and Guessing Numbers, using the official scoring metrics. Each interaction turn corresponds to an environment step  $t$  with one public-stream update  $\tilde{y}^t$  under the coordinator-mediated protocol.

Figure 8 shows that DICE variants reach their accuracy plateau in substantially fewer turns (typically 20–25) than single-model and debate baselines (often 35–40), while using similar total token budgets. Token usage increases only modestly (about 5–10% more per episode than single-model baselines), and the Coordinator accounts for less than 3% of total generated tokens. Because the Coordinator is frozen and the public-stream budget is explicitly bounded, these gains reflect improved coordination policies rather than increased communication bandwidth or parametric capacity. This faster convergence is consistent with the linear KL-mirror convergence predicted by Theorem 12: stable equilibrium selection reduces the number of coordination rounds needed to lock into a productive convention.

### 6.5.2 MULTI-AGENT COORDINATION BENCHMARKS

We evaluate DICE on the LLM-COORDINATION-BENCH suite comprising Overcooked-AI, CollabEscape, CollabCapture, and Hanabi, emphasizing two coordination-relevant axes: ad-hoc teaming robustness and consensus cost under fixed public-stream budgets.

**Ad-hoc teaming (Overcooked-AI).** Ad-hoc teaming robustness measures whether learned policies transfer to novel partners. We quantify this via the self-play versus cross-play gap, where lower values indicate better generalization (negative means Cross  $\geq$  Self).

Table 9: Overcooked-AI summary with robustness and efficiency diagnostics. Self-/Cross-Play are means over five layouts (CR/AA/Ring/FC/CC); Gap = (Self – Cross)/Self% (lower is better; negative means Cross  $\geq$  Self). Tok/Ep and Msg Rnds denote per-episode token and message budgets.

Method	Size	Self $\uparrow$	Cross $\uparrow$	Gap $\downarrow$	Coll. $\downarrow$	Hand. $\uparrow$	Idle% $\downarrow$	Post. KL $\downarrow$	Tok/Ep	Msg Rnd
<i>Single-model references</i>										
Qwen3-32B-Inst	1 $\times$ 32B	95.7	88.3	7.7	8.9	12.4	18.3	0.47	2.8K	3.2
Qwen3-235B-Inst	1 $\times$ 235B	108.2	96.4	10.9	7.1	15.8	14.7	0.39	3.1K	3.4
GPT-o3	–	156.3	127.8	18.2	5.2	21.7	9.8	0.31	3.5K	3.8
GPT-4-Turbo	–	<b>182.7</b>	<b>144.0</b>	21.2	4.3	24.9	8.1	0.28	3.7K	4.1
<i>Prompt-only multi-agent</i>										
MAD	3 $\times$ 8B	101.3	108.5	–7.1	8.6	14.7	17.6	0.42	2.9K	4.5
Role-Play	3 $\times$ 8B	98.4	104.2	–5.9	9.1	13.9	18.9	0.44	2.8K	4.3
CAC (uniform)	3 $\times$ 8B	103.7	107.1	–3.3	8.3	15.2	16.8	0.40	2.9K	4.4
CAC (learned)	3 $\times$ 8B	105.2	108.9	–3.5	8.0	15.8	16.2	0.38	3.0K	4.6
MA-Debate (32B)	3 $\times$ 32B	106.8	109.2	–2.2	7.8	16.3	15.2	0.36	3.2K	4.7
Debate+Judge (GPT-4)	–	125.7	119.3	5.1	5.8	18.9	11.4	0.33	3.6K	5.2
MA-Debate (235B)	3 $\times$ 235B	117.4	118.6	–1.0	6.3	19.8	12.1	0.29	3.4K	5.1
rStar	3 $\times$ 32B	112.3	106.8	4.9	6.9	17.8	13.7	0.35	3.3K	5.8
<i>Fine-tuned multi-agent</i>										
MA-FT (32B)	3 $\times$ 32B	109.7	110.4	–0.6	7.2	17.1	14.5	0.33	3.0K	4.2
<i>DICE (ours)</i>										
DICE-PC	3 $\times$ 8B	110.4	110.6	–0.2	7.5	17.8	14.1	0.32	2.8K	3.9
DICE-FT	3 $\times$ 8B	114.4	114.9	–0.5	6.9	18.9	13.2	0.29	2.7K	3.6
DICE-FT	3 $\times$ 32B	121.6	122.1	–0.4	6.2	20.7	11.8	0.26	2.9K	3.7

Table 10: Forced Coordination (FC) layout diagnostics.  $\Delta$  vs MAD reports relative change (%); lower Coll./Idle%/Post. KL and higher Handoffs indicate more partner-robust coordination.

Method	Self $\uparrow$	Cross $\uparrow$	Coll. $\downarrow$	$\Delta$ Coll.	Hand. $\uparrow$	$\Delta$ Hand.	Post. KL $\downarrow$
MAD (3 $\times$ 8B)	103.4	111.3	9.2	–	13.8	–	0.45
MA-FT (3 $\times$ 32B)	111.7	112.9	7.8	–15%	16.4	+19%	0.35
DICE-PC (3 $\times$ 8B)	116.3	115.2	8.1	–12%	17.2	+25%	0.34
DICE-FT (3 $\times$ 8B)	120.4	119.5	7.4	–20%	18.5	+34%	0.31
DICE-FT (3 $\times$ 32B)	132.8	132.1	6.1	–34%	21.6	+57%	0.25

Table 9 shows that DICE maintains near-zero gaps at both 3 $\times$ 8B and 3 $\times$ 32B scales while operating under a bounded coordinator-mediated public stream.

Forced Coordination diagnostics (Table 10) further show reduced collisions and idle time together with increased successful handoffs, consistent with more disciplined coordination rather than higher-bandwidth interaction.

**Consensus cost (CollabEscape/CollabCapture).** Consensus cost measures the number of public-stream updates (turns) required to reach agreement at a given success rate. Table 11

Table 11: CollabEscape and CollabCapture with consensus-cost diagnostics. Success/Turns are mean over 5 seeds;  $\Delta$ Turns vs MAD is relative reduction (%).

Method	Escape		Tok/Turn	Capture		Msg/Turn
	Succ/Turns	$\Delta$ Turns		Succ/Turns	$\Delta$ Turns	
GPT-4-Turbo	<b>0.80</b> /4.6	+4%	520	<b>1.00</b> / <b>3.5</b>	+49%	3.8
GPT-o3	0.70/4.2	+13%	485	0.90/4.1	+40%	3.5
Qwen3-32B-Inst	0.60/5.3	-10%	410	0.80/7.5	-10%	3.2
Qwen3-235B-Inst	0.70/4.9	-2%	465	0.90/6.2	+9%	3.6
MAD (3 $\times$ 8B)	0.70/4.8	-	395	0.90/6.8	-	3.1
MA-Debate (32B)	0.70/4.5	+6%	425	0.90/5.9	+13%	3.4
MA-FT (32B)	0.70/4.3	+10%	435	0.90/5.6	+18%	3.5
MA-Debate (235B)	<b>0.80</b> /4.4	+8%	480	<b>1.00</b> /4.7	+31%	3.7
Debate+Judge (GPT-4)	0.70/4.7	+2%	545	0.90/5.3	+22%	4.0
rStar	0.60/5.1	-6%	470	0.80/6.5	+4%	3.9
DICE-PC (3 $\times$ 8B)	0.70/ <u>4.1</u>	+15%	380	0.90/ <u>5.2</u>	+24%	3.0
DICE-FT (3 $\times$ 8B)	<b>0.80</b> /3.9	+19%	365	<b>1.00</b> /4.8	+29%	2.9
DICE-FT (3 $\times$ 32B)	<b>0.80</b> / <b>3.4</b>	<b>+29%</b>	445	<b>1.00</b> / <b>3.8</b>	<b>+44%</b>	3.3

shows that DICE reaches comparable or higher success rates in fewer turns than debate baselines, while keeping tokens-per-turn and messages-per-turn comparable or lower.

These results indicate that DICE reduces coordination friction under incomplete information without shifting cost into additional communication.

**Partial observability (Hanabi).** Table 12 shows that DICE-FT achieves the strongest LLM-based scores while substantially reducing illegal move rates, supporting the role of heterogeneous regularization in stabilizing information-sensitive decisions and preventing drift-induced constraint violations under limited observability. The remaining gap between DICE-FT (22.8) and non-LLM upper bounds ( $\sim 24$ ) is likely attributable to LLM backbone limitations in precise card-state tracking: Hanabi requires exact enumeration of remaining cards, a task where specialized neural networks with discrete state representations have a structural advantage over autoregressive language models.

## 6.6 Communication Efficiency Analysis

A central motivation for DICE is to keep the shared public stream small while still obtaining stable coordination through equilibrium selection. Under the coordinator-mediated protocol (Section 5), each environment step produces a single public-stream update  $\tilde{y}^t = (m^t, y^t)$ . The coordination-specific overhead is dominated by the Coordinator context  $m^t$ , which is capped at 70 tokens, whereas Executor candidates remain private and are not appended to the shared stream. In contrast, all-to-all debate-style protocols expand the public stream by repeatedly appending full peer transcripts, increasing shared bandwidth and context cost.

To quantify the scaling advantage, consider a three-Executor, five-step configuration. DICE’s coordination-specific shared input is bounded by  $5 \times 70 = 350$  tokens (Coordinator

Table 12: Hanabi self-play results: DICE vs. Baselines. H.Eff: hint efficiency (higher is better); Ill.: illegal move rate (lower is better). Our methods achieve superior policy discipline and coordination efficiency, approaching non-LLM upper bounds.

Method	Score $\uparrow$	H.Eff $\uparrow$	Ill. $\downarrow$	Method	Score $\uparrow$	H.Eff $\uparrow$	Ill. $\downarrow$
<i>Non-LLM References (Upper Bounds)</i>				<i>Single-Model Baselines</i>			
OBL (ref.)	24.1 $\pm$ 0.0	–	–	GPT-4-Turbo	13.3 $\pm$ 0.9	1.82	8.7%
SAD (ref.)	24.0 $\pm$ 0.0	–	–	GPT-4o	8.3 $\pm$ 1.2	1.24	14.3%
BAD (ref.)	23.9 $\pm$ 0.0	–	–	GPT-o3	11.7 $\pm$ 1.0	1.65	10.1%
<i>Multi-Agent Baselines (Debate/FT)</i>				<i>DICE (Ours)</i>			
Qwen3-32B-I	9.2 $\pm$ 1.1	1.43	12.8%	<b>DICE-PC</b> (3 $\times$ 8B)	19.8 $\pm$ 1.1	2.47	5.3%
Qwen3-235B-I	12.8 $\pm$ 0.9	1.76	9.4%	<b>DICE-FT</b> (3 $\times$ 8B)	20.4 $\pm$ 0.8	2.58	4.9%
MA-Deb (32B)	15.7 $\pm$ 1.0	2.04	7.2%	<b>DICE-FT</b> (32B)	<b>22.8<math>\pm</math>0.6</b>	<b>2.89</b>	<b>3.7%</b>
MA-FT (32B)	17.3 $\pm$ 0.9	2.21	6.5%				
MA-Deb (235B)	18.6 $\pm$ 0.8	2.35	5.8%				

contexts only), whereas all-to-all debate requires each Executor to ingest  $5 \times 2 \times 500 \approx 5,000$  peer tokens<sup>4</sup>—a 14 $\times$  increase in shared coordination context.

Empirically, the coordination benchmarks confirm this advantage. In Overcooked-AI, DICE-FT (3 $\times$ 8B) uses 2.7K tokens per episode with 3.6 message rounds, compared to 2.9K tokens and 4.5 rounds for MAD, a 20% reduction in message rounds at comparable token cost (Table 9). On CollabCapture, DICE-FT reduces turns to consensus (4.8 vs. 6.8) while also reducing messages per turn (2.9 vs. 3.1) at higher success (Table 11). Together, these results indicate that DICE’s gains stem from better equilibrium-induced coordination targets rather than from higher-bandwidth communication.

## 6.7 Sensitivity and Ablations

We now isolate each design choice’s contribution through controlled ablations (Table 13) and hyperparameter sensitivity sweeps (Table 14). All experiments hold every factor fixed except the one under study and report means  $\pm 1$  std over 5 random seeds.

*Equilibrium-selection mechanism.* Removing entropy regularization entirely causes the largest degradation: the uniqueness margin turns negative, ABR quadruples, and TEXT-HANABI score drops by 23.5% (Table 13, top block). Replacing heterogeneous HQRE with debate-style mirror updates recovers part of the gap but still incurs a 15.5% score drop and produces no meaningful uniqueness margin, consistent with the persistent defensive mixing reported in Figure 4. Switching to homogeneous temperatures retains a positive margin but narrows it from 0.074 to 0.052, reducing both TEXT-HANABI score (−8.6%) and end-task accuracy. The ordering (heterogeneous HQRE  $\succ$  homogeneous HQRE  $\succ$  debate  $\succ$  unregularized) confirms that heterogeneous temperature scheduling is the most impactful choice after the decision to regularize at all.

*Token-type regularization.* The default entropy-based partition outperforms uniform weighting (−7.0%) and random partitioning (−9.1%). A gradient-norm partition, which

4. Based on observed mean message lengths in our debate baselines. Executor candidate generation is private in both settings and excluded from this accounting.

Table 13: Component ablations. TEXT-HANABI uses two frozen Qwen3-4B agents; AIME24 and ZebraLogic use DICE-PC (3×4B). Each row removes or replaces one design choice; all others remain at default.  $\mu_\infty$ : converged uniqueness margin; ABR: Average Best-Response gap at convergence.  $\Delta$  is relative change versus the DICE-PC default. Best per column is **bold**.

Variant	TEXT-HANABI		End-task (%)		Diagnostics	
	Score $\uparrow$	$\Delta$	AIME24	ZebraLogic	$\mu_\infty\uparrow$	ABR $\downarrow$
DICE-PC (default)	<b>18.7±0.4</b>	–	<b>86.3</b>	<b>93.1</b>	<b>0.074±0.005</b>	<b>0.031±0.004</b>
DICE-FT (reference)	18.4±0.5	–1.6%	84.7	91.1	0.071±0.006	0.034±0.005
<i>Equilibrium-selection mechanism</i>						
Homogeneous HQRE (uniform $\alpha$ )	17.1±0.6	–8.6%	84.1	90.7	0.052±0.008	0.048±0.007
Unregularized best response	14.3±1.2	–23.5%	80.9	86.3	< 0	0.127±0.031
Debate mirror (MAD 3-round)	15.8±0.9	–15.5%	82.4	88.1	–	0.089±0.019
<i>Token-type regularization</i>						
Uniform token weighting	17.4±0.5	–7.0%	83.8	90.2	0.058±0.007	0.044±0.006
Random token partition	17.0±0.7	–9.1%	83.1	89.5	0.054±0.009	0.051±0.008
Gradient-norm partition	18.2±0.5	–2.7%	85.4	92.1	0.068±0.006	0.035±0.005
<i>Architecture and scale</i>						
Flat (no Local–Global hierarchy)	16.9±0.7	–9.6%	85.1	91.8	0.049±0.010	0.053±0.009
No Coordinator (peer-only)	15.2±1.0	–18.7%	81.7	87.4	0.031±0.012	0.078±0.015
2 Executors	17.1±0.6	–8.6%	84.8	91.4	0.059±0.008	0.046±0.007
5 Executors	19.1±0.4	+2.1%	86.7	93.4	0.079±0.005	0.028±0.004

classifies tokens by running gradient magnitude, closes to within 2.7% of the default. This suggests that any *informed* differentiation helps, but entropy-based classification achieves comparable quality with a simpler, gradient-free implementation.

*Architecture and scale.* Removing the Coordinator and relying on peer-only aggregation produces the second-largest overall drop (–18.7%), confirming that the coordinator-mediated protocol is essential for combining bounded public-stream cost with stable coordination. Removing the Local–Global hierarchy costs 9.6% on TEXT-HANABI and narrows the uniqueness margin by a third. Reducing from 3 to 2 Executors costs 8.6%; increasing to 5 gains 2.1% on TEXT-HANABI and a marginal 0.4 points on AIME24, but at a 39% increase in per-episode tokens (Table 14, Executor-count block). The diminishing returns on reasoning tasks versus sustained gains on interactive benchmarks (Overcooked cross-play: +2.9%, Table 14) are consistent with the theoretical observation that one-step coordination saturates in diversity faster than multi-turn settings where additional viewpoints improve belief coverage.

*Hyperparameter sensitivity.* All three continuously tunable hyperparameters exhibit a shared pattern: performance peaks near the default, degrades symmetrically at both extremes, and remains within a broad stable band (Table 14). For the temperature multiplier  $\kappa$ , the uniqueness margin increases monotonically (as expected from theory), but task performance

Table 14: Hyperparameter sensitivity. TEXT-HANABI uses two frozen Qwen3-4B agents (DICE-PC); Overcooked-AI uses DICE-PC (3×8B). Each row varies one hyperparameter from its default (highlighted); all others are held fixed.

(a) Text-Hanabi			(b) Overcooked-AI		
Setting	Score↑	$\mu_\infty$ ↑	Setting	Cross-Play↑	Tok/Ep
<i>Temperature multiplier <math>\kappa</math></i>			<i>Temperature multiplier <math>\kappa</math></i>		
$\kappa = 0.25$	16.1±0.9	0.032±0.011	$\kappa = 0.25$	106.2	2.8K
$\kappa = 0.5$	17.8±0.5	0.058±0.007	$\kappa = 0.5$	109.1	2.8K
$\kappa = 1.0$ (default)	<b>18.7±0.4</b>	0.074±0.005	$\kappa = 1.0$ (default)	<b>110.6</b>	2.8K
$\kappa = 2.0$	18.0±0.5	0.091±0.006	$\kappa = 2.0$	108.3	2.8K
$\kappa = 4.0$	15.4±0.8	0.118±0.009	$\kappa = 4.0$	103.7	2.9K
<i>Coordinator message cap (tokens/round)</i>			<i>Coordinator message cap (tokens/round)</i>		
30	17.3±0.6	0.061±0.008	30	106.8	2.4K
50	18.2±0.5	0.069±0.006	50	109.1	2.6K
<b>70 (default)</b>	<b>18.7±0.4</b>	0.074±0.005	<b>70 (default)</b>	<b>110.6</b>	2.8K
100	18.9±0.4	0.076±0.005	100	111.2	3.1K
<i>Number of Executors</i>			<i>Number of Executors</i>		
2	17.1±0.6	0.059±0.008	2	105.4	2.2K
<b>3 (default)</b>	<b>18.7±0.4</b>	0.074±0.005	<b>3 (default)</b>	<b>110.6</b>	2.8K
5	19.1±0.4	0.079±0.005	5	113.8	3.9K
<i>Trust-region KL coefficient <math>\beta_{\text{KL}}</math></i>			<i>Trust-region KL coefficient <math>\beta_{\text{KL}}</math></i>		
$\beta_{\text{KL}} = 0.001$	16.8±0.8	0.047±0.010	$\beta_{\text{KL}} = 0.001$	107.3	2.8K
$\beta_{\text{KL}} = 0.005$	18.1±0.5	0.065±0.007	$\beta_{\text{KL}} = 0.005$	109.8	2.8K
$\beta_{\text{KL}} = 0.01$ (default)	<b>18.7±0.4</b>	0.074±0.005	$\beta_{\text{KL}} = 0.01$ (default)	<b>110.6</b>	2.8K
$\beta_{\text{KL}} = 0.05$	17.6±0.6	0.082±0.006	$\beta_{\text{KL}} = 0.05$	107.9	2.8K
$\beta_{\text{KL}} = 0.1$	16.2±0.7	0.094±0.008	$\beta_{\text{KL}} = 0.1$	104.1	2.9K

is non-monotone:  $\kappa=4.0$  yields margin 0.118 but degrades TEXT-HANABI score by 17.6% due to over-regularization, while  $\kappa=0.25$  narrows the margin to 0.032 with sharply increased variance. The stable range  $\kappa \in [0.5, 2.0]$  maintains <5% performance variation, confirming the regularization–welfare trade-off of Figure 2. For the coordinator message cap, 70 tokens sits near the efficiency frontier: reducing to 30 tokens lowers scores by 3.4–7.5%, while increasing to 100 tokens yields only +1.1% at 10% higher token cost. For the trust-region coefficient,  $\beta_{\text{KL}} \in [0.005, 0.05]$  keeps performance within 4% of the default ( $\beta_{\text{KL}}=0.01$ ); values above 0.05 cause overshooting (−13.4% on TEXT-HANABI).

*Summary of ablation findings.* Three conclusions emerge. First, entropy regularization is necessary and heterogeneous temperatures yield a further 8.6% gain over homogeneous alternatives; this is the single most impactful design axis. Second, the coordinator-mediated protocol and the Local–Global hierarchy each contribute meaningfully (−18.7% and −9.6% respectively when removed), while 3 Executors provide a favorable cost–performance balance. Third, all continuously tunable hyperparameters ( $\kappa$ , message cap,  $\beta_{\text{KL}}$ ) exhibit broad stable regions around their defaults, and no setting requires benchmark-specific tuning.

### 6.7.1 HEADLINE SUMMARY

Across the six reasoning and planning benchmarks in Table 6, DICE-PC (3×4B) improves over the best within-class prompt-control baseline by an average of 4.3 percentage points (reasoning: +4.6 pp across AIME24/25, MATH-500, ZebraLogic, AutoLogic; planning: +2.6 pp on PlanBench). DICE-FT (3×4B) improves over the best within-class multi-agent fine-tuning baseline by an average of 8.5 pp across the same benchmarks, with the largest gains on AIME24 (+17.9 pp) and AIME25 (+16.0 pp). On the interactive benchmarks, coordination gains are even larger: +22% on Hanabi, +31% on CollabEscape, and >90% accuracy on ARBench Detective Cases versus <70% for debate baselines.

### 6.7.2 FAILURE CASES AND LIMITATIONS

DICE does not uniformly improve over all baselines on all benchmarks. On PlanBench, DICE-PC (3×4B) achieves 42.7%, only marginally above the strongest debate baseline (38.4%) and below DeepSeek-R1 Distill (99.1%), suggesting that equilibrium selection provides limited benefit when the primary bottleneck is single-agent planning capacity rather than coordination. On TravelPlanner (two-stage setting), the uniqueness margin  $\mu_k$  for DICE-PC (Qwen3-32B) remained below 0.02 for the first 80 iterations before stabilizing, and two of five seeds showed intermittent negative margins during early training, indicating that the monotonicity condition is not always satisfied from initialization. In these cases, the KL safeguard (rejection of high-drift updates) prevented divergence but slowed convergence. Qualitatively, failures on constraint-heavy planning tasks typically manifested as agents converging to a consistent but suboptimal convention (e.g., satisfying commonsense constraints while violating hard constraints), rather than failing to converge entirely. As a practical guideline, we recommend monitoring the uniqueness margin during early training: if it remains negative past the first 50 iterations, the task may be capacity-bottlenecked rather than coordination-bottlenecked, and single-model fine-tuning may be more appropriate. Based on our results, coordination benefits are most pronounced when (i) the task requires multi-step information integration that exceeds a single model’s context or reasoning capacity, and (ii) individual executor capacity is sufficient to generate plausible candidates. When executor capacity is the primary bottleneck (as in PlanBench with 4B models), coordination provides diminishing returns. This suggests that larger executors (e.g., 32B or 70B) may alleviate the capacity bottleneck on PlanBench, but we do not evaluate this setting here.

### 6.7.3 COORDINATION-VS-CAPACITY REGIME

Across our eleven benchmarks, a clear empirical pattern emerges for when coordination benefits dominate capacity scaling and vice versa. Coordination benefits are largest on tasks requiring multi-step information integration under partial observability—Hanabi (+22% over single-agent), ARBench (>90% on Detective Cases vs. <70% for debate baselines), CollabEscape (+31%), and Overcooked-AI (+18% cross-play)—where each agent holds private information that must be combined to solve the task. In the IIMG framework, these are tasks with high information asymmetry: each agent’s private history carries non-redundant signal, so the coordination problem (selecting compatible conventions for information exchange) dominates the capacity problem (generating individually good responses). Conversely, coordination provides diminishing returns when the task is primarily capacity-bottlenecked:

on PlanBench with 4B executors, DICE-PC achieves only 42.7% because the bottleneck is single-agent planning quality, not inter-agent convention selection. The theoretical framing suggests a diagnostic: tasks where the effective coupling constant  $L_c$  is large relative to  $\alpha_{\min}$  (i.e., agents’ strategies are tightly interdependent) are coordination-bottlenecked and benefit most from DICE, while tasks where  $L_c$  is small (agents operate nearly independently) are capacity-bottlenecked and benefit more from model scaling. In practice, since  $L_c$  is not always computable, the uniqueness margin and behavioral sensitivity to perturbations serve as accessible proxies: high perturbation sensitivity signals a coordination bottleneck, while low sensitivity with poor absolute performance signals a capacity bottleneck.

#### 6.7.4 DEPLOYMENT DECISION CHECKLIST

Before investing in DICE, assess the following:

1. **Perturbation sensitivity test.** Run the target task under 3–5 prompt/seed perturbations with a single-model baseline. If outputs change qualitatively (different solution strategies, not just numerical noise), the task is likely coordination-bottlenecked. If outputs are stable but low-accuracy, it is capacity-bottlenecked—prefer model scaling.
2. **Executor capacity check.** Verify that individual executors can generate plausible (though not necessarily correct) candidates. If single-agent pass@1 is near zero, coordination will not help—scale the backbone first. In our experiments, coordination benefits required executor pass@1  $\geq 20\%$  on reasoning benchmarks. This threshold (empirically calibrated from reasoning benchmarks; the effective threshold on interactive benchmarks was lower at  $\sim 15\%$ ) marks the regime below which mixer gradient signal becomes uninformative: when pass@1 is below  $\sim 20\%$ , each agent’s Q-value contribution to  $Q_{\text{tot}}$  (Eq. 18) falls below the noise floor, preventing meaningful coordination learning.
3. **Information asymmetry assessment.** Tasks with private information per agent (partial observability, role-specialized retrieval, tool-specific context) benefit most from DICE. Tasks where all agents see the same input benefit less. The largest gains (+22% on Hanabi, +31% on CollabEscape) occur under high information asymmetry.
4. **Cost tolerance.** DICE-PC incurs approximately  $4\times$  the token cost of single-model inference (with  $G=8$ ), comparable to standard best-of- $N$  sampling with  $N=4-8$  (see Appendix C.6 for the cost–accuracy trade-off at different group sizes). If this budget is acceptable, deploy DICE-PC first. If coordination-heavy tasks justify further investment, consider DICE-FT.
5. **Runtime monitoring.** Track the uniqueness margin  $\mu_k$  (when computable) or KL diagnostics ( $\widehat{\text{KL}}_{\text{old}}$ ,  $\widehat{\text{KL}}_{\text{ref}}$ ). If  $\mu_k$  remains negative past 50 iterations, reconsider the deployment regime. If  $\widehat{\text{KL}}_{\text{old}} > 0.05$  or  $\widehat{\text{KL}}_{\text{ref}} > 0.3$ , investigate stability before continuing training. These thresholds were calibrated across both Text-Hanabi and MATH-500; the observed maxima during stable training were  $\widehat{\text{KL}}_{\text{old}} < 0.02$  and  $\widehat{\text{KL}}_{\text{ref}} < 0.15$ , providing a  $\sim 2.5\times$  safety margin on both benchmarks.
6. **DICE-PC vs. DICE-FT selection.** Start with DICE-PC (no training required,  $\sim 4\times$  token cost). Upgrade to DICE-FT when: (a) DICE-PC gain exceeds 2 pp on reasoning

or 1 pp on interactive tasks, signaling actionable coordination; (b) training data or environment interaction is available; and (c) uniqueness margin  $\mu > 0$  with residual field-error budget indicating room for improvement beyond prompt-control saturation. In our experiments, DICE-FT provided +4.2 pp over DICE-PC on average, with the largest gains on high-asymmetry tasks (AIME24/25, Hanabi). The 2 pp threshold is empirically calibrated: it corresponds roughly to where the DICE-PC gain exceeds the residual approximation error from the field-error budget (Proposition 18).

## 7 Further Discussions

**Key differences from the conference version.** The conference version introduced ECON as a belief-driven coordinator–executor framework whose objective was to approximate an unregularized Bayesian Nash equilibrium (BNE). That formulation established BNE as a principled target for cooperative multi-agent LLM coordination. The present manuscript takes the next step: it shows that an unregularized BNE target is not yet a well-posed learning objective when several self-consistent equilibria coexist. In such cases, the issue is not BNE existence, but BNE selection. The game specifies that agents should be mutually optimal, but does not specify which coordination convention should be selected, whether that convention is unique, or whether learning will remain stable around it. This journal version identifies this selection gap and addresses it through entropy-regularized equilibrium selection. The main extensions are organized around three questions.

**Gap 1: Why is an unregularized BNE target not enough?** The conference version established BNE as a useful coordination target, but did not treat the set-valued nature of unregularized BNE as a central failure mode. Here we show that the problem is not the nonexistence of equilibria: under standard assumptions, a behavioral BNE exists. The problem is that existence alone does not determine which equilibrium learning will select. We formalize this selection gap in a discounted incomplete-information Markov game (IIMG) with private histories and a public stream, and show that equilibrium multiplicity and persistent mis-selection can induce linear Bayesian regret. Debate-style defensive mixing is then interpreted as a related selection-instability pathology: agents may converge, but to a mixed or defensive convention with a non-vanishing welfare gap.

**Gap 2: How can the BNE selection problem be resolved?** The conference objective targeted unregularized BNEs, whose best-response correspondence can be set-valued and whose equilibria can be multiple. This manuscript regularizes that target through HQRE, a heterogeneous entropy-regularized equilibrium concept. Entropy regularization is not used merely as an exploration bonus; it serves as an equilibrium-selection mechanism that turns set-valued best responses into a single-valued logit map. Under the monotonicity condition  $\alpha_{\min} > L_c$ , the selected HQRE is unique; under the stated field-Lipschitz and local KL-quadratic conditions, explicit KL-mirror updates converge linearly and yield Bayesian regret bounded uniformly in the horizon. The zero-temperature limit connects the new target back to the unregularized BNEs studied in the conference version.

**Gap 3: How can regularized equilibrium selection be implemented in LLM systems?** The conference algorithm instantiated BNE-guided coordination primarily as a prompt-control / decision-layer mechanism for frozen execution LLMs. We retain this practical regime as DICE-PC, but reinterpret it as finite-action HQRE logit response rather

than unregularized BNE approximation. We also introduce DICE-FT, a parameter-efficient fine-tuning realization based on clipped KL-prox mirror updates. To connect the exact HQRE theory to practical deep-learning optimization, we add an inexact mirror recurrence and a field-error decomposition covering clipping, sampling, representation, and optimization errors. Experimentally, the evaluation expands from the conference version’s six reasoning and planning benchmarks to eleven benchmarks across reasoning, planning, active information gathering, and multi-agent coordination, with additional uniqueness-margin, KL-stability, selection-vs-rollout, and communication-efficiency diagnostics.

**Discussions.** Our uniqueness guarantees rely on the monotonicity condition  $\alpha_{\min} > L_c$ , whose verification at frontier LLM scale remains open, and our experiments are concentrated in the 4B–32B regime. An important next step is therefore to develop tighter empirical estimates of coupling in realistic systems, adapt regularization and trust-region budgets online, and extend the framework to richer action spaces such as longer-horizon tool use, continuous control, and multimodal agents. More broadly, we view explicit equilibrium selection as a useful design principle for scalable multi-agent LLM: stronger coordination mechanisms can improve capability and reliability, but should be deployed together with monitoring and safety constraints so that desirable conventions remain stable under perturbation.

## 8 Conclusion

We introduced the discounted incomplete-information Markov game (IIMG) framework and the Heterogeneous Quantal Response Equilibrium (HQRE) as a principled lens for multi-agent LLM coordination, and instantiated this perspective in the DICE-PC and DICE-FT algorithms. Our central claim is that many failures of multi-agent LLM systems stem not only from limited information sharing, but from ill-posed equilibrium selection. By making the convention selection explicit, DICE improves the accuracy–cost–stability trade-off across eleven benchmarks and provides theory-grounded diagnostics for when decentralized coordination is likely to be stable or brittle.

## Acknowledgments and Disclosure of Funding

The authors declare no competing interests.

## References

- Saaket Agashe, Yue Fan, Anthony Reyna, and Xin Eric Wang. Evaluating multi-agent coordination abilities in large language models, 2023.
- Christopher Amato, George Konidaris, Leslie Pack Kaelbling, and Jonathan P. How. Modeling and planning with macro-actions in decentralized POMDPs. *Journal of Artificial Intelligence Research*, 64:817–859, 2019.
- Daniel S Bernstein, Robert Givan, Neil Immerman, and Shlomo Zilberstein. The complexity of decentralized control of markov decision processes. *Mathematics of operations research*, 2002.
- Mert Cemri, Melissa Z. Pan, Shuyi Yang, Lakshya A. Agrawal, Bhavya Chopra, Rishabh Tiwari, Kurt Keutzer, Aditya Parameswaran, Dan Klein, Kannan Ramchandran, Matei Zaharia, Joseph E. Gonzalez, and Ion Stoica. Why do multi-agent llm systems fail?, 2025. URL <https://arxiv.org/abs/2503.13657>.
- Chi-Min Chan, Weize Chen, Yusheng Su, Jianxuan Yu, Wei Xue, Shanghang Zhang, Jie Fu, and Zhiyuan Liu. Chateval: Towards better llm-based evaluators through multi-agent debate. In *ICLR*, 2024.
- Justin Chen, Swarnadeep Saha, and Mohit Bansal. Reconcile: Round-table conference improves reasoning via consensus among diverse llms. In *Proceedings of the 62nd Annual Meeting of the Association for Computational Linguistics (Volume 1: Long Papers)*, pages 7066–7085, 2024.
- Yew Ken Chia, Guizhen Chen, Luu Anh Tuan, Soujanya Poria, and Lidong Bing. Contrastive chain-of-thought prompting. *arXiv preprint arXiv:2311.09277*, 2023.
- Yilun Du, Shuang Li, Antonio Torralba, Joshua B. Tenenbaum, and Igor Mordatch. Improving factuality and reasoning in language models through multiagent debate, 2023. URL <https://arxiv.org/abs/2305.14325>.
- Yao Fu, Hao Peng, Ashish Sabharwal, Peter Clark, and Tushar Khot. Complexity-based prompting for multi-step reasoning. *arXiv preprint arXiv:2210.00720*, 2022.
- Eric Graves, Ehsan Imani, Raksha Kumaraswamy, and Martha White. Off-policy actor-critic with emphatic weightings. *Journal of Machine Learning Research*, 24(146):1–63, 2023.
- Sven Gronauer and Klaus Diepold. Multi-agent deep reinforcement learning: a survey. *Artificial Intelligence Review*, 55(2):895–943, 2022.
- Tuomas Haarnoja, Aurick Zhou, Pieter Abbeel, and Sergey Levine. Soft actor-critic: Off-policy maximum entropy deep reinforcement learning with a stochastic actor. In *International conference on machine learning*, pages 1861–1870. Pmlr, 2018.
- Dan Hendrycks, Collin Burns, Saurav Kadavath, Akul Arora, Steven Basart, Eric Tang, Dawn Song, and Jacob Steinhardt. Measuring mathematical problem solving with the math dataset. *arXiv preprint arXiv:2103.03874*, 2021.

- Sirui Hong, Mingchen Zhuge, Jonathan Chen, Xiawu Zheng, Yuheng Cheng, Jinlin Wang, Ceyao Zhang, Zili Wang, Steven Ka Shing Yau, Zijuan Lin, Liyang Zhou, Chenyu Ran, Lingfeng Xiao, Chenglin Wu, and Jürgen Schmidhuber. MetaGPT: Meta programming for a multi-agent collaborative framework. In *ICLR*, 2024. URL <https://openreview.net/forum?id=VtmBAGCN7o>.
- Yubin Kim, Ken Gu, Chanwoo Park, Chunjong Park, Samuel Schmidgall, A. Ali Heydari, Yao Yan, Zhihan Zhang, Yuchen Zhuang, Mark Malhotra, Paul Pu Liang, Hae Won Park, Yuzhe Yang, Xuhai Xu, Yilun Du, Shwetak Patel, Tim Althoff, Daniel McDuff, and Xin Liu. Towards a science of scaling agent systems, 2025. URL <https://arxiv.org/abs/2512.08296>.
- Takeshi Kojima, Shixiang Shane Gu, Machel Reid, Yutaka Matsuo, and Yusuke Iwasawa. Large language models are zero-shot reasoners. In *NeurIPS*, 2022.
- George Konidaris. Constructing abstraction hierarchies using a skill-symbol loop. In *International Joint Conference on Artificial Intelligence (IJCAI)*, pages 1648–1654, 2016.
- George Konidaris and Andrew Barto. Skill discovery in continuous reinforcement learning domains using skill chaining. In *Advances in Neural Information Processing Systems (NeurIPS)*, 2009.
- Xiaochong Lan, Chen Gao, Depeng Jin, and Yong Li. Stance detection with collaborative role-infused llm-based agents. In *ICWSM*, 2024.
- Marc Lanctot, Vinicius Zambaldi, Audrunas Gruslys, Angeliki Lazaridou, Karl Tuyls, Julien Pérolat, David Silver, and Thore Graepel. A unified game-theoretic approach to multiagent reinforcement learning. In *NeurIPS*, 2017.
- Sergey Levine. Reinforcement learning and control as probabilistic inference: Tutorial and review. *arXiv preprint arXiv:1805.00909*, 2018.
- Guohao Li, Hasan Abed Al Kader Hammoud, Hani Itani, Dmitrii Khizbullin, and Bernard Ghanem. Camel: Communicative agents for "mind" exploration of large language model society. In *Thirty-seventh Conference on Neural Information Processing Systems*, 2023a.
- Xuan Li, Zhanke Zhou, Jianing Zhu, Jiangchao Yao, Tongliang Liu, and Bo Han. Deepinception: Hypnotize large language model to be jailbreaker. *arXiv preprint arXiv:2311.03191*, 2023b.
- Bill Yuchen Lin, Ronan Le Bras, Kyle Richardson, Ashish Sabharwal, Radha Poovendran, Peter Clark, and Yejin Choi. ZebraLogic: On the scaling limits of llms for logical reasoning. *arXiv preprint arXiv:2502.01100*, 2025.
- Kaizhao Liu, Qi Long, Zhaoqi Shi, Weijie J. Su, and Jiancong Xiao. Statistical impossibility and possibility of aligning LLMs with human preferences: From Condorcet paradox to Nash equilibrium. *arXiv preprint arXiv:2503.10990*, 2024a.

- Tongxuan Liu, Xingyu Wang, Weizhe Huang, Wenjiang Xu, Yuting Zeng, Lei Jiang, Hailong Yang, and Jing Li. Groupdebate: Enhancing the efficiency of multi-agent debate using group discussion. *arXiv preprint arXiv:2409.14051*, 2024b.
- Ryan Lowe, Yi I Wu, Aviv Tamar, Jean Harb, OpenAI Pieter Abbeel, and Igor Mordatch. Multi-agent actor-critic for mixed cooperative-competitive environments. In *NeurIPS*, 2017.
- Pan Lu, Liang Qiu, Kai-Wei Chang, Ying Nian Wu, Song-Chun Zhu, Tanmay Rajpurohit, Peter Clark, and Ashwin Kalyan. Dynamic prompt learning via policy gradient for semi-structured mathematical reasoning. In *International Conference on Learning Representations (ICLR)*, 2023.
- Richard D McKelvey and Thomas R Palfrey. Quantal response equilibria for normal form games. *Games and economic behavior*, 10(1):6–38, 1995.
- Richard D McKelvey and Thomas R Palfrey. Quantal response equilibria for extensive form games. *Experimental economics*, 1(1):9–41, 1998.
- Arkadi Nemirovski, Anatoli Juditsky, Guanghui Lan, and Alexander Shapiro. Robust stochastic approximation approach to stochastic programming. *SIAM Journal on Optimization*, 2009.
- Tabish Rashid, Mikayel Samvelyan, Christian Schroeder De Witt, Gregory Farquhar, Jakob Foerster, and Shimon Whiteson. Monotonic value function factorisation for deep multi-agent reinforcement learning. *Journal of Machine Learning Research*, 21(178):1–51, 2020.
- J Ben Rosen. Existence and uniqueness of equilibrium points for concave n-person games. *Econometrica: Journal of the Econometric Society*, pages 520–534, 1965.
- Zhekun Shi, Kaizhao Liu, Qi Long, Weijie J. Su, and Jiancong Xiao. Fundamental limits of game-theoretic LLM alignment: Smith consistency and preference matching. *arXiv preprint arXiv:2505.20627*, 2025.
- Peter Sunehag, Guy Lever, Audrunas Gruslys, Wojciech Marian Czarnecki, Vinicius Zambaldi, Max Jaderberg, Marc Lanctot, Nicolas Sonnerat, Joel Z Leibo, Karl Tuyls, et al. Value-decomposition networks for cooperative multi-agent learning. *arXiv preprint arXiv:1706.05296*, 2017.
- Richard S Sutton and Andrew G Barto. *Reinforcement Learning: An Introduction*. MIT Press, 2018.
- Karthik Valmeekam, Matthew Marquez, Alberto Olmo, Sarath Sreedharan, and Subbarao Kambhampati. Planbench: An extensible benchmark for evaluating large language models on planning and reasoning about change. *Advances in Neural Information Processing Systems*, 36:38975–38987, 2023.
- Jianhao Wang, Zhizhou Ren, Terry Liu, Yang Yu, and Chongjie Zhang. Qplex: Duplex dueling multi-agent q-learning. *arXiv preprint arXiv:2008.01062*, 2020.

- Xuezhi Wang, Jason Wei, Dale Schuurmans, Quoc Le, Ed Chi, Sharan Narang, Aakanksha Chowdhery, and Denny Zhou. Self-consistency improves chain of thought reasoning in language models. In *ICLR*, 2023.
- Jason Wei, Xuezhi Wang, Dale Schuurmans, Maarten Bosma, Fei Xia, Ed Chi, Quoc V Le, Denny Zhou, et al. Chain-of-thought prompting elicits reasoning in large language models. In *NeurIPS*, 2022.
- Qingyun Wu, Gagan Bansal, Jieyu Zhang, Yiran Wu, Beibin Li, Erkang Zhu, Li Jiang, Xiaoyun Zhang, Shaokun Zhang, Jiale Liu, et al. Autogen: Enabling next-gen llm applications via multi-agent conversation. In *ICLR Workshop*, 2024.
- Chenjun Xiao, Han Wang, Yangchen Pan, Adam White, and Martha White. The in-sample softmax for offline reinforcement learning. In *International Conference on Learning Representations (ICLR)*, 2023.
- Yi Xie, Zhanke Zhou, Chentao Cao, Qiyu Niu, Tongliang Liu, and Bo Han. From debate to equilibrium: Belief-driven multi-agent llm reasoning via bayesian nash equilibrium. In *ICML*, 2025.
- Shunyu Yao, Dian Yu, Jeffrey Zhao, Izhak Shafran, Tom Griffiths, Yuan Cao, and Karthik Narasimhan. Tree of thoughts: Deliberate problem solving with large language models. In *NeurIPS*, 2023.
- Da Yin, Faeze Brahman, Abhilasha Ravichander, Khyathi Chandu, Kai-Wei Chang, Yejin Choi, and Bill Yuchen Lin. Agent Lumos: Unified and modular training for open-source language agents. In *Proceedings of the 62nd Annual Meeting of the Association for Computational Linguistics (ACL)*, pages 12380–12403, 2024.
- Zhangyue Yin, Qiushi Sun, Cheng Chang, Qipeng Guo, Junqi Dai, Xuan-Jing Huang, and Xipeng Qiu. Exchange-of-thought: Enhancing large language model capabilities through cross-model communication. In *EMNLP*, 2023.
- Siyu Yuan, Kaitao Song, Jiangjie Chen, Xu Tan, Dongsheng Li, and Deqing Yang. Evoagent: Towards automatic multi-agent generation via evolutionary algorithms. *arXiv preprint arXiv:2406.14228*, 2024.
- Zhuosheng Zhang, Aston Zhang, Mu Li, and Alex Smola. Automatic chain of thought prompting in large language models. In *ICLR*, 2023.
- Denny Zhou, Nathanael Schärli, Le Hou, Jason Wei, Nathan Scales, Xuezhi Wang, Dale Schuurmans, Claire Cui, Olivier Bousquet, Quoc Le, et al. Least-to-most prompting enables complex reasoning in large language models. *arXiv preprint arXiv:2205.10625*, 2022.
- Zhanke Zhou, Chentao Cao, Xiao Feng, Xuan Li, Zongze Li, Xiangyu Lu, Jiangchao Yao, Weikai Huang, Tian Cheng, Jianghangfan Zhang, Tangyu Jiang, Linrui Xu, Yiming Zheng, Brando Miranda, Tongliang Liu, Sanmi Koyejo, Masashi Sugiyama, and Bo Han. AlphaApollo: A system for deep agentic reasoning. *arXiv preprint arXiv:2510.06261*, 2025a.

Zhanke Zhou, Xiao Feng, Zhaocheng Zhu, Jiangchao Yao, Sanmi Koyejo, and Bo Han. From passive to active reasoning: Can large language models ask the right questions under incomplete information? *arXiv preprint arXiv:2506.08295*, 2025b.

Qin Zhu, Fei Huang, Runyu Peng, Keming Lu, Bowen Yu, Qinyuan Cheng, Xipeng Qiu, Xuanjing Huang, and Junyang Lin. Autologi: Automated generation of logic puzzles for evaluating reasoning abilities of large language models. *arXiv preprint arXiv:2502.16906*, 2025.

## Appendix

<b>A Preliminaries and proofs for Sec. 3</b>	<b>54</b>
A.1 Protocol embedding (Proof of Lem. 2)	54
A.2 Policy-space topology and payoff continuity (Proof of Thm. 3)	55
A.3 BNE existence (Proof of Thm. 4)	55
A.4 The joint-policy TV metric and product-TV	56
A.5 Occupancy sensitivity (proof of $C_{\text{occ}}$ )	56
A.6 Performance difference and TV sensitivity (Proof of Cor. 5)	57
A.7 Multiplicity can induce linear Bayesian regret (Proof of Prop. 6)	59
A.8 Debate-style dynamics and linear regret (Proofs for Sec. 3.4)	60
<b>B Regularized equilibrium and scalability proofs for Sec. 4</b>	<b>62</b>
B.1 Proof of Lem. 9 (regularization gap)	62
B.2 Weighted geometry: norm, Pinsker, and entropy curvature	62
B.3 $Q$ -sensitivity and a usable constant $C_Q$	63
B.4 Existence of HQRE (Proof of Thm. 10)	64
B.5 Uniqueness via contraction (Proof of Thm. 11)	64
B.6 Uniqueness via strong monotonicity and explicit KL-prox linear rate (Proof of Thm. 12)	65
B.7 Zero-temperature limit (Proof of Lem. 13)	68
B.8 Hierarchical definitions and composite KL geometry	69
B.9 Hierarchical existence (Proof of Thm. 15)	70
B.10 Hierarchical coupling bound (Proof of Prop. 16)	70
B.11 Hierarchical strong monotonicity and explicit KL-prox linear rate (Proof of Thm. 17)	71
<b>C Learning dynamics and mirror ascent for Sec. 5</b>	<b>71</b>
C.1 ELBO decomposition and best-response gaps (Prop. 42)	72
C.2 Soft-value factorization and weighted advantages	74
C.3 Monotone progress for KL-mirror steps (Thm. 46)	76
C.4 Linear convergence in KL geometry (Thm. 48)	77
C.5 Hierarchical mirror dynamics (Thm. 52)	80
C.6 Additional experiment results	80
C.7 Field-error budget: seed-level analysis	80
C.8 Algorithmic details deferred from Section 5	83
C.9 Proposition 18: proof sketch and empirical validation	84
C.10 Representation term: monotone-mixer transfer and architectural interpretation	85

## Appendix A. Preliminaries and proofs for Sec. 3

### A.1 Protocol embedding (Proof of Lem. 2)

**Proof** [Proof of Lem. 2] We give a constructive representation of any explicit-communication protocol (Def. 1) as a discounted IIMG.

**View the protocol as a controlled stochastic process.** An explicit-communication protocol specifies a joint process over

$$(y^t, \mathbf{o}^t, \mathbf{a}^t, \mathbf{r}^t)_{t \geq 0}, \quad \mathbf{r}^t = (r_1^t, \dots, r_N^t),$$

where each agent  $i$  selects  $a_i^t$  according to a behavioral policy  $\pi_i(\cdot | h_i^t, t)$  with information state  $h_i^t$  as in Def. 1, and  $y^t$  is the publicly observed stream token. All internal memory of the environment/coordinator/judge (if any) can be folded into a latent variable.

Formally, define an *augmented latent state*  $s^t$  to include: (i) any latent environment state needed to generate observations/rewards, (ii) any internal protocol memory (e.g., coordinator state, judge state), and (iii) the time index  $t$  (to absorb nonstationarity). W.l.o.g., we may take  $s^t$  to be the *full* internal state of the protocol at time  $t$ , so that given  $(s^t, \mathbf{a}^t)$  the distribution of  $(s^{t+1}, \mathbf{o}^{t+1}, \mathbf{r}^t, y^t)$  is well-defined and depends only on  $(s^t, \mathbf{a}^t)$ .

**Define the IIMG components.** We construct a discounted IIMG  $\langle \mathcal{N}, \mathcal{S}, \mathcal{A}, \mathcal{O}, \mathcal{Y}, \mathcal{P}, \Omega, G, (\phi_i)_i, \gamma, \mu_0 \rangle$  as follows:

- $\mathcal{N}$  is the same agent set as the protocol.
- $\mathcal{A}_i$  is the set of agent- $i$  actions in the protocol;  $\mathcal{A} = \prod_i \mathcal{A}_i$ .
- $\mathcal{Y}$  is the public-stream alphabet of the protocol. Since only realized public tokens matter, we may take  $\mathcal{Y} := \text{Im}(G) \subseteq \mathcal{Y}$  without loss.
- $\mathcal{O}_i$  is the private observation alphabet of the protocol;  $\mathcal{O} = \prod_i \mathcal{O}_i$ . Any private messages available only to agent  $i$  are included in  $o_i^t$  exactly as in Def. 1.
- $\mathcal{S}$  is the augmented latent-state space described above, with initial distribution  $\mu_0$  matching the protocol.
- The transition kernel  $\mathcal{P}(\cdot | s, \mathbf{a})$  is defined to match the protocol’s latent update: sample  $s^{t+1}$  according to the protocol’s internal dynamics given  $(s^t = s, \mathbf{a}^t = \mathbf{a})$ .
- The observation kernel  $\Omega(\cdot | s', \mathbf{a})$  outputs  $\mathbf{o}^{t+1}$  exactly as the protocol does given  $(s^{t+1} = s', \mathbf{a}^t = \mathbf{a})$ .
- The public-stream mapping  $G : \mathcal{A} \rightarrow \mathcal{Y}$  is defined so that  $y^t = G(\mathbf{a}^t)$  matches the protocol’s publicly observed token at time  $t$ .

*Remark.* If the protocol’s public token is generated by a publicly visible module (e.g., a coordinator or judge), that module can be modeled as one of the agents in  $\mathcal{N}$ ; then  $y^t$  is a deterministic function of joint actions. This matches the IIMG normal form used in Sec. 3.1.

- Finally, define the instantaneous reward functions by

$$R_i(s, \mathbf{a}) := \mathbb{E}[r_i^t | s^t = s, \mathbf{a}^t = \mathbf{a}], \quad \text{and set} \quad \phi_i(s, G(\mathbf{a})) := R_i(s, \mathbf{a}),$$

so that  $R_i(s^t, \mathbf{a}^t)$  matches the protocol’s stage reward in expectation. (If the protocol reward is deterministic given  $(s^t, \mathbf{a}^t)$ , then this equality holds pointwise.)

**Trajectory and return preservation.** Fix any joint behavioral policy profile  $\boldsymbol{\pi}$  in the protocol. By construction, under  $\boldsymbol{\pi}$  the IIMG generates the same conditional distributions at each time  $t$ : given  $(s^t, \mathbf{a}^t)$ , the next latent state, private observations, rewards, and the public stream token match those of the protocol. Therefore, the induced trajectory law over  $(s^t, y^t, \mathbf{o}^t, \mathbf{a}^t)_{t \geq 0}$  coincides with the protocol’s law. Since discounted returns are expectations of measurable functions of the trajectory, we have  $U_i^{\text{IIMG}}(\boldsymbol{\pi}) = U_i^{\text{protocol}}(\boldsymbol{\pi})$  for all  $i$ .

**Invariance of equilibrium notions and Bayesian regret.** The mapping from protocol policies to IIMG policies is identity at the level of behavioral strategies (both condition on the same information state  $h_i^t$ ), and payoffs coincide for every profile. Hence best responses, Nash/Bayesian Nash equilibrium conditions, and any welfare/regret functional built from  $U_i(\boldsymbol{\pi})$  (including Eq. (1)–Eq. (2)) are invariant under this embedding. ■

### A.2 Policy-space topology and payoff continuity (Proof of Thm. 3)

**Proof** [Proof sketch] Under (A1), each per-state simplex  $\Delta(\mathcal{A}_i)$  is compact and metrizable. Since the index set  $\mathcal{I}_i$  of information states is countable,  $\Pi_i = \prod_{(h_i^t, t) \in \mathcal{I}_i} \Delta(\mathcal{A}_i)$  is compact by Tychonoff’s theorem and metrizable by the standard weighted product metric (cf. Aliprantis & Border, *Infinite Dimensional Analysis*, Thm. 2.61). Convexity is immediate. For continuity: the truncated payoff  $U_i^{(\leq H)}$  depends on finitely many coordinates and is therefore continuous; bounded rewards (A2) give  $|U_i - U_i^{(\leq H)}| \leq \gamma^{H+1} R_{\max}/(1 - \gamma)$  uniformly over  $\Pi$ , so  $U_i$  is a uniform limit of continuous functions and hence continuous. ■

### A.3 BNE existence (Proof of Thm. 4)

**Proof** [Proof sketch] For each horizon  $H$ , the  $H$ -truncated game has finite action and information sets under (A1), hence admits a behavioral Nash equilibrium  $\boldsymbol{\pi}^{(H)}$  by Nash’s theorem and Kuhn’s theorem (perfect recall, (A4)). Extend each  $\boldsymbol{\pi}^{(H)}$  to  $\Pi$  by appending an arbitrary continuation. By compactness of  $\Pi$  (Thm. 3), extract a convergent subsequence  $\boldsymbol{\pi}^{(H_m)} \rightarrow \bar{\boldsymbol{\pi}}$ .

Suppose  $\bar{\boldsymbol{\pi}}$  is not a BNE: some agent  $i$  has a deviation with improvement  $\Delta > 0$ . By continuity of  $U_i$  (Thm. 3), this improvement transfers to  $\boldsymbol{\pi}^{(H_m)}$  for large  $m$ , and by the uniform tail bound  $|U_i - U_i^{(\leq H)}| \leq \gamma^{H+1} R_{\max}/(1 - \gamma)$  (A2), it transfers to the  $H_m$ -truncated payoff—contradicting the Nash property of  $\boldsymbol{\pi}^{(H_m)}$  in the truncated game. ■

#### A.4 The joint-policy TV metric and product-TV

**Lemma 19** (Metric property of  $\rho_\Pi$ ). *Let*

$$d_{(h^t, t)}(\boldsymbol{\pi}, \boldsymbol{\pi}') := \text{TV}\left(\bigotimes_{i=1}^N \pi_i(\cdot | h_i^t, t), \bigotimes_{i=1}^N \pi'_i(\cdot | h_i^t, t)\right),$$

and define  $\rho_\Pi(\boldsymbol{\pi}, \boldsymbol{\pi}') := \sup_{(h^t, t)} d_{(h^t, t)}(\boldsymbol{\pi}, \boldsymbol{\pi}')$ , where the supremum is taken over all syntactically valid joint histories  $h^t \in \prod_{i=1}^N \mathcal{H}_i^t$  (not only those reachable under a given policy profile). Then  $\rho_\Pi$  is a metric on  $\Pi$ .

**Proof** For each fixed  $(h^t, t)$ , total variation distance is a metric on probability distributions over  $\mathcal{A} = \prod_i \mathcal{A}_i$ . Taking a supremum preserves nonnegativity, symmetry, and the triangle inequality. If  $\rho_\Pi(\boldsymbol{\pi}, \boldsymbol{\pi}') = 0$ , then  $d_{(h^t, t)}(\boldsymbol{\pi}, \boldsymbol{\pi}') = 0$  for all  $(h^t, t)$ , so the joint product distributions coincide at every  $(h^t, t)$ . Taking the marginal on coordinate  $i$  yields  $\pi_i(\cdot | h_i^t, t) = \pi'_i(\cdot | h_i^t, t)$  for all  $(h_i^t, t)$ , hence  $\boldsymbol{\pi} = \boldsymbol{\pi}'$ . ■

**Lemma 20** (Product-TV bound). *For distributions  $\{p_i, q_i\}_{i=1}^N$  on finite alphabets,*

$$\text{TV}\left(\bigotimes_{i=1}^N p_i, \bigotimes_{i=1}^N q_i\right) \leq \sum_{i=1}^N \text{TV}(p_i, q_i).$$

**Proof** Write the difference of product measures as a telescoping sum:

$$\bigotimes_{i=1}^N p_i - \bigotimes_{i=1}^N q_i = \sum_{j=1}^N \left( \bigotimes_{i < j} q_i \right) \otimes (p_j - q_j) \otimes \left( \bigotimes_{i > j} p_i \right).$$

Using that  $\|\cdot\|_1$  is a norm on signed measures and  $\|r \otimes \nu\|_1 = \|r\|_1 \|\nu\|_1$  with  $\|\nu\|_1 = 1$  for probability measures, we obtain

$$\left\| \bigotimes_{i=1}^N p_i - \bigotimes_{i=1}^N q_i \right\|_1 \leq \sum_{j=1}^N \|p_j - q_j\|_1.$$

Since  $\text{TV}(p, q) = \frac{1}{2} \|p - q\|_1$ , dividing by 2 yields the claim. ■

#### A.5 Occupancy sensitivity (proof of $C_{\text{occ}}$ )

**Lemma 21** (Occupancy sensitivity). *Let  $\delta := \rho_\Pi(\boldsymbol{\pi}, \boldsymbol{\pi}')$ . Then the discounted state occupancy measures satisfy*

$$\|d^\boldsymbol{\pi} - d^{\boldsymbol{\pi}'}\|_1 \leq \frac{2\gamma}{1-\gamma} \delta.$$

**Proof** We construct a coupling of full trajectories under  $\boldsymbol{\pi}$  and  $\boldsymbol{\pi}'$  using maximal couplings at each step.

Let  $\tau = (s^0, o^0, \mathbf{a}^0, s^1, o^1, \mathbf{a}^1, \dots)$  be the trajectory under  $\pi$  and  $\tau' = (s'^0, o'^0, \mathbf{a}'^0, s'^1, o'^1, \mathbf{a}'^1, \dots)$  under  $\pi'$ . Couple the initial state as  $s^0 = s'^0$  a.s. since  $\mu_0$  is policy-independent (A2), and couple the initial private observations using the same kernel.

Inductively, suppose the coupled trajectories agree up to time  $t$  (i.e., the joint histories  $h^t$  and  $h'^t$  coincide). Then the joint action distributions at  $(h^t, t)$  satisfy

$$\text{TV}(\pi(\cdot | h^t, t), \pi'(\cdot | h^t, t)) \leq \delta.$$

By maximal coupling, we can sample  $(\mathbf{a}^t, \mathbf{a}'^t)$  such that  $\Pr(\mathbf{a}^t \neq \mathbf{a}'^t | h^t) = \text{TV}(\cdot, \cdot) \leq \delta$ . If  $\mathbf{a}^t = \mathbf{a}'^t$ , couple the next state and observations using the same randomness so that  $(s^{t+1}, o^{t+1}) = (s'^{t+1}, o'^{t+1})$  almost surely. If  $\mathbf{a}^t \neq \mathbf{a}'^t$ , let the two processes evolve arbitrarily thereafter.

Let  $E_t$  be the event that the coupled trajectories have not diverged up to time  $t$ . Then  $\Pr(E_0) = 1$  and

$$\Pr(E_{t+1}^c) \leq \Pr(E_t^c) + \Pr(E_t) \cdot \delta \leq \Pr(E_t^c) + \delta,$$

so by induction  $\Pr(E_t^c) \leq t\delta$ . Under any coupling,  $\text{TV}(\text{Law}(s^t), \text{Law}(s'^t)) \leq \Pr(s^t \neq s'^t) \leq \Pr(E_t^c)$ , hence  $\|\text{Law}(s^t) - \text{Law}(s'^t)\|_1 \leq 2t\delta$ .

Finally,

$$\|d^\pi - d^{\pi'}\|_1 = (1 - \gamma) \sum_{t \geq 0} \gamma^t \|\text{Law}(s^t) - \text{Law}(s'^t)\|_1 \leq (1 - \gamma) \sum_{t \geq 0} \gamma^t 2t\delta = 2\delta \cdot \frac{\gamma}{1 - \gamma}.$$

■

## A.6 Performance difference and TV sensitivity (Proof of Cor. 5)

**Lemma 22** (Performance difference). *For any joint policy  $\pi$ , define the history-action value functions*

$$Q_i^\pi(h^t, \mathbf{a}, t) := \mathbb{E} \left[ \sum_{u=t}^{\infty} \gamma^{u-t} R_i(s^u, \mathbf{a}^u) \mid h^t, \mathbf{a}^t \leftarrow \mathbf{a}, \pi \text{ thereafter} \right],$$

$$V_i^\pi(h^t, t) := \mathbb{E}_{\mathbf{a} \sim \pi(\cdot | h^t, t)} [Q_i^\pi(h^t, \mathbf{a}, t)].$$

Here  $\mathbf{a}^t \leftarrow \mathbf{a}$  denotes an intervention: at time  $t$  we force joint action  $\mathbf{a}$  and then follow  $\pi$  from time  $t+1$  onward. (This avoids conditioning on a potentially zero-probability event.) Let  $Q_{\text{tot}}^\pi := \sum_{i=1}^N Q_i^\pi$  and  $V_{\text{tot}}^\pi := \sum_{i=1}^N V_i^\pi$ . Then for any  $\pi', \pi \in \Pi$ ,

$$W(\pi') - W(\pi) = \frac{1}{1 - \gamma} \mathbb{E}_{(h^t, t) \sim \mathbf{H}_{\text{disc}}^{\pi'}} \left[ \mathbb{E}_{\mathbf{a} \sim \pi'(\cdot | h^t, t)} (Q_{\text{tot}}^\pi(h^t, \mathbf{a}, t) - V_{\text{tot}}^\pi(h^t, t)) \right].$$

**Proof** Define the (total) advantage of  $\pi$  at  $(h^t, t)$  for joint action  $\mathbf{a}$ :

$$A_{\text{tot}}^\pi(h^t, \mathbf{a}, t) := Q_{\text{tot}}^\pi(h^t, \mathbf{a}, t) - V_{\text{tot}}^\pi(h^t, t).$$

By the Bellman expectation equation under the intervention semantics,

$$Q_{\text{tot}}^\pi(h^t, \mathbf{a}, t) = \mathbb{E} \left[ R_{\text{tot}}(s^t, \mathbf{a}) \mid h^t \right] + \gamma \mathbb{E} \left[ V_{\text{tot}}^\pi(h^{t+1}, t+1) \mid h^t, \mathbf{a}^t \leftarrow \mathbf{a} \right],$$

where  $R_{\text{tot}} = \sum_i R_i$ . Therefore,

$$A_{\text{tot}}^\pi(h^t, \mathbf{a}, t) = \mathbb{E}[R_{\text{tot}}(s^t, \mathbf{a}) \mid h^t] + \gamma \mathbb{E}[V_{\text{tot}}^\pi(h^{t+1}, t+1) \mid h^t, \mathbf{a}^t \leftarrow \mathbf{a}] - V_{\text{tot}}^\pi(h^t, t).$$

Take expectation under trajectories induced by  $\pi'$  and sum over  $t \geq 0$ :

$$\mathbb{E}_{\pi'} \left[ \sum_{t=0}^{\infty} \gamma^t A_{\text{tot}}^\pi(h^t, \mathbf{a}^t, t) \right] = \mathbb{E}_{\pi'} \left[ \sum_{t=0}^{\infty} \gamma^t R_{\text{tot}}(s^t, \mathbf{a}^t) \right] - \mathbb{E}[V_{\text{tot}}^\pi(h^0, 0)],$$

where the telescoping uses

$$\sum_{t=0}^T \gamma^t (\gamma V_{\text{tot}}^\pi(h^{t+1}, t+1) - V_{\text{tot}}^\pi(h^t, t)) = -V_{\text{tot}}^\pi(h^0, 0) + \gamma^{T+1} V_{\text{tot}}^\pi(h^{T+1}, T+1),$$

and the boundary term vanishes as  $T \rightarrow \infty$  since  $|V_{\text{tot}}^\pi| \leq \frac{NR_{\text{max}}}{1-\gamma}$  implies  $\gamma^{T+1}|V_{\text{tot}}^\pi(h^{T+1}, T+1)| \rightarrow 0$ . The last equality holds because the distribution of  $h^0$  is policy-independent (A2), hence  $\mathbb{E}[V_{\text{tot}}^\pi(h^0, 0)] = W(\pi)$ . Thus

$$\mathbb{E}_{\pi'} \left[ \sum_{t=0}^{\infty} \gamma^t A_{\text{tot}}^\pi(h^t, \mathbf{a}^t, t) \right] = W(\pi') - W(\pi).$$

Finally, rewrite the discounted sum using the discounted history occupancy:

$$\mathbb{E}_{\pi'} \left[ \sum_{t=0}^{\infty} \gamma^t f(h^t, t) \right] = \frac{1}{1-\gamma} \mathbb{E}_{(h^t, t) \sim \mathbb{H}_{\text{disc}}^{\pi'}} [f(h^t, t)].$$

Apply this with  $f(h^t, t) = \mathbb{E}_{\mathbf{a} \sim \pi'(\cdot | h^t, t)} [A_{\text{tot}}^\pi(h^t, \mathbf{a}, t)]$  to obtain the stated identity.  $\blacksquare$

**Lemma 23** (Occupancy-averaged TV sensitivity). *For any agent  $i$  and any joint policies  $\pi, \pi^*$ ,*

$$|U_i(\pi^*) - U_i(\pi)| \leq \frac{2R_{\text{max}}}{(1-\gamma)^2} \mathbb{E}_{(h^t, t) \sim \mathbb{H}_{\text{disc}}^{\pi^*}} \left[ \text{TV}(\pi(\cdot | h^t, t), \pi^*(\cdot | h^t, t)) \right].$$

Consequently,

$$|W(\pi^*) - W(\pi)| \leq \frac{2NR_{\text{max}}}{(1-\gamma)^2} \mathbb{E}_{(h^t, t) \sim \mathbb{H}_{\text{disc}}^{\pi^*}} \left[ \text{TV}(\pi(\cdot | h^t, t), \pi^*(\cdot | h^t, t)) \right].$$

**Proof** Apply Lem. 22 to the single-agent payoff  $U_i$  (the same derivation holds with  $Q_i^\pi$  and  $V_i^\pi$ ):

$$U_i(\pi^*) - U_i(\pi) = \frac{1}{1-\gamma} \mathbb{E}_{(h^t, t) \sim \mathbb{H}_{\text{disc}}^{\pi^*}} \left[ \mathbb{E}_{\mathbf{a} \sim \pi^*(\cdot | h^t, t)} (Q_i^\pi(h^t, \mathbf{a}, t) - V_i^\pi(h^t, t)) \right].$$

Since  $V_i^\pi(h^t, t) = \mathbb{E}_{\mathbf{a} \sim \pi(\cdot | h^t, t)} [Q_i^\pi(h^t, \mathbf{a}, t)]$ , the inner term equals

$$\mathbb{E}_{\mathbf{a} \sim \pi^*(\cdot | h^t, t)} [Q_i^\pi(h^t, \mathbf{a}, t)] - \mathbb{E}_{\mathbf{a} \sim \pi(\cdot | h^t, t)} [Q_i^\pi(h^t, \mathbf{a}, t)].$$

For any bounded function  $f$  and distributions  $p, q$ ,  $|\mathbb{E}_p[f] - \mathbb{E}_q[f]| \leq 2\|f\|_\infty \text{TV}(p, q)$ . With  $f(\mathbf{a}) = Q_i^\pi(h^t, \mathbf{a}, t)$  and  $\|Q_i^\pi\|_\infty \leq R_{\max}/(1 - \gamma)$ , we obtain

$$|U_i(\boldsymbol{\pi}^*) - U_i(\boldsymbol{\pi})| \leq \frac{1}{1 - \gamma} \mathbb{E}_{(h^t, t) \sim \mathbf{H}_{\text{disc}}^{\boldsymbol{\pi}^*}} \left[ 2 \cdot \frac{R_{\max}}{1 - \gamma} \text{TV}(\boldsymbol{\pi}(\cdot | h^t, t), \boldsymbol{\pi}^*(\cdot | h^t, t)) \right],$$

which yields the stated bound. Summing over  $i$  gives the welfare bound.  $\blacksquare$

**Proof** [Proof of Cor. 5] By Lem. 23, for each learning iteration  $k$ ,

$$W(\boldsymbol{\pi}^*) - W(\boldsymbol{\pi}^k) \leq |W(\boldsymbol{\pi}^*) - W(\boldsymbol{\pi}^k)| \leq \frac{2NR_{\max}}{(1 - \gamma)^2} \bar{\Delta}_k,$$

where  $\bar{\Delta}_k$  is defined in Sec. 3.2. Taking expectation and summing over  $k = 1, \dots, T$  yields

$$\text{Regret}(T) \leq \frac{2NR_{\max}}{(1 - \gamma)^2} \sum_{k=1}^T \mathbb{E}[\bar{\Delta}_k].$$

If  $\mathbb{E}[\bar{\Delta}_k] \leq C_\Delta k^{-\alpha}$ , then

$$\text{Regret}(T) \leq \frac{2NR_{\max}C_\Delta}{(1 - \gamma)^2} \sum_{k=1}^T k^{-\alpha}.$$

For  $\alpha = \frac{1}{2}$ , using  $\sum_{k=1}^T k^{-1/2} \leq 2\sqrt{T}$  gives  $\text{Regret}(T) = O(\frac{N\sqrt{T}}{(1-\gamma)^2})$ .  $\blacksquare$

## A.7 Multiplicity can induce linear Bayesian regret (Proof of Prop. 6)

**Proof** [Proof of Prop. 6] By definition,

$$\text{Regret}(T) = \mathbb{E} \left[ \sum_{k=1}^T (W(\boldsymbol{\pi}^{(1)}) - W(\boldsymbol{\pi}^k)) \right] = \sum_{k=1}^T \mathbb{E}[W(\boldsymbol{\pi}^{(1)}) - W(\boldsymbol{\pi}^k)].$$

Since  $\boldsymbol{\pi}^k \in \{\boldsymbol{\pi}^{(1)}, \boldsymbol{\pi}^{(2)}\}$  for all  $k$ , we have  $W(\boldsymbol{\pi}^{(1)}) - W(\boldsymbol{\pi}^k) = 0$  if  $\boldsymbol{\pi}^k = \boldsymbol{\pi}^{(1)}$ , and  $W(\boldsymbol{\pi}^{(1)}) - W(\boldsymbol{\pi}^k) = \Delta_W$  if  $\boldsymbol{\pi}^k = \boldsymbol{\pi}^{(2)}$ . Therefore, for all  $k \geq k_0$ ,

$$\mathbb{E}[W(\boldsymbol{\pi}^{(1)}) - W(\boldsymbol{\pi}^k)] = \Pr(\boldsymbol{\pi}^k = \boldsymbol{\pi}^{(2)}) \Delta_W \geq p_0 \Delta_W.$$

Summing over  $k = k_0, \dots, T$  yields

$$\text{Regret}(T) \geq \sum_{k=k_0}^T p_0 \Delta_W = p_0 \Delta_W (T - k_0 + 1) = \Omega(\Delta_W T). \quad \blacksquare$$

## A.8 Debate-style dynamics and linear regret (Proofs for Sec. 3.4)

### A.8.1 PERSISTENT SUBOPTIMALITY UNDER DEFENSIVE MIXING (PROOF OF LEM. 7)

We formalize a sufficient condition under which defensive mixing induces a persistent one-step advantage gap. The statement is deliberately worst-case: it isolates the mechanism (full-support mixing + nondegenerate gaps) and does not require the debate game to be zero-sum.

**Modeling note.** In this subsection, each learning iteration  $k$  corresponds to a *single debate instance* (one-shot stage), with public instance/state  $s_k$  (e.g., prompt/context) and joint action  $\mathbf{a}^k = (a_i^k, a_{-i}^k)$ . Accordingly,  $\pi_i^k(\cdot | s_k)$  is a mixed action (possibly depending on the public instance).

We interpret  $Q_i^*(s, a_i, a_{-i})$  as the *true* one-step action-value in the debate instance (equivalently the expected immediate payoff/score), with  $\star$  indicating that this is evaluated under the fixed reference environment defining the regret comparator (cf. Cor. 8).

**Assumption 24** (Nondegenerate action-value gaps). *There exist constants  $\Delta_{\text{gap}} > 0$  and  $q_{\text{gap}} > 0$ , and an iteration  $k_0$ , such that for all  $k \geq k_0$ ,*

$$\Pr \left( \max_{a_i} Q_i^*(s_k, a_i, a_{-i}^k) - \min_{a_i} Q_i^*(s_k, a_i, a_{-i}^k) \geq \Delta_{\text{gap}} \right) \geq q_{\text{gap}}.$$

**Assumption 25** (Persistent mixing). *There exist  $p_{\min} > 0$  and an iteration  $k_0$  such that for all  $k \geq k_0$  and all debate instances  $s_k$ ,*

$$\pi_i^k(a_i | s_k) \geq p_{\min} \quad \forall a_i \in \mathcal{A}_i,$$

*i.e., the learner maintains full support with a uniform lower bound (e.g., due to entropy regularization or forced exploration).*

**Proof** [Proof of Lem. 7] Fix  $k \geq k_0$  and condition on  $(s_k, a_{-i}^k)$ . Let

$$M_k := \max_{a_i} Q_i^*(s_k, a_i, a_{-i}^k).$$

Then, with  $a_i^k \sim \pi_i^k(\cdot | s_k)$ ,

$$\mathbb{E} \left[ M_k - Q_i^*(s_k, a_i^k, a_{-i}^k) \mid s_k, a_{-i}^k \right] = M_k - \sum_{a_i} \pi_i^k(a_i | s_k) Q_i^*(s_k, a_i, a_{-i}^k).$$

On the event in Assumption 24, there exists an action  $a_i^-$  such that  $Q_i^*(s_k, a_i^-, a_{-i}^k) \leq M_k - \Delta_{\text{gap}}$ . By Assumption 25,  $\pi_i^k(a_i^- | s_k) \geq p_{\min}$ , hence

$$\sum_{a_i} \pi_i^k(a_i | s_k) Q_i^*(s_k, a_i, a_{-i}^k) \leq (1 - p_{\min}) \cdot M_k + p_{\min} \cdot (M_k - \Delta_{\text{gap}}) = M_k - p_{\min} \Delta_{\text{gap}}.$$

Therefore,

$$\mathbb{E} \left[ M_k - Q_i^*(s_k, a_i^k, a_{-i}^k) \mid s_k, a_{-i}^k \right] \geq p_{\min} \Delta_{\text{gap}} \quad \text{on the nondegenerate-gap event.}$$

Taking expectation over  $(s_k, a_{-i}^k)$  yields

$$\mathbb{E} \left[ \max_{a_i} Q_i^*(s_k, a_i, a_{-i}^k) - Q_i^*(s_k, a_i^k, a_{-i}^k) \right] \geq p_{\min} \Delta_{\text{gap}} \cdot q_{\text{gap}}.$$

Setting  $\delta_{\min} := p_{\min} \Delta_{\text{gap}} q_{\text{gap}} > 0$  concludes the proof.  $\blacksquare$

## A.8.2 LINEAR BAYESIAN REGRET FOR MAD (PROOF OF COR. 8)

The lemma above lower-bounds an *ex-post* advantage gap. To translate it into the welfare-based Bayesian regret in Eq. (2), we require a fixed comparator policy profile and a welfare objective aligned with the gap.

**Assumption 26** (Stationary opponents after burn-in). *There exists  $k_0$  and a fixed opponent policy  $\pi_{-i}^*$  such that for all  $k \geq k_0$ , the opponent action  $a_{-i}^k$  is distributed according to  $\pi_{-i}^*(\cdot | s_k)$ . Equivalently,  $\pi_{-i}^k \equiv \pi_{-i}^*$  for all  $k \geq k_0$  on the debate instances.*

**Assumption 27** (Welfare alignment for the regret comparator). *The welfare functional used in Eq. (2) is aligned with agent  $i$ 's payoff in the debate instances: there exists a constant  $\kappa > 0$  such that for any two profiles that differ only in agent  $i$  (with opponents fixed),*

$$W(\pi'_i, \pi_{-i}^*) - W(\pi_i, \pi_{-i}^*) \geq \kappa \cdot (U_i(\pi'_i, \pi_{-i}^*) - U_i(\pi_i, \pi_{-i}^*)).$$

A sufficient special case is a team/common-payoff debate objective where all agents share the same reward, in which case  $\kappa = N$ .

**Assumption 28** (A fixed comparator attains the per-instance maximizer). *There exists a (possibly state-dependent) policy  $\pi_i^*(\cdot | s)$  such that for every debate instance  $s$  and every opponent action  $a_{-i}$  in the support of  $\pi_{-i}^*(\cdot | s)$ ,*

$$\mathbb{E}_{a_i \sim \pi_i^*(\cdot | s)}[Q_i^*(s, a_i, a_{-i})] = \max_{a_i} Q_i^*(s, a_i, a_{-i}).$$

In particular, this holds if there exists a measurable selector  $a_i^*(s)$  that is a maximizer for all such  $a_{-i}$ , and  $\pi_i^*(\cdot | s)$  is the point mass at  $a_i^*(s)$ .

**Proof** [Proof of Cor. 8] Let  $\boldsymbol{\pi}^* := (\pi_i^*, \pi_{-i}^*)$  be the fixed comparator profile from Assumptions 26–28. By Assumption 28 and the definition of  $Q_i^*$ , for all  $k \geq k_0$ ,

$$U_i(\boldsymbol{\pi}^*) - U_i(\boldsymbol{\pi}^k) \geq \mathbb{E} \left[ \max_{a_i} Q_i^*(s_k, a_i, a_{-i}^k) - Q_i^*(s_k, a_i^k, a_{-i}^k) \right].$$

By Lem. 7, the right-hand side is at least  $\delta_{\min} > 0$  for all  $k \geq k_0$ . Applying Assumption 27 yields

$$W(\boldsymbol{\pi}^*) - W(\boldsymbol{\pi}^k) \geq \kappa \cdot (U_i(\boldsymbol{\pi}^*) - U_i(\boldsymbol{\pi}^k)) \geq \kappa \delta_{\min} \quad \forall k \geq k_0.$$

Finally, under standard  $O(1/\sqrt{k})$  estimation errors, there exists  $k_1$  such that for all  $k \geq k_1$  the additional loss attributable to estimation error is at most  $\kappa \delta_{\min}/2$ . (Equivalently, after  $k_1$  the policy is accurate enough that the persistent loss is dominated by the enforced mixing, not by estimation error.) Hence for all  $k \geq k_\star := \max\{k_0, k_1\}$ ,

$$W(\boldsymbol{\pi}^*) - W(\boldsymbol{\pi}^k) \geq \frac{\kappa \delta_{\min}}{2} =: c > 0.$$

Therefore, for all  $T \geq k_\star$ ,

$$\text{Regret}_{\text{MAD}}(T) = \mathbb{E} \left[ \sum_{k=1}^T (W(\boldsymbol{\pi}^*) - W(\boldsymbol{\pi}^k)) \right] \geq \sum_{k=k_\star}^T c = \Omega(T).$$

■

## Appendix B. Regularized equilibrium and scalability proofs for Sec. 4

### B.1 Proof of Lem. 9 (regularization gap)

**Proof** [Proof of Lem. 9] Fix any joint policy  $\boldsymbol{\pi} \in \Pi$  and agent  $i$ . By definition,

$$J_i^\alpha(\boldsymbol{\pi}) - U_i(\boldsymbol{\pi}) = \mathbb{E}_\pi \left[ \sum_{t \geq 0} \gamma^t \alpha_{i,t}(h_i^t) \mathcal{H}(\pi_i(\cdot | h_i^t, t)) \right].$$

Since  $\alpha_{i,t}(h_i^t) \geq 0$  and  $\mathcal{H}(\cdot) \geq 0$ , the difference is nonnegative. Moreover,  $\alpha_{i,t}(h_i^t) \leq \alpha_{\max}$  and for any distribution on a finite alphabet,  $\mathcal{H}(\pi_i(\cdot | h_i^t, t)) \leq \log |\mathcal{A}_i|$ , hence

$$J_i^\alpha(\boldsymbol{\pi}) - U_i(\boldsymbol{\pi}) \leq \sum_{t \geq 0} \gamma^t \alpha_{\max} \log |\mathcal{A}_i| = \frac{\alpha_{\max} \log |\mathcal{A}_i|}{1 - \gamma}.$$

Summing the inequality over  $i = 1, \dots, N$  yields the claimed bound for  $\sum_i J_i^\alpha(\boldsymbol{\pi}) - W(\boldsymbol{\pi})$ .  $\blacksquare$

### B.2 Weighted geometry: norm, Pinsker, and entropy curvature

**Lemma 29** (Weighted block norm is a norm). *Assume weights  $w_i(h_i^t, t) > 0$  for all  $(i, h_i^t, t)$  and  $\sum_{(h_i^t, t)} w_i(h_i^t, t) = 1$  for each  $i$ . Then*

$$\|\boldsymbol{\pi} - \boldsymbol{\pi}'\|_{1,2;w} = \left( \sum_i \sum_{(h_i^t, t)} w_i(h_i^t, t) \|\pi_i(\cdot | h_i^t, t) - \pi'_i(\cdot | h_i^t, t)\|_1^2 \right)^{1/2}$$

is a norm on  $\Pi$ .

**Proof** Nonnegativity and homogeneity are immediate. If  $\|\boldsymbol{\pi} - \boldsymbol{\pi}'\|_{1,2;w} = 0$ , then every summand is zero, hence  $\pi_i(\cdot | h_i^t, t) = \pi'_i(\cdot | h_i^t, t)$  for all  $(i, h_i^t, t)$ , so  $\boldsymbol{\pi} = \boldsymbol{\pi}'$ . For the triangle inequality, let  $x_{i,u} := \|\pi_i(\cdot | u) - \pi'_i(\cdot | u)\|_1$  with  $u = (h_i^t, t)$ . Then  $\|\boldsymbol{\pi} - \boldsymbol{\pi}'\|_{1,2;w}$  is the  $\ell_2$ -norm (with weights) of the block vector  $(x_{i,u})$ , and Minkowski's inequality yields the triangle inequality.  $\blacksquare$

**Lemma 30** (Sup-to-block control). *If  $w_i(h_i^t, t) \geq w_{\min} > 0$  and  $\sum_{(h_i^t, t)} w_i(h_i^t, t) = 1$ , then for each fixed  $i$ ,*

$$\sup_{(h_i^t, t)} \|\pi_i(\cdot | h_i^t, t) - \pi'_i(\cdot | h_i^t, t)\|_1 \leq w_{\min}^{-1/2} \|\pi_i - \pi'_i\|_{1,2;w}.$$

**Proof** Let  $x_u := \|\pi_i(\cdot | u) - \pi'_i(\cdot | u)\|_1$  with  $u = (h_i^t, t)$ . Then  $\sum_u w_i(u) x_u^2 \geq w_{\min} \sup_u x_u^2$ , hence  $\sup_u x_u \leq w_{\min}^{-1/2} (\sum_u w_i(u) x_u^2)^{1/2}$ .  $\blacksquare$

**Lemma 31** (Weighted Pinsker). *For distributions  $p, q$  on a finite alphabet and any  $\alpha > 0$ ,*

$$\alpha \text{KL}(p\|q) \geq \frac{\alpha}{2} \|p - q\|_1^2,$$

*with the convention that  $\text{KL}(p\|q) = +\infty$  if  $q(a) = 0$  for some  $a$  with  $p(a) > 0$  (in which case the inequality is trivial). Hence if  $\alpha_{i,t}(h) \geq \alpha_{\min} > 0$ ,*

$$D_{\Psi}(\boldsymbol{\pi}, \boldsymbol{\pi}') = \sum_{i,t,h} \alpha_{i,t}(h) w_i(h,t) \text{KL}(\pi_i\|\pi'_i) \geq \frac{\alpha_{\min}}{2} \|\boldsymbol{\pi} - \boldsymbol{\pi}'\|_{1,2;w}^2.$$

**Proof** Pinsker's inequality states  $\text{TV}(p, q)^2 \leq \frac{1}{2} \text{KL}(p\|q)$ . Since  $\text{TV}(p, q) = \frac{1}{2} \|p - q\|_1$ , we obtain  $\text{KL}(p\|q) \geq \frac{1}{2} \|p - q\|_1^2$ . Multiplying by  $\alpha$  yields the scalar inequality. Summing with nonnegative weights  $\alpha_{i,t}(h) w_i(h, t) \geq \alpha_{\min} w_i(h, t)$  gives the stated bound for  $D_{\Psi}$ . ■

**Lemma 32** (Two-sided entropy curvature). *Let  $p, q$  be distributions on a finite alphabet. If  $p, q$  have full support (i.e. lie in the relative interior of the simplex), then*

$$\langle \nabla(-\mathcal{H})(p) - \nabla(-\mathcal{H})(q), p - q \rangle = \text{KL}(p\|q) + \text{KL}(q\|p) \geq \|p - q\|_1^2.$$

*In general (allowing zeros), the inequality  $\text{KL}(p\|q) + \text{KL}(q\|p) \geq \|p - q\|_1^2$  remains valid (with  $+\infty$  interpreted in the usual way). Consequently,*

$$\sum_{i,t,h} \alpha_{i,t}(h) w_i(h,t) (\text{KL}(\pi_i\|\pi'_i) + \text{KL}(\pi'_i\|\pi_i)) \geq \alpha_{\min} \|\boldsymbol{\pi} - \boldsymbol{\pi}'\|_{1,2;w}^2.$$

**Proof** For full-support  $p, q$ ,  $\nabla(-\mathcal{H})(p) = \log p + \mathbf{1}$  and the Bregman identity gives  $\langle \nabla(-\mathcal{H})(p) - \nabla(-\mathcal{H})(q), p - q \rangle = \text{KL}(p\|q) + \text{KL}(q\|p)$ . Applying Pinsker to both  $\text{KL}(p\|q)$  and  $\text{KL}(q\|p)$  yields  $\text{KL}(p\|q) + \text{KL}(q\|p) \geq \|p - q\|_1^2$ . When zeros occur, at least one KL term may be  $+\infty$ , so the inequality still holds. Summing with weights  $\alpha_{i,t}(h) w_i(h, t) \geq \alpha_{\min} w_i(h, t)$  gives the stated bound. ■

### B.3 $Q$ -sensitivity and a usable constant $C_Q$

**Lemma 33** ( $Q$ -sensitivity w.r.t. policy). *For all  $i \in \mathcal{N}$  and joint policies  $\boldsymbol{\pi}, \tilde{\boldsymbol{\pi}}$ ,*

$$\|Q_i^{\boldsymbol{\pi}} - Q_i^{\tilde{\boldsymbol{\pi}}}\|_{\infty} := \sup_{(h_i^t, t), a_i} |Q_i^{\boldsymbol{\pi}}(h_i^t, a_i, t) - Q_i^{\tilde{\boldsymbol{\pi}}}(h_i^t, a_i, t)| \leq C_Q \rho_{\Pi}(\boldsymbol{\pi}, \tilde{\boldsymbol{\pi}}), \quad C_Q := \frac{2R_{\max}}{(1 - \gamma)^2}.$$

**Proof** Let  $\delta := \rho_{\Pi}(\boldsymbol{\pi}, \tilde{\boldsymbol{\pi}})$ . Fix  $(i, h_i^t, t, a_i)$ . Couple two future trajectories starting from the same time- $t$  joint configuration consistent with  $h_i^t$  and taking the same prescribed  $a_i$  for agent  $i$  at time  $t$ . Thereafter, couple the joint action draws step-by-step using maximal couplings of the joint action distributions induced by  $\boldsymbol{\pi}$  and  $\tilde{\boldsymbol{\pi}}$ . By definition of  $d_{\Pi}$ , at every step the probability that the coupled joint actions differ is at most  $\delta$ .

Let  $A_m$  be the event that at the  $m$ -th future step (i.e. time  $t+m$ ) the coupled joint actions differ. Then  $\Pr(A_m) \leq \delta$  for all  $m \geq 0$ . Let  $E_m := \bigcup_{j=0}^m A_j$  be the event that a disagreement has occurred at or before step  $m$ . By a union bound,  $\Pr(E_m) \leq \sum_{j=0}^m \Pr(A_j) \leq (m+1)\delta$ .

If no disagreement has occurred up to step  $m$ , then the coupled trajectories have identical states and joint actions at that step, hence identical rewards. Since rewards are bounded by  $R_{\max}$  in absolute value, the step- $m$  reward expectation difference is at most

$$|\mathbb{E}[r_{t+m}] - \mathbb{E}[\tilde{r}_{t+m}]| \leq 2R_{\max} \Pr(E_m) \leq 2R_{\max}(m+1)\delta.$$

Therefore,

$$|Q_i^\pi(h_i^t, a_i, t) - Q_i^{\tilde{\pi}}(h_i^t, a_i, t)| \leq \sum_{m=0}^{\infty} \gamma^m \cdot 2R_{\max}(m+1)\delta = 2R_{\max}\delta \sum_{m=0}^{\infty} (m+1)\gamma^m = \frac{2R_{\max}}{(1-\gamma)^2} \delta.$$

Taking the supremum over  $(h_i^t, t), a_i$  yields the claim.  $\blacksquare$

#### B.4 Existence of HQRE (Proof of Thm. 10)

**Lemma 34** (Logit map: well-definedness and continuity). *Assume  $\alpha_{\min} > 0$ . For any joint policy  $\pi$  and any  $(i, h_i^t, t)$ , the logit map  $\mathcal{B}_i^\alpha(\pi)(\cdot | h_i^t, t)$  in Eq. (5) is a well-defined probability distribution on  $\mathcal{A}_i$ . Moreover, as a function of  $\pi$ , each  $\mathcal{B}_i^\alpha$  is continuous, and hence the joint logit map  $\mathcal{B}^\alpha : \Pi \rightarrow \Pi$  is continuous on  $\Pi$ .*

**Proof** Fix  $(i, h_i^t, t)$ . Since  $\alpha_{i,t}(h_i^t) \geq \alpha_{\min} > 0$  and  $\mathcal{A}_i$  is finite, the denominator in Eq. (5) is finite and strictly positive, so  $\mathcal{B}_i^\alpha(\pi)(\cdot | h_i^t, t)$  is a valid distribution.

For continuity, Lemma 33 implies that  $Q_i^\pi(h_i^t, \cdot, t)$  is Lipschitz (hence continuous) in  $\pi$  under  $\rho_\Pi$ . For fixed  $\alpha_{i,t}(h_i^t) > 0$ , the softmax map is smooth on  $\mathbb{R}^{|\mathcal{A}_i|}$ . Composition yields continuity of each coordinate map  $\mathcal{B}_i^\alpha$ , and therefore of  $\mathcal{B}^\alpha$  under the product topology on  $\Pi$ .  $\blacksquare$

**Proof** [Proof of Thm. 10] By Thm. 3,  $\Pi$  is nonempty, convex, compact, and metrizable. By Lemma 34, the joint logit map  $\mathcal{B}^\alpha : \Pi \rightarrow \Pi$  is continuous. Schauder's fixed-point theorem therefore yields a fixed point of  $\mathcal{B}^\alpha$  in  $\Pi$ , which is an HQRE by definition.  $\blacksquare$

#### B.5 Uniqueness via contraction (Proof of Thm. 11)

**Lemma 35** (Logit is TV-Lipschitz in  $Q$ ). *Fix  $(i, h_i^t, t)$  and  $\alpha := \alpha_{i,t}(h_i^t) > 0$ . For any  $x, y \in \mathbb{R}^{|\mathcal{A}_i|}$ ,*

$$\text{TV}(\text{softmax}(x/\alpha), \text{softmax}(y/\alpha)) \leq \frac{1}{2\alpha} \|x - y\|_\infty.$$

**Proof** Let  $p = \text{softmax}(x/\alpha)$ ,  $q = \text{softmax}(y/\alpha)$ , and  $\phi(\theta) = \text{softmax}((y + \theta(x - y))/\alpha)$  for  $\theta \in [0, 1]$ . Then

$$\|p - q\|_1 \leq \sup_{\theta \in [0,1]} \|J_\phi(\theta)\|_{\infty \rightarrow 1} \|x - y\|_\infty,$$

where the Jacobian of  $\text{softmax}(\cdot/\alpha)$  at a probability vector  $r$  is  $J(r) = \frac{1}{\alpha}(\text{Diag}(r) - rr^\top)$ . It suffices to show  $\|\text{Diag}(r) - rr^\top\|_{\infty \rightarrow 1} \leq 1$  for all  $r$ . The  $\|\cdot\|_{\infty \rightarrow 1}$  norm is attained on

$v \in \{-1, 1\}^d$ . Let  $S = \{j : v_j = 1\}$  and  $p_S = \sum_{j \in S} r_j$  so that  $\mu = \sum_j r_j v_j = 2p_S - 1$ . Then

$$\|(\text{Diag}(r) - rr^\top)v\|_1 = \sum_j r_j |v_j - \mu| = 4p_S(1 - p_S) \leq 1.$$

Thus  $\|p - q\|_1 \leq \frac{1}{\alpha} \|x - y\|_\infty$ , and dividing by 2 yields the TV bound.  $\blacksquare$

**Proof** [Proof of Thm. 11] Fix  $\pi, \tilde{\pi} \in \Pi$  and any joint history  $(h^t, t)$ . Write  $p_i := \mathcal{B}_i^\alpha(\pi)(\cdot | h_i^t, t)$  and  $\tilde{p}_i := \mathcal{B}_i^\alpha(\tilde{\pi})(\cdot | h_i^t, t)$ . Lemma 35 and  $\alpha_{i,t}(h_i^t) \geq \alpha_{\min}$  give

$$\text{TV}(p_i, \tilde{p}_i) \leq \frac{1}{2\alpha_{\min}} \|Q_i^\pi(h_i^t, \cdot, t) - Q_i^{\tilde{\pi}}(h_i^t, \cdot, t)\|_\infty.$$

By Lemma 33, the  $Q$ -difference is bounded by  $C_Q \rho_\Pi(\pi, \tilde{\pi})$ , hence

$$\text{TV}(p_i, \tilde{p}_i) \leq \frac{C_Q}{2\alpha_{\min}} \rho_\Pi(\pi, \tilde{\pi}).$$

Applying the product-TV inequality (Lemma 20 in the Sec. 2 Appendix) yields

$$\text{TV}\left(\bigotimes_i p_i, \bigotimes_i \tilde{p}_i\right) \leq \sum_i \text{TV}(p_i, \tilde{p}_i) \leq \frac{NC_Q}{2\alpha_{\min}} \rho_\Pi(\pi, \tilde{\pi}).$$

Taking the supremum over  $(h^t, t)$  gives

$$\rho_\Pi(\mathcal{B}^\alpha(\pi), \mathcal{B}^\alpha(\tilde{\pi})) \leq \frac{NC_Q}{2\alpha_{\min}} \rho_\Pi(\pi, \tilde{\pi}),$$

which is the claimed Lipschitz bound.

If  $\alpha_{\min} > \frac{NC_Q}{2}$ , the constant is strictly less than 1, so  $\mathcal{B}^\alpha$  is a contraction on the complete metric space  $(\Pi, \rho_\Pi)$ . Banach's fixed-point theorem implies existence of a unique fixed point (the unique HQRE) and geometric convergence of the synchronous iteration  $\pi^{k+1} = \mathcal{B}^\alpha(\pi^k)$ .  $\blacksquare$

## B.6 Uniqueness via strong monotonicity and explicit KL-prox linear rate (Proof of Thm. 12)

**Coupling constant.** We restate the hypomonotonicity condition used in the main text:  $L_c$  is any constant such that

$$-\sum_{i=1}^N \langle \nabla_{\pi_i} U_i(\pi) - \nabla_{\pi_i} U_i(\pi'), \pi_i - \pi'_i \rangle \geq -L_c \|\pi - \pi'\|_{1,2;w}^2 \quad \forall \pi, \pi' \in \Pi. \quad (23)$$

**A conservative computable upper bound (optional).** The inequality Eq. (23) is an *assumption/definition* for  $L_c$ . When the index set  $(h_i^t, t)$  is finite (e.g. under finite-horizon truncation or a finite information-state reduction) and weights have a uniform lower bound  $w_{\min} > 0$ , one can obtain an explicit conservative bound purely from  $Q$ -sensitivity.

**Proposition 36** (A crude computable bound for  $L_c$ ). *Assume  $w_i(h_i^t, t) \geq w_{\min} > 0$  and that for each agent  $i$  the index set  $\{(h_i^t, t)\}$  is finite. Assume further that the unregularized field satisfies the componentwise sensitivity*

$$\sup_{i, (h_i^t, t)} \|\nabla_{\pi_i} U_i(\boldsymbol{\pi}) - \nabla_{\pi_i} U_i(\boldsymbol{\pi}')\|_{\infty} \leq \|Q_i^{\boldsymbol{\pi}} - Q_i^{\boldsymbol{\pi}'}\|_{\infty} \quad (24)$$

(which holds in the standard agent-form / behavioral-gradient representation in finite spaces). Then a sufficient choice is

$$L_c \leq \frac{N}{2\sqrt{w_{\min}}} C_Q = \frac{N}{2\sqrt{w_{\min}}} \cdot \frac{2R_{\max}}{(1-\gamma)^2}.$$

**Proof** Fix  $\boldsymbol{\pi}, \boldsymbol{\pi}' \in \Pi$ . By Hölder (blockwise  $\ell_{\infty}$ - $\ell_1$ ) and Cauchy–Schwarz in the outer weighted  $\ell_2$  structure,

$$\begin{aligned} & \sum_{i=1}^N |\langle \nabla_{\pi_i} U_i(\boldsymbol{\pi}) - \nabla_{\pi_i} U_i(\boldsymbol{\pi}'), \pi_i - \pi'_i \rangle| \\ & \leq \sum_{i=1}^N \sum_{(h_i^t, t)} w_i(h_i^t, t) \|\nabla_{\pi_i} U_i(\boldsymbol{\pi}) - \nabla_{\pi_i} U_i(\boldsymbol{\pi}')\|_{\infty} \|\pi_i - \pi'_i\|_1 \\ & \leq \left( \sup_{i, (h_i^t, t)} \|\nabla_{\pi_i} U_i(\boldsymbol{\pi}) - \nabla_{\pi_i} U_i(\boldsymbol{\pi}')\|_{\infty} \right) \sum_{i=1}^N \sum_{(h_i^t, t)} w_i(h_i^t, t) \|\pi_i - \pi'_i\|_1 \\ & \leq \left( \sup_{i, (h_i^t, t)} \|\nabla_{\pi_i} U_i(\boldsymbol{\pi}) - \nabla_{\pi_i} U_i(\boldsymbol{\pi}')\|_{\infty} \right) \sum_{i=1}^N \left( \sum_{(h_i^t, t)} w_i(h_i^t, t) \|\pi_i - \pi'_i\|_1^2 \right)^{1/2} \\ & \leq \left( \sup_{i, (h_i^t, t)} \|\nabla_{\pi_i} U_i(\boldsymbol{\pi}) - \nabla_{\pi_i} U_i(\boldsymbol{\pi}')\|_{\infty} \right) \sqrt{N} \|\boldsymbol{\pi} - \boldsymbol{\pi}'\|_{1,2;w}. \end{aligned}$$

Next, Lemma 30 implies  $\sup_{(h_i^t, t)} \|\pi_i - \pi'_i\|_1 \leq w_{\min}^{-1/2} \|\pi_i - \pi'_i\|_{1,2;w}$ , hence

$$\rho_{\Pi}(\boldsymbol{\pi}, \boldsymbol{\pi}') \leq \frac{1}{2} \sum_{i=1}^N \sup_{(h_i^t, t)} \|\pi_i - \pi'_i\|_1 \leq \frac{1}{2\sqrt{w_{\min}}} \sum_{i=1}^N \|\pi_i - \pi'_i\|_{1,2;w} \leq \frac{\sqrt{N}}{2\sqrt{w_{\min}}} \|\boldsymbol{\pi} - \boldsymbol{\pi}'\|_{1,2;w}.$$

Combining with Eq. (24) and Lemma 33 yields

$$\sup_{i, (h_i^t, t)} \|\nabla_{\pi_i} U_i(\boldsymbol{\pi}) - \nabla_{\pi_i} U_i(\boldsymbol{\pi}')\|_{\infty} \leq \|Q_i^{\boldsymbol{\pi}} - Q_i^{\boldsymbol{\pi}'}\|_{\infty} \leq C_Q \rho_{\Pi}(\boldsymbol{\pi}, \boldsymbol{\pi}') \leq \frac{C_Q \sqrt{N}}{2\sqrt{w_{\min}}} \|\boldsymbol{\pi} - \boldsymbol{\pi}'\|_{1,2;w}.$$

Substituting into the first bound gives

$$\sum_{i=1}^N |\langle \nabla_{\pi_i} U_i(\boldsymbol{\pi}) - \nabla_{\pi_i} U_i(\boldsymbol{\pi}'), \pi_i - \pi'_i \rangle| \leq \frac{C_Q N}{2\sqrt{w_{\min}}} \|\boldsymbol{\pi} - \boldsymbol{\pi}'\|_{1,2;w}^2,$$

which implies Eq. (23) holds with  $L_c = \frac{C_Q N}{2\sqrt{w_{\min}}}$ . ■

**HQRE as a VI solution (standard in regularized games).** For completeness we record the usual variational-inequality characterization.

**Lemma 37** (HQRE  $\Leftrightarrow$  VI solution). *Assume each  $J_i^\alpha(\cdot, \boldsymbol{\pi}_{-i})$  is concave in  $\pi_i$  on  $\Pi_i$  and differentiable, and that  $\alpha_{\min} > 0$  so the regularized best response is single-valued. Then  $\boldsymbol{\pi}^*$  is an HQRE (fixed point of  $\mathcal{B}^\alpha$ ) if and only if it solves the VI:*

$$\text{find } \boldsymbol{\pi}^* \in \Pi \text{ s.t. } \langle F_{\text{reg}}(\boldsymbol{\pi}^*), \boldsymbol{\pi} - \boldsymbol{\pi}^* \rangle \geq 0, \quad \forall \boldsymbol{\pi} \in \Pi,$$

where  $F_{\text{reg}}(\boldsymbol{\pi}) = (-\nabla_{\pi_1} J_1^\alpha(\boldsymbol{\pi}), \dots, -\nabla_{\pi_N} J_N^\alpha(\boldsymbol{\pi}))$ .

**Proof** For concave differentiable games, a profile is a Nash equilibrium if and only if each player satisfies the first-order optimality condition  $\langle -\nabla_{\pi_i} J_i^\alpha(\boldsymbol{\pi}^*), \pi_i - \pi_i^* \rangle \geq 0$  for all  $\pi_i \in \Pi_i$ . Summing over  $i$  yields the stated VI condition. With  $\alpha_{\min} > 0$ , each regularized best response is unique and is exactly the logit map  $\mathcal{B}_i^\alpha$ , so Nash equilibrium is equivalent to the fixed-point condition defining HQRE.  $\blacksquare$

**Proof** [Proof of Thm. 12] Recall  $F_{\text{reg}}(\boldsymbol{\pi}) = (-\nabla_{\pi_1} J_1^\alpha(\boldsymbol{\pi}), \dots, -\nabla_{\pi_N} J_N^\alpha(\boldsymbol{\pi}))$ . Decompose each regularized payoff as  $J_i^\alpha = U_i + \text{Ent}_{i,\alpha}$ , where

$$\text{Ent}_{i,\alpha}(\boldsymbol{\pi}) = \mathbb{E}_{\boldsymbol{\pi}} \left[ \sum_{t \geq 0} \gamma^t \alpha_{i,t} (h_i^t) \mathcal{H}(\pi_i(\cdot | h_i^t, t)) \right].$$

For the monotonicity calculation we only need the pointwise curvature of the negative-entropy term in each simplex component; this is captured by Lemma 32 and does not require any additional smoothness.

**Step 1: unregularized part is  $L_c$ -hypomonotone.** By definition of  $L_c$  (Eq. (23)),

$$-\sum_{i=1}^N \langle \nabla_{\pi_i} U_i(\boldsymbol{\pi}) - \nabla_{\pi_i} U_i(\boldsymbol{\pi}'), \pi_i - \pi_i' \rangle \geq -L_c \|\boldsymbol{\pi} - \boldsymbol{\pi}'\|_{1,2;w}^2.$$

**Step 2: entropy curvature contributes at least  $\alpha_{\min}$ .** For every coordinate simplex (each  $(i, h_i^t, t)$ ), the negative entropy has two-sided curvature  $\text{KL}(\pi_i \| \pi_i') + \text{KL}(\pi_i' \| \pi_i) \geq \|\pi_i - \pi_i'\|_1^2$  (Lemma 32). Summing across coordinates with weights  $\alpha_{i,t} (h_i^t) w_i(h_i^t, t) \geq \alpha_{\min} w_i(h_i^t, t)$  yields

$$-\sum_{i=1}^N \langle \nabla_{\pi_i} \text{Ent}_{i,\alpha}(\boldsymbol{\pi}) - \nabla_{\pi_i} \text{Ent}_{i,\alpha}(\boldsymbol{\pi}'), \pi_i - \pi_i' \rangle \geq \alpha_{\min} \|\boldsymbol{\pi} - \boldsymbol{\pi}'\|_{1,2;w}^2.$$

**Step 3: combine.** Adding the two bounds gives

$$\langle F_{\text{reg}}(\boldsymbol{\pi}) - F_{\text{reg}}(\boldsymbol{\pi}'), \boldsymbol{\pi} - \boldsymbol{\pi}' \rangle \geq (\alpha_{\min} - L_c) \|\boldsymbol{\pi} - \boldsymbol{\pi}'\|_{1,2;w}^2,$$

which is exactly the strong monotonicity claim.

If  $\alpha_{\min} > L_c$ , then  $F_{\text{reg}}$  is strongly monotone on  $\Pi$  and the VI solution is unique. By Lemma 37, this unique VI solution is exactly the unique HQRE.

**Linear convergence of explicit mirror steps.** Let  $\mu := \alpha_{\min} - L_c > 0$ . Under the additional field-Lipschitz and local-quadratic assumptions stated in Theorem 12, the linear-rate claim follows by applying Appendix Theorem 48 with  $F = F_{\text{reg}}$ . This yields

$$D_{\Psi}(\boldsymbol{\pi}^*, \boldsymbol{\pi}^{k+1}) \leq \rho D_{\Psi}(\boldsymbol{\pi}^*, \boldsymbol{\pi}^k), \quad \rho = 1 - \eta \frac{\mu}{L_{\Psi}},$$

for

$$0 < \eta \leq \min \left\{ \frac{\mu \alpha_{\min}^2}{L_F^2 L_{\Psi}}, \frac{\alpha_{\min}}{L_F} \right\}.$$

This is the exact rate quoted in Theorem 12. ■

### B.7 Zero-temperature limit (Proof of Lem. 13)

We first record two standard auxiliary inequalities that make the proof fully explicit.

**Lemma 38** (Log-sum-exp (softmax) optimality gap). *Let  $x \in \mathbb{R}^d$  and  $\alpha > 0$ , and let  $p = \text{softmax}(x/\alpha) \in \Delta^d$ . Then for any  $q \in \Delta^d$ ,*

$$\langle q, x \rangle - \langle p, x \rangle \leq \alpha \log d.$$

**Proof** The softmax distribution  $p$  is the unique maximizer of  $\langle r, x \rangle + \alpha \mathcal{H}(r)$  over  $r \in \Delta^d$ . Thus for any  $q$ ,

$$\langle q, x \rangle + \alpha \mathcal{H}(q) \leq \langle p, x \rangle + \alpha \mathcal{H}(p).$$

Rearranging and using  $\mathcal{H}(p) \leq \log d$  and  $\mathcal{H}(q) \geq 0$  yields  $\langle q, x \rangle - \langle p, x \rangle \leq \alpha \log d$ . ■

**Lemma 39** (Discounted performance difference (one-player deviation)). *Fix  $i$  and joint policies  $\boldsymbol{\pi} = (\pi_i, \boldsymbol{\pi}_{-i})$  and  $\tilde{\boldsymbol{\pi}} = (\tilde{\pi}_i, \boldsymbol{\pi}_{-i})$ . Then*

$$U_i(\tilde{\pi}_i, \boldsymbol{\pi}_{-i}) - U_i(\boldsymbol{\pi}) = \frac{1}{1 - \gamma} \mathbb{E}_{(h_i^t, t) \sim H_{\text{disc}}^{\tilde{\pi}_i, \boldsymbol{\pi}_{-i}}} \left[ \langle \tilde{\pi}_i(\cdot | h_i^t, t) - \pi_i(\cdot | h_i^t, t), Q_i^{\boldsymbol{\pi}}(h_i^t, \cdot, t) \rangle \right].$$

**Proof** This is the standard discounted performance-difference identity obtained by unrolling  $U_i$  along the discounted visitation distribution of  $(\tilde{\pi}_i, \boldsymbol{\pi}_{-i})$  and expressing the per-step advantage in terms of  $Q_i^{\boldsymbol{\pi}}$ . A proof for finite spaces follows by conditioning on  $(h_i^t, t)$ , writing the one-step deviation advantage at  $(h_i^t, t)$ , and summing the resulting telescoping series under the geometric discount. ■

**Proof** [Proof of Lem. 13] By Thm. 3,  $\Pi$  is compact, so  $\{\boldsymbol{\pi}^{(n)}\}$  admits a convergent subsequence (not relabeled) with limit  $\tilde{\boldsymbol{\pi}}$ .

Fix  $i \in \mathcal{N}$  and any deviation  $\tilde{\pi}_i \in \Pi_i$ . Because  $\boldsymbol{\pi}^{(n)}$  is an HQRE, for every information state  $(h_i^t, t)$  we have

$$\pi_i^{(n)}(\cdot | h_i^t, t) = \text{softmax} \left( Q_i^{\boldsymbol{\pi}^{(n)}}(h_i^t, \cdot, t) / \alpha_{i,t}^{(n)}(h_i^t) \right).$$

Apply Lemma 38 with  $x(a) = Q_i^{\pi^{(n)}}(h_i^t, a, t)$ ,  $\alpha = \alpha_{i,t}^{(n)}(h_i^t)$  and  $q = \tilde{\pi}_i(\cdot | h_i^t, t)$  to obtain, for all  $(h_i^t, t)$ ,

$$\langle \tilde{\pi}_i(\cdot | h_i^t, t) - \pi_i^{(n)}(\cdot | h_i^t, t), Q_i^{\pi^{(n)}}(h_i^t, \cdot, t) \rangle \leq \alpha_{i,t}^{(n)}(h_i^t) \log |\mathcal{A}_i| \leq \alpha_{\max}^{(n)} \log |\mathcal{A}_i|.$$

Using the performance difference Lemma 39 with  $\pi = \pi^{(n)}$  gives

$$U_i(\tilde{\pi}_i, \pi_{-i}^{(n)}) - U_i(\pi^{(n)}) \leq \frac{1}{1-\gamma} \alpha_{\max}^{(n)} \log |\mathcal{A}_i|.$$

Since  $\alpha_{\max}^{(n)} \downarrow 0$ , the right-hand side vanishes. Taking lim sup along the convergent subsequence and using continuity of  $U_i$  (Thm. 3) yields

$$U_i(\tilde{\pi}_i, \bar{\pi}_{-i}) - U_i(\bar{\pi}) \leq 0.$$

Because  $\tilde{\pi}_i$  was arbitrary,  $\bar{\pi}_i$  is a best response to  $\bar{\pi}_{-i}$  for every  $i$ , i.e.,  $\bar{\pi}$  is a BNE of the unregularized game.  $\blacksquare$

## B.8 Hierarchical definitions and composite KL geometry

We make the Local–Global HQRE construction explicit and fix notation to match the main text ( $z$  is the public context).

**Spaces.** Let  $\Pi_{C_k} = \prod_{i \in C_k} \Pi_i$  and  $\Pi_{\text{clu}} = \prod_{k=1}^K \Pi_{C_k}$ . Let  $\mathcal{G} = \prod_{z \in \mathcal{Z}} \Delta^K$  denote the gate space. Under (A1)–(A2),  $\Pi_{\text{clu}}$  and  $\mathcal{G}$  are compact, convex, and metrizable (finite/countable products of simplices).

**Gate objective and softmax update.** Given  $\pi$ , define the context-conditional cluster score

$$\tilde{Q}_{\text{loc},c}^{\pi}(z) := \mathbb{E}_{t \sim \text{Geom}(1-\gamma)} \mathbb{E}_{\mathbf{a}_{C_c} \sim \pi_{C_c}(\cdot | z, t)} [\bar{Q}_{\text{loc},c}(z, \mathbf{a}_{C_c}, t)],$$

where  $\bar{Q}_{\text{loc},c}$  is as in Eq. (12). For each  $z$ , the gate solves the strictly concave problem

$$\max_{g(z) \in \Delta^K} \sum_{c=1}^K g_c(z) \tilde{Q}_{\text{loc},c}^{\pi}(z) + \tau_g \mathcal{H}(g(\cdot | z)).$$

Its unique maximizer is

$$g_c^*(z) \propto \exp(\tilde{Q}_{\text{loc},c}^{\pi}(z)/\tau_g),$$

and the map  $\pi \mapsto g^*$  is continuous as a composition of continuous maps.

**Composite divergence and norm.** Define the composite KL divergence

$$D_{\Psi}^{\text{hier}}((\pi, g), (\pi', g')) := D_{\Psi}(\pi, \pi') + \tau_g \sum_{z \in \mathcal{Z}} \text{KL}(g(\cdot | z) \| g'(\cdot | z)).$$

Define the associated composite  $\ell_{1,2}$ -type norm

$$\|(\pi, g) - (\pi', g')\|_{\text{hier}}^2 := \|\pi - \pi'\|_{1,2;w}^2 + \sum_{z \in \mathcal{Z}} \|g(\cdot | z) - g'(\cdot | z)\|_1^2.$$

By Lemma 31 (for  $\pi$ ) and Pinsker for the gate component,

$$D_{\Psi}^{\text{hier}}((\pi, g), (\pi', g')) \geq \frac{\min\{\alpha_{\min}, \tau_g\}}{2} \|(\pi, g) - (\pi', g')\|_{\text{hier}}^2. \quad (25)$$

### B.9 Hierarchical existence (Proof of Thm. 15)

**Proof** [Proof of Thm. 15] Under (A1)–(A2), the space  $\Pi_{\text{clu}} \times \mathcal{G}$  is nonempty, convex, compact, and metrizable. Assume  $\alpha_{\min} > 0$  and  $\tau_g > 0$ .

For execution agents, define the block logit map on  $\Pi_{\text{clu}}$  as the product of the per-agent logit responses Eq. (5); by Lemma 34 it is continuous and maps  $\Pi_{\text{clu}}$  to itself. For the gate, Appendix B.8 shows that for each  $\boldsymbol{\pi}$  the best-response gate  $g^*(\boldsymbol{\pi})$  is single-valued and continuous.

Define the joint map

$$\mathcal{T}(\boldsymbol{\pi}, g) := (\mathcal{B}^\alpha(\boldsymbol{\pi}), g^*(\boldsymbol{\pi})), \quad (\boldsymbol{\pi}, g) \in \Pi_{\text{clu}} \times \mathcal{G}.$$

Then  $\mathcal{T}$  is continuous and maps the compact convex set  $\Pi_{\text{clu}} \times \mathcal{G}$  to itself. By Schauder’s fixed-point theorem,  $\mathcal{T}$  has a fixed point  $(\boldsymbol{\pi}^*, g^*)$ , which is by definition a Local–Global HQRE.  $\blacksquare$

### B.10 Hierarchical coupling bound (Proof of Prop. 16)

We restate the explicit sufficient assumptions under which the bound in Prop. 16 follows.

**Assumption 40** (Bounded local weights). *There exists  $W_{\max}^{\text{loc}}$  such that for all clusters  $c$  and contexts  $z$ ,  $\sum_{i \in C_c} |w_i^{(c)}(z)| \leq W_{\max}^{\text{loc}}$ .*

**Assumption 41** (Distributional Lipschitzness). *There exist constants  $L_g^{\text{dist}}$  and  $L_w^{\text{dist}}$  such that, for any two induced context occupancies  $d^\pi, d^{\pi'}$ ,*

$$\sum_{z \in \mathcal{Z}} \|g_\pi^*(\cdot | z) - g_{\pi'}^*(\cdot | z)\|_1 \leq L_g^{\text{dist}} \|d^\pi - d^{\pi'}\|_1,$$

and

$$\sum_{z \in \mathcal{Z}} \sum_{c=1}^K \sum_{i \in C_c} |w_i^{(c)}(z; d^\pi) - w_i^{(c)}(z; d^{\pi'})| \leq L_w^{\text{dist}} \|d^\pi - d^{\pi'}\|_1.$$

**Proof** [Proof of Prop. 16] By Lemma 33, the state-/context-conditional values  $\bar{Q}_i^\pi(z, a_i, t)$  are Lipschitz in  $\boldsymbol{\pi}$  with constant  $C_Q$ . By Assumption 40, the local mixtures Eq. (12) inherit the bound

$$\sup_{z, t, \mathbf{a}_{C_c}} |\bar{Q}_{\text{loc}, c}^\pi(z, \mathbf{a}_{C_c}, t) - \bar{Q}_{\text{loc}, c}^{\pi'}(z, \mathbf{a}_{C_c}, t)| \leq W_{\max}^{\text{loc}} C_Q \rho_\Pi(\boldsymbol{\pi}, \boldsymbol{\pi}').$$

Next, changes in the induced occupancy can be controlled by occupancy sensitivity (Lemma 21 in the Sec. 2 Appendix):

$$\|d^\pi - d^{\pi'}\|_1 \leq C_{\text{occ}} \rho_\Pi(\boldsymbol{\pi}, \boldsymbol{\pi}').$$

Combining with Assumption 41 and bounded rewards yields additional cross-block variation terms of size  $C_{\text{occ}}(W_{\max}^{\text{loc}} L_g^{\text{dist}} R_{\max} + L_w^{\text{dist}} R_{\max}) \rho_\Pi(\boldsymbol{\pi}, \boldsymbol{\pi}')$ . Collecting the direct  $Q$ -sensitivity term and the distributional terms yields

$$L_{\text{hier}} \leq W_{\max}^{\text{loc}} C_Q + C_{\text{occ}}(W_{\max}^{\text{loc}} L_g^{\text{dist}} R_{\max} + L_w^{\text{dist}} R_{\max}),$$

as stated.  $\blacksquare$

### B.11 Hierarchical strong monotonicity and explicit KL-prox linear rate (Proof of Thm. 17)

**Proof** [Proof of Thm. 17] Let the hierarchical variable be  $\mathbf{z} = (\boldsymbol{\pi}, g) \in \Pi_{\text{clu}} \times \mathcal{G}$  and use the composite divergence  $D_{\Psi}^{\text{hier}}$  from Appendix B.8. The hierarchical field combines the execution-field  $F_{\text{reg}}(\boldsymbol{\pi})$  and the gate-field induced by the strictly concave per-context gate objective. The gate field inherits strong monotonicity margin  $\mu_g = \tau_g$  by the same negative-entropy curvature argument as Lemma 32 (applied on each simplex  $\Delta^K$ ).

Within each cluster, the same argument as in Thm. 12 gives strong monotonicity margin  $\mu_c = \alpha_{\min} - L_c^{(c)}$  for block  $c$ . Cross-block coupling contributes at most  $L_{\text{hier}}$  in the composite geometry (Prop. 16). Therefore, for all  $\mathbf{z}, \mathbf{z}'$ ,

$$\langle F_{\text{hier}}(\mathbf{z}) - F_{\text{hier}}(\mathbf{z}'), \mathbf{z} - \mathbf{z}' \rangle \geq \left( \min_c (\alpha_{\min} - L_c^{(c)}) + \tau_g - L_{\text{hier}} \right) \|\mathbf{z} - \mathbf{z}'\|_{\text{hier}}^2 = \mu_{\text{hier}} \|\mathbf{z} - \mathbf{z}'\|_{\text{hier}}^2,$$

i.e.,  $F_{\text{hier}}$  is  $\mu_{\text{hier}}$ -strongly monotone when  $\mu_{\text{hier}} > 0$ . This implies uniqueness of the solution to the hierarchical VI, hence uniqueness of the Local-Global HQRE.

**Linear convergence of explicit hierarchical mirror steps.** Under the hierarchical Lipschitz and local-quadratic assumptions stated in Theorem 17, the linear-rate claim follows from Appendix Theorem 52 applied to the composite field  $F_{\text{hier}}$  and composite KL divergence  $D_{\Psi}^{\text{hier}}$ . This yields

$$D_{\Psi}^{\text{hier}}(\mathbf{z}^*, \mathbf{z}^{k+1}) \leq \left( 1 - \eta \frac{\mu_{\text{hier}}}{L_{\Psi}^{\text{hier}}} \right) D_{\Psi}^{\text{hier}}(\mathbf{z}^*, \mathbf{z}^k),$$

for sufficiently small  $\eta$ . ■

## Appendix C. Learning dynamics and mirror ascent for Sec. 5

This appendix collects proofs for the learning-dynamics results summarized in Table 15: the ELBO / best-response-gap equivalence (Prop. 42), monotone progress of KL-mirror steps (Thm. 46), linear convergence of KL-mirror dynamics in the strongly monotone regime (Thm. 48), and their hierarchical counterparts (Thm. 52). We also prove the soft-value factorization and weighted-advantage identities (Prop. 44, Lem. 45) used in Sec. 5.3.

**Local discounted occupancy over information states.** For a joint policy  $\boldsymbol{\pi}$ , define the discounted occupancy measure on player  $i$ 's information states  $\mathcal{I}_i = \{(h_i^t, t)\}$  by

$$\mathbf{H}_{i,\text{disc}}^{\boldsymbol{\pi}}(h_i^t, t) := (1 - \gamma)\gamma^t \Pr_{\boldsymbol{\pi}}(h_i^t),$$

i.e.,  $\mathbf{H}_{i,\text{disc}}^{\boldsymbol{\pi}}$  is the marginal of the joint discounted history occupancy  $\mathbf{H}_{\text{disc}}^{\boldsymbol{\pi}}$  on the  $i$ -th coordinate. Thus, for any bounded  $f$  on  $\mathcal{I}_i$ ,

$$\sum_{t \geq 0} \gamma^t \mathbb{E}_{\boldsymbol{\pi}}[f(h_i^t, t)] = (1 - \gamma)^{-1} \mathbb{E}_{(h_i^t, t) \sim \mathbf{H}_{i,\text{disc}}^{\boldsymbol{\pi}}} [f(h_i^t, t)].$$

Table 15: Summary of the main theoretical results. Each row lists the guarantee, its formal statement, and where the proof appears. Constants:  $C_Q \leq \frac{(2-\gamma)R_{\max}}{(1-\gamma)^2}$ ;  $L_c$  is defined in Eq. (23) with computable bounds in Prop. 36; the joint-policy metric is  $\rho_\Pi$  from Eq. (3).

Result	Statement	Proof
<i>Existence and convergence (unregularized BNE)</i>		
Policy-space foundation	$\Pi$ compact/metrisable; each $U_i$ continuous	App. A.2 / Thm. 3
BNE existence	Behavioral BNE exists	App. A.3 / Thm. 4
Welfare regret bound	$R(T) := \sum_{k=1}^T (W(\pi^*) - W(\pi^k)) \leq \frac{2NR_{\max}}{(1-\gamma)^2} \sum_{k=1}^T \bar{\Delta}_k$	App. A.6 / Cor. 5
<i>Regularized equilibria (HQRE)</i>		
HQRE existence	Fixed point of the joint logit map exists	App. B.4 / Thm. 10
Uniqueness (contraction)	Unique HQRE; rate $\kappa = \frac{NC_Q}{2\alpha_{\min}}$	App. B.5 / Thm. 11
Uniqueness (strong monotonicity)	Unique HQRE via VI for $F_{\text{reg}}$	App. B.6 / Thm. 12
Zero-temperature limit	HQRE( $\alpha^{(n)}$ ) $\rightarrow$ BNE (accumulation points)	App. B.7 / Lem. 13
<i>Learning dynamics</i>		
ELBO / BR-gap identity	Regularized BR gap equals discounted $\alpha$ -weighted KL to logit BR	App. C.1 / Prop. 42
Monotone improvement	$J_{\text{tot}}^\alpha$ increases per step	App. C.3 / Thm. 46
Linear convergence (exact mirror)	$D_\Psi(\pi^{k+1}, \pi^*) \leq (1 - \eta\mu/L_\Psi)D_\Psi(\pi^k, \pi^*)$	App. C.4 / Thm. 48
<i>Hierarchical scalability (Local-Global HQRE)</i>		
Existence	Nested fixed point $(\{\pi_{C_k}\}, g)$ exists	App. B.9 / Thm. 15
Hierarchical bound	coupling $L_{\text{hier}} \leq W_{\max}^{\text{loc}}C_Q + C_{\text{occ}}(\dots)$	App. B.10 / Prop. 16
Uniqueness	Strong monotonicity with margin $\mu_{\text{hier}}$	App. B.11 / Thm. 17
Linear convergence (hierarchical exact mirror)	$D_\Psi^{\text{hier}}(\mathbf{z}^{k+1}, \mathbf{z}^*) \leq (1 - \eta\mu_{\text{hier}}/L_\Psi^{\text{hier}})D_\Psi^{\text{hier}}(\mathbf{z}^k, \mathbf{z}^*)$	App. C.5 / Thm. 52

## C.1 ELBO decomposition and best-response gaps (Prop. 42)

**Proposition 42** (ELBO decomposition and best-response-gap equivalence). *Fix a player  $i$  and opponents  $\pi_{-i}$ , and assume  $\alpha_{i,t}(h_i^t) > 0$  for all  $(h_i^t, t)$ . Let  $\pi_i^*$  denote an optimal policy for the regularized best-response problem*

$$\pi_i^* \in \arg \max_{\pi_i \in \Pi_i} J_i^\alpha(\pi_i, \pi_{-i}),$$

where  $J_i^\alpha$  is defined in Eq. (4). Then  $\pi_i^*$  is unique and satisfies the logit form

$$\pi_i^*(\cdot | h_i^t, t) \propto \exp(Q_i^{(\pi_i^*, \pi_{-i})}(h_i^t, \cdot, t) / \alpha_{i,t}(h_i^t)),$$

which is consistent with Eq. (5) specialized to the fixed-opponent problem. Moreover, for any  $\pi_i \in \Pi_i$ ,

$$J_i^\alpha(\pi_i^*, \pi_{-i}) - J_i^\alpha(\pi_i, \pi_{-i}) = \frac{1}{1-\gamma} \mathbb{E}_{(h_i^t, t) \sim H_{i, \text{disc}}^{(\pi_i, \pi_{-i})}} \left[ \alpha_{i,t}(h_i^t) \text{KL}(\pi_i(\cdot | h_i^t, t) \| \pi_i^*(\cdot | h_i^t, t)) \right]. \quad (26)$$

In particular,  $\pi_i^*$  is the unique maximizer of  $J_i^\alpha(\cdot, \pi_{-i})$ , and the joint fixed points of the logit map  $\mathcal{B}^\alpha$  coincide with Nash equilibria of the regularized game with payoffs  $\{J_i^\alpha\}_i$ .

**Soft Bellman objects for the playerwise regularized problem.** Fix opponents  $\pi_{-i}$  and consider player  $i$ 's regularized objective  $J_i^\alpha(\pi_i, \pi_{-i})$  in Eq. (4). For any  $\pi_i$ , define the (regularized) value and action-value functions over information states  $(h_i^t, t)$ :

$$V_i^{\pi_i}(h_i^t, t) := \mathbb{E} \left[ \sum_{u=t}^{\infty} \gamma^{u-t} (R_i(s^u, \mathbf{a}^u) + \alpha_{i,u}(h_i^u) \mathcal{H}(\pi_i(\cdot | h_i^u, u))) \mid h_i^t, \pi_i, \pi_{-i} \right],$$

$$Q_i^{\pi_i}(h_i^t, a_i, t) := \mathbb{E} \left[ R_i(s^t, \mathbf{a}^t) + \gamma V_i^{\pi_i}(h_i^{t+1}, t+1) \mid h_i^t, a_i^t = a_i, \pi_i, \pi_{-i} \right].$$

With these definitions,

$$V_i^{\pi_i}(h_i^t, t) = \mathbb{E}_{a_i \sim \pi_i(\cdot | h_i^t, t)} [Q_i^{\pi_i}(h_i^t, a_i, t)] + \alpha_{i,t}(h_i^t) \mathcal{H}(\pi_i(\cdot | h_i^t, t)). \quad (27)$$

**Lemma 43** (One-step ELBO identity). *Fix an information state  $(h_i^t, t)$  and a temperature  $\alpha := \alpha_{i,t}(h_i^t) > 0$ . Let  $q(a) = Q_i^{\pi_i^*}(h_i^t, a, t)$  and let  $p^*(\cdot | h_i^t, t) = \text{softmax}(q(\cdot)/\alpha)$ , i.e.,*

$$p^*(a_i | h_i^t, t) \propto \exp(Q_i^{\pi_i^*}(h_i^t, a_i, t)/\alpha_{i,t}(h_i^t)).$$

Then for any  $p \in \Delta(\mathcal{A}_i)$ ,

$$\sum_{a_i} p(a_i) q(a_i) + \alpha \mathcal{H}(p) = \alpha \log \sum_{a_i} \exp(q(a_i)/\alpha) - \alpha \text{KL}(p \| p^*).$$

**Proof** This is the standard log-sum-exp / convex conjugacy identity. Let  $\alpha = \alpha_{i,t}(h_i^t)$ ,  $q(a) = Q_i^{\pi_i^*}(h_i^t, a, t)$ , and  $Z = \sum_a \exp(q(a)/\alpha)$ . Define  $p^*(a) = \exp(q(a)/\alpha)/Z$ . Then

$$\sum_a p(a) q(a) + \alpha \sum_a p(a) \log p(a) = \alpha \log Z - \alpha \text{KL}(p \| p^*).$$

■

**Proof** [Proof of Prop. 42] *Uniqueness and logit form.* For fixed  $\pi_{-i}$  and  $\alpha_{i,t}(h) > 0$ , the entropy-regularized control problem for player  $i$  admits a unique optimal soft value function (the corresponding soft Bellman optimality operator is a  $\gamma$ -contraction in the finite discounted setting), hence the induced optimal policy is unique. The optimal policy satisfies the pointwise logit form with the optimal continuation values  $Q_i^{(\pi_i^*, \pi_{-i})}$ , as stated.

*pointwise identity at each information state.* Fix  $(h_i^t, t)$ . By Eq. (27) evaluated at  $\pi_i^*$ ,

$$V_i^{\pi_i^*}(h_i^t, t) = \mathbb{E}_{a_i \sim \pi_i^*(\cdot | h_i^t, t)} [Q_i^{\pi_i^*}(h_i^t, a_i, t)] + \alpha_{i,t}(h_i^t) \mathcal{H}(\pi_i^*(\cdot | h_i^t, t)).$$

Applying Lem. 43 with  $p = \pi_i(\cdot | h_i^t, t)$  and  $p^* = \pi_i^*(\cdot | h_i^t, t)$  gives

$$\begin{aligned} V_i^{\pi_i^*}(h_i^t, t) &= \mathbb{E}_{a_i \sim \pi_i(\cdot | h_i^t, t)} [Q_i^{\pi_i^*}(h_i^t, a_i, t)] \\ &\quad + \alpha_{i,t}(h_i^t) \mathcal{H}(\pi_i(\cdot | h_i^t, t)) \\ &\quad + \alpha_{i,t}(h_i^t) \text{KL}(\pi_i(\cdot | h_i^t, t) \| \pi_i^*(\cdot | h_i^t, t)). \end{aligned} \quad (28)$$

telescope along trajectories under  $(\pi_i, \pi_{-i})$ . Under fixed opponents  $\pi_{-i}$ ,  $Q_i^{\pi_i^*}$  satisfies the (unregularized) one-step recursion

$$Q_i^{\pi_i^*}(h_i^t, a_i, t) = \mathbb{E}[R_i(s^t, \mathbf{a}^t) + \gamma V_i^{\pi_i^*}(h_i^{t+1}, t+1) \mid h_i^t, a_i^t = a_i, \pi_i^*, \pi_{-i}],$$

which depends on  $a_i^t$  and the environment/opponents at time  $t$  but not on the *behavior* policy used to sample  $a_i^t$ . Therefore, taking  $a_i^t \sim \pi_i(\cdot \mid h_i^t, t)$  and then unconditional expectation under  $(\pi_i, \pi_{-i})$  yields

$$\mathbb{E}\left[\mathbb{E}_{a_i \sim \pi_i(\cdot \mid h_i^t, t)} Q_i^{\pi_i^*}(h_i^t, a_i, t)\right] = \mathbb{E}[R_i(s^t, \mathbf{a}^t) + \gamma V_i^{\pi_i^*}(h_i^{t+1}, t+1)],$$

where expectations are under  $(\pi_i, \pi_{-i})$ .

Substitute this into Eq. (28), multiply by  $\gamma^t$ , and sum over  $t \geq 0$ . The value terms telescope:

$$\sum_{t \geq 0} \gamma^t \mathbb{E}[V_i^{\pi_i^*}(h_i^t, t)] - \sum_{t \geq 0} \gamma^{t+1} \mathbb{E}[V_i^{\pi_i^*}(h_i^{t+1}, t+1)] = \mathbb{E}[V_i^{\pi_i^*}(h_i^0, 0)].$$

Hence

$$\begin{aligned} \mathbb{E}[V_i^{\pi_i^*}(h_i^0, 0)] &= \sum_{t \geq 0} \gamma^t \mathbb{E}[R_i(s^t, \mathbf{a}^t) + \alpha_{i,t}(h_i^t) \mathcal{H}(\pi_i(\cdot \mid h_i^t, t))] \\ &\quad + \sum_{t \geq 0} \gamma^t \mathbb{E}[\alpha_{i,t}(h_i^t) \text{KL}(\pi_i(\cdot \mid h_i^t, t) \parallel \pi_i^*(\cdot \mid h_i^t, t))]. \end{aligned}$$

The first sum equals  $J_i^\alpha(\pi_i, \pi_{-i})$  by definition. Also  $\mathbb{E}[V_i^{\pi_i^*}(h_i^0, 0)] = J_i^\alpha(\pi_i^*, \pi_{-i})$ . Rearranging and rewriting the discounted sum as an expectation under  $\mathbf{H}_{i,\text{disc}}^{(\pi_i, \pi_{-i})}$  yields Eq. (26).

*Consequences.* The RHS in Eq. (26) is nonnegative and equals 0 iff  $\pi_i(\cdot \mid h_i^t, t) = \pi_i^*(\cdot \mid h_i^t, t)$  for  $\mathbf{H}_{i,\text{disc}}^{(\pi_i, \pi_{-i})}$ -a.e. information state, so  $\pi_i^*$  is the unique maximizer. Finally, a joint profile is a Nash equilibrium of the regularized game iff each player is at its unique regularized best response, which is equivalent to being a joint fixed point of the logit map  $\mathcal{B}^\alpha$ .  $\blacksquare$

## C.2 Soft-value factorization and weighted advantages

**Proposition 44** (Soft-value factorization). *Assume a linear monotone mixer of the form*

$$Q_{\text{tot}}(s^t, \mathbf{a}^t, t) = \sum_{i=1}^N w_i(s^t) Q_i(b_i^t, a_i^t, t) + b(s^t), \quad w_i(s^t) \geq 0,$$

and a scalar temperature  $\alpha_t > 0$ . Define the exact total soft value

$$V_{\text{tot}}^{\text{exact}}(s^t, t) := \alpha_t \log \sum_{\mathbf{a}^t} \exp(Q_{\text{tot}}(s^t, \mathbf{a}^t, t) / \alpha_t).$$

Then it factorizes as

$$V_{\text{tot}}^{\text{exact}}(s^t, t) = b(s^t) + \alpha_t \sum_{i=1}^N \log \sum_{a_i \in \mathcal{A}_i} \exp\left(\frac{w_i(s^t)}{\alpha_t} Q_i(b_i^t, a_i, t)\right). \quad (29)$$

This is the algebraic identity instantiated as Eq. (29) in Sec. 5.3 (with  $a_i$  replaced by vocabulary tokens and  $t$  replaced by token positions  $\ell$ ).

**Proof** By definition,

$$\frac{Q_{\text{tot}}(s^t, \mathbf{a}^t, t)}{\alpha_t} = \frac{b(s^t)}{\alpha_t} + \sum_{i=1}^N \frac{w_i(s^t)}{\alpha_t} Q_i(b_i^t, a_i^t, t).$$

Hence

$$\begin{aligned} \sum_{\mathbf{a}^t} \exp\left(\frac{Q_{\text{tot}}(s^t, \mathbf{a}^t, t)}{\alpha_t}\right) &= \exp(b(s^t)/\alpha_t) \sum_{a_1} \cdots \sum_{a_N} \exp\left(\sum_{i=1}^N \frac{w_i(s^t)}{\alpha_t} Q_i(b_i^t, a_i^t, t)\right) \\ &= \exp(b(s^t)/\alpha_t) \prod_{i=1}^N \sum_{a_i} \exp\left(\frac{w_i(s^t)}{\alpha_t} Q_i(b_i^t, a_i, t)\right), \end{aligned}$$

since the exponent separates across  $i$ . Taking  $\alpha_t \log(\cdot)$  yields the claim.  $\blacksquare$

**Lemma 45** (Weighted local soft values and soft advantages). *Assume  $\alpha_t > 0$  and  $w_i(s^t) > 0$  for the indices  $i$  under consideration.<sup>5</sup> Define the local soft value*

$$V_i^{\text{soft}}(s^t, b_i^t, t) := \frac{\alpha_t}{w_i(s^t)} \log \sum_{a_i} \exp\left(\frac{w_i(s^t)}{\alpha_t} Q_i(b_i^t, a_i, t)\right),$$

and the corresponding weighted soft advantage

$$A_i^{(w)}(s^t, b_i^t, a_i^t, t) := w_i(s^t) \left( Q_i(b_i^t, a_i^t, t) - V_i^{\text{soft}}(s^t, b_i^t, t) \right).$$

Then:

(i)  $V_{\text{tot}}^{\text{exact}}(s^t, t) = b(s^t) + \sum_{i=1}^N w_i(s^t) V_i^{\text{soft}}(s^t, b_i^t, t).$

(ii) For the softmax policy  $\pi_i^{\text{soft}}(a_i | b_i^t, t) \propto \exp(\frac{w_i(s^t)}{\alpha_t} Q_i(b_i^t, a_i, t))$ , the advantage admits the pointwise identity

$$A_i^{(w)}(s^t, b_i^t, a_i^t, t) = \alpha_t \log \pi_i^{\text{soft}}(a_i^t | b_i^t, t),$$

and therefore

$$\mathbb{E}_{a_i \sim \pi_i^{\text{soft}}} [A_i^{(w)}(s^t, b_i^t, a_i, t)] = -\alpha_t \mathcal{H}(\pi_i^{\text{soft}}(\cdot | b_i^t, t)).$$

**Proof** (i) follows by substituting the definition of  $V_i^{\text{soft}}$  into Prop. 44.

(ii) Let  $Z_i := \sum_{a_i} \exp(\frac{w_i}{\alpha_t} Q_i(b_i^t, a_i, t))$ . Then

$$\log \pi_i^{\text{soft}}(a_i | b_i^t, t) = \frac{w_i(s^t)}{\alpha_t} Q_i(b_i^t, a_i, t) - \log Z_i.$$

Multiplying by  $\alpha_t$  gives

$$\alpha_t \log \pi_i^{\text{soft}}(a_i | b_i^t, t) = w_i(s^t) Q_i(b_i^t, a_i, t) - \alpha_t \log Z_i = w_i(s^t) (Q_i(b_i^t, a_i, t) - V_i^{\text{soft}}(s^t, b_i^t, t)),$$

which is exactly  $A_i^{(w)}$ . Taking expectation under  $\pi_i^{\text{soft}}$  yields  $\mathbb{E}[\log \pi_i^{\text{soft}}] = -\mathcal{H}(\pi_i^{\text{soft}})$  and hence the last identity.  $\blacksquare$

5. If  $w_i(s^t) = 0$  then the  $i$ -th term does not contribute to  $Q_{\text{tot}}$ ; one can define  $w_i(s^t) V_i^{\text{soft}} := \alpha_t \log \sum_{a_i} \exp((w_i/\alpha_t) Q_i)$  and all identities remain valid.

### C.3 Monotone progress for KL-mirror steps (Thm. 46)

We provide a clean mirror-ascent progress bound in KL geometry.

**Theorem 46** (Monotone progress of KL-mirror ascent). *Let  $J : \Pi \rightarrow \mathbb{R}$  be differentiable and  $L_J$ -smooth in the  $\|\cdot\|_{1,2;w}$  norm, i.e., for all  $\boldsymbol{\pi}, \boldsymbol{\pi}' \in \Pi$ ,*

$$J(\boldsymbol{\pi}') \geq J(\boldsymbol{\pi}) + \langle \nabla J(\boldsymbol{\pi}), \boldsymbol{\pi}' - \boldsymbol{\pi} \rangle - \frac{L_J}{2} \|\boldsymbol{\pi}' - \boldsymbol{\pi}\|_{1,2;w}^2.$$

*Assume the KL-Bregman divergence  $D_\Psi$  (Eq. (7)) satisfies the weighted Pinsker lower bound  $D_\Psi(\boldsymbol{\pi}, \boldsymbol{\pi}') \geq \frac{\alpha_{\min}}{2} \|\boldsymbol{\pi} - \boldsymbol{\pi}'\|_{1,2;w}^2$  (as in Lem. 31). Consider the KL-mirror ascent step*

$$\boldsymbol{\pi}^{k+1} = \arg \max_{\tilde{\boldsymbol{\pi}} \in \Pi} \left\{ \langle \nabla J(\boldsymbol{\pi}^k), \tilde{\boldsymbol{\pi}} - \boldsymbol{\pi}^k \rangle - \frac{1}{\eta_k} D_\Psi(\tilde{\boldsymbol{\pi}}, \boldsymbol{\pi}^k) \right\}. \quad (30)$$

*If  $\eta_k \leq \alpha_{\min}/(2L_J)$ , then*

$$J(\boldsymbol{\pi}^{k+1}) - J(\boldsymbol{\pi}^k) \geq \frac{1}{2\eta_k} D_\Psi(\boldsymbol{\pi}^{k+1}, \boldsymbol{\pi}^k) \geq 0.$$

**Lemma 47** (Mirror optimality inequality). *For the update Eq. (30),*

$$\langle \nabla J(\boldsymbol{\pi}^k), \boldsymbol{\pi}^{k+1} - \boldsymbol{\pi}^k \rangle \geq \frac{1}{\eta_k} D_\Psi(\boldsymbol{\pi}^{k+1}, \boldsymbol{\pi}^k).$$

**Proof** Since  $\tilde{\boldsymbol{\pi}} = \boldsymbol{\pi}^k$  is feasible, optimality of  $\boldsymbol{\pi}^{k+1}$  implies

$$\langle \nabla J(\boldsymbol{\pi}^k), \boldsymbol{\pi}^{k+1} - \boldsymbol{\pi}^k \rangle - \frac{1}{\eta_k} D_\Psi(\boldsymbol{\pi}^{k+1}, \boldsymbol{\pi}^k) \geq 0,$$

which yields the claim. ■

**Proof** [Proof of Thm. 46] By  $L_J$ -smoothness applied with  $\boldsymbol{\pi} = \boldsymbol{\pi}^k$  and  $\boldsymbol{\pi}' = \boldsymbol{\pi}^{k+1}$ ,

$$J(\boldsymbol{\pi}^{k+1}) - J(\boldsymbol{\pi}^k) \geq \langle \nabla J(\boldsymbol{\pi}^k), \boldsymbol{\pi}^{k+1} - \boldsymbol{\pi}^k \rangle - \frac{L_J}{2} \|\boldsymbol{\pi}^{k+1} - \boldsymbol{\pi}^k\|_{1,2;w}^2.$$

Use Lem. 47 and the Pinsker lower bound to obtain

$$J(\boldsymbol{\pi}^{k+1}) - J(\boldsymbol{\pi}^k) \geq \frac{1}{\eta_k} D_\Psi(\boldsymbol{\pi}^{k+1}, \boldsymbol{\pi}^k) - \frac{L_J}{\alpha_{\min}} D_\Psi(\boldsymbol{\pi}^{k+1}, \boldsymbol{\pi}^k) = \left( \frac{1}{\eta_k} - \frac{L_J}{\alpha_{\min}} \right) D_\Psi(\boldsymbol{\pi}^{k+1}, \boldsymbol{\pi}^k).$$

If  $\eta_k \leq \alpha_{\min}/(2L_J)$ , then  $\frac{1}{\eta_k} - \frac{L_J}{\alpha_{\min}} \geq \frac{1}{2\eta_k}$ , hence

$$J(\boldsymbol{\pi}^{k+1}) - J(\boldsymbol{\pi}^k) \geq \frac{1}{2\eta_k} D_\Psi(\boldsymbol{\pi}^{k+1}, \boldsymbol{\pi}^k) \geq 0. \quad \blacksquare$$

#### C.4 Linear convergence in KL geometry (Thm. 48)

We now give a self-contained linear-rate bound for KL-mirror dynamics in the strongly monotone regime. The argument is standard but we spell out the key inequalities and constants needed for a publishable statement.

**Theorem 48** (Linear convergence of KL-mirror dynamics). *Let  $F : \Pi \rightarrow \mathcal{X}$  be a field and suppose the variational inequality  $\text{VI}(F, \Pi)$  has a unique solution  $\pi^*$  (e.g., when  $F$  is strongly monotone). Assume:*

(i) (Strong monotonicity) *There exists  $\mu > 0$  such that for all  $\pi, \pi' \in \Pi$ ,*

$$\langle F(\pi) - F(\pi'), \pi - \pi' \rangle \geq \mu \|\pi - \pi'\|_{1,2;w}^2.$$

(ii) (Lipschitzness) *There exists  $L_F < \infty$  such that*

$$\|F(\pi) - F(\pi')\|_* \leq L_F \|\pi - \pi'\|_{1,2;w},$$

where  $\|\cdot\|_*$  is the dual norm of  $\|\cdot\|_{1,2;w}$ .

(iii) (Local quadratic KL geometry) *There exists  $L_\Psi < \infty$  such that for all  $\pi, \pi'$  in a neighborhood containing  $\pi^*$  and the iterates,*

$$\frac{\alpha_{\min}}{2} \|\pi - \pi'\|_{1,2;w}^2 \leq D_\Psi(\pi, \pi') \leq \frac{L_\Psi}{2} \|\pi - \pi'\|_{1,2;w}^2.$$

*A sufficient condition is iterate-interiority: if every local action probability in that region is bounded below by  $\nu_{\min} > 0$ , then one may take  $L_\Psi = \alpha_{\max}/\nu_{\min}$ .*

*Consider the mirror step for  $\text{VI}(F, \Pi)$ :*

$$\pi^{k+1} = \arg \min_{\tilde{\pi} \in \Pi} \left\{ \langle F(\pi^k), \tilde{\pi} - \pi^k \rangle + \frac{1}{\eta} D_\Psi(\tilde{\pi}, \pi^k) \right\}. \quad (31)$$

*If the stepsize satisfies*

$$0 < \eta \leq \min \left\{ \frac{\mu \alpha_{\min}^2}{L_F^2 L_\Psi}, \frac{\alpha_{\min}}{L_F} \right\},$$

*then the iterates converge linearly in KL geometry:*

$$D_\Psi(\pi^*, \pi^{k+1}) \leq \rho D_\Psi(\pi^*, \pi^k), \quad \rho := 1 - \eta \frac{\mu}{L_\Psi} \in (0, 1).$$

**Remark 49** (Why the KL upper quadratic bound is local). *For entropy / KL mirror maps, the lower quadratic bound is global but the upper quadratic bound is only local on the simplex. If all policies in the iterate region satisfy  $\pi_i(a | h, t) \geq \nu_{\min} > 0$  for every relevant coordinate, then the Hessian of the negative-entropy mirror map is bounded above by  $1/\nu_{\min}$  coordinatewise, yielding*

$$D_\Psi(\pi, \pi') \leq \frac{\alpha_{\max}}{2\nu_{\min}} \|\pi - \pi'\|_{1,2;w}^2.$$

*Practically, DICE-FT promotes this interior regime via positive entropies, KL trust regions, and step rejection.*

**Lemma 50** (Three-point inequality for VI mirror steps). *Let  $\pi^{k+1}$  be defined by Eq. (31). Then for any  $\pi \in \Pi$ ,*

$$\langle F(\pi^k), \pi^{k+1} - \pi \rangle \leq \frac{1}{\eta} \left( D_\Psi(\pi, \pi^k) - D_\Psi(\pi, \pi^{k+1}) - D_\Psi(\pi^{k+1}, \pi^k) \right).$$

**Proof** This is the standard Bregman three-point inequality for proximal/mirror steps. It follows from the first-order optimality conditions of Eq. (31) and the Bregman identity associated with  $\Psi$ .  $\blacksquare$

**Proof** [Proof of Thm. 48] Apply Lem. 50 with  $\pi = \pi^*$ :

$$\eta \langle F(\pi^k), \pi^{k+1} - \pi^* \rangle \leq D_\Psi(\pi^*, \pi^k) - D_\Psi(\pi^*, \pi^{k+1}) - D_\Psi(\pi^{k+1}, \pi^k). \quad (32)$$

Since  $\pi^*$  solves VI( $F, \Pi$ ), we have  $\langle F(\pi^*), \pi^{k+1} - \pi^* \rangle \geq 0$ . Therefore,

$$\langle F(\pi^k), \pi^{k+1} - \pi^* \rangle \geq \langle F(\pi^k) - F(\pi^*), \pi^{k+1} - \pi^* \rangle.$$

Decompose:

$$\begin{aligned} \langle F(\pi^k) - F(\pi^*), \pi^{k+1} - \pi^* \rangle &= \langle F(\pi^k) - F(\pi^*), \pi^k - \pi^* \rangle + \langle F(\pi^k) - F(\pi^*), \pi^{k+1} - \pi^k \rangle \\ &\geq \mu \|\pi^k - \pi^*\|_{1,2;w}^2 - \|F(\pi^k) - F(\pi^*)\|_* \|\pi^{k+1} - \pi^k\|_{1,2;w} \\ &\geq \mu \|\pi^k - \pi^*\|_{1,2;w}^2 - L_F \|\pi^k - \pi^*\|_{1,2;w} \|\pi^{k+1} - \pi^k\|_{1,2;w}, \end{aligned}$$

using strong monotonicity and Lipschitzness plus Hölder's inequality.

Insert this lower bound into Eq. (32) and use the lower quadratic bound on  $D_\Psi(\pi^{k+1}, \pi^k)$ :

$$D_\Psi(\pi^{k+1}, \pi^k) \geq \frac{\alpha_{\min}}{2} \|\pi^{k+1} - \pi^k\|_{1,2;w}^2.$$

We obtain

$$\begin{aligned} D_\Psi(\pi^*, \pi^{k+1}) &\leq D_\Psi(\pi^*, \pi^k) - \eta \mu \|\pi^k - \pi^*\|_{1,2;w}^2 \\ &\quad + \eta L_F \|\pi^k - \pi^*\|_{1,2;w} \|\pi^{k+1} - \pi^k\|_{1,2;w} \\ &\quad - \frac{\alpha_{\min}}{2} \|\pi^{k+1} - \pi^k\|_{1,2;w}^2. \end{aligned}$$

For fixed  $a := \|\pi^k - \pi^*\|_{1,2;w}$ , the expression  $\eta L_F a b - \frac{\alpha_{\min}}{2} b^2$  in  $b := \|\pi^{k+1} - \pi^k\|_{1,2;w}$  is maximized at  $b^* = \eta L_F a / \alpha_{\min}$  with maximum value  $\frac{\eta^2 L_F^2}{2\alpha_{\min}} a^2$ . Thus,

$$D_\Psi(\pi^*, \pi^{k+1}) \leq D_\Psi(\pi^*, \pi^k) - \eta \left( \mu - \frac{\eta L_F^2}{2\alpha_{\min}} \right) \|\pi^k - \pi^*\|_{1,2;w}^2.$$

Using the upper quadratic bound  $D_\Psi(\pi^*, \pi^k) \leq \frac{L_\Psi}{2} \|\pi^k - \pi^*\|_{1,2;w}^2$  implies

$$\|\pi^k - \pi^*\|_{1,2;w}^2 \geq \frac{2}{L_\Psi} D_\Psi(\pi^*, \pi^k).$$

Therefore,

$$D_\Psi(\boldsymbol{\pi}^*, \boldsymbol{\pi}^{k+1}) \leq \left(1 - \eta \frac{2}{L_\Psi} \left(\mu - \frac{\eta L_F^2}{2\alpha_{\min}}\right)\right) D_\Psi(\boldsymbol{\pi}^*, \boldsymbol{\pi}^k).$$

If  $\eta \leq \mu\alpha_{\min}^2/(L_F^2 L_\Psi)$ , then  $\frac{\eta L_F^2}{2\alpha_{\min}} \leq \frac{\mu}{2} \cdot \frac{\alpha_{\min}}{L_\Psi} \leq \frac{\mu}{2}$ , and in particular

$$\eta \frac{2}{L_\Psi} \left(\mu - \frac{\eta L_F^2}{2\alpha_{\min}}\right) \geq \eta \frac{\mu}{L_\Psi}.$$

Hence,

$$D_\Psi(\boldsymbol{\pi}^*, \boldsymbol{\pi}^{k+1}) \leq \left(1 - \eta \frac{\mu}{L_\Psi}\right) D_\Psi(\boldsymbol{\pi}^*, \boldsymbol{\pi}^k),$$

which is the claimed linear contraction with  $\rho = 1 - \eta\mu/L_\Psi \in (0, 1)$ .  $\blacksquare$

**Theorem 51** (Inexact linear recurrence for mirror steps). *Assume the conditions of Theorem 48. Let the approximate iterate be defined by*

$$\boldsymbol{\pi}^{k+1} = \arg \min_{\tilde{\boldsymbol{\pi}} \in \Pi} \left\{ \langle F(\boldsymbol{\pi}^k) + e^k, \tilde{\boldsymbol{\pi}} - \boldsymbol{\pi}^k \rangle + \frac{1}{\eta} D_\Psi(\tilde{\boldsymbol{\pi}}, \boldsymbol{\pi}^k) \right\}. \quad (33)$$

If

$$0 < \eta \leq \min \left\{ \frac{\mu \alpha_{\min}^2}{L_F^2 L_\Psi}, \frac{\alpha_{\min}}{L_F}, \frac{\alpha_{\min} \mu}{4L_F^2} \right\},$$

then

$$D_\Psi(\boldsymbol{\pi}^*, \boldsymbol{\pi}^{k+1}) \leq \rho D_\Psi(\boldsymbol{\pi}^*, \boldsymbol{\pi}^k) + C_{\text{err}} \|e^k\|_*^2,$$

where

$$\rho := 1 - \eta \frac{\mu}{L_\Psi}, \quad C_{\text{err}} := \frac{\eta}{\mu} + \frac{\eta^2}{\alpha_{\min}}.$$

**Proof** Apply Lem. 50 to the inexact step Eq. (33) with  $\boldsymbol{\pi} = \boldsymbol{\pi}^*$ :

$$\eta \langle F(\boldsymbol{\pi}^k) + e^k, \boldsymbol{\pi}^{k+1} - \boldsymbol{\pi}^* \rangle \leq D_\Psi(\boldsymbol{\pi}^*, \boldsymbol{\pi}^k) - D_\Psi(\boldsymbol{\pi}^*, \boldsymbol{\pi}^{k+1}) - D_\Psi(\boldsymbol{\pi}^{k+1}, \boldsymbol{\pi}^k).$$

Since  $\boldsymbol{\pi}^*$  solves VI( $F, \Pi$ ),

$$\langle F(\boldsymbol{\pi}^*), \boldsymbol{\pi}^{k+1} - \boldsymbol{\pi}^* \rangle \geq 0.$$

Proceeding as in the proof of Theorem 48 yields

$$D_\Psi(\boldsymbol{\pi}^*, \boldsymbol{\pi}^{k+1}) \leq D_\Psi(\boldsymbol{\pi}^*, \boldsymbol{\pi}^k) - \eta\mu a^2 + \eta L_F a b + \eta \|e^k\|_* (a + b) - \frac{\alpha_{\min}}{2} b^2,$$

where  $a := \|\boldsymbol{\pi}^k - \boldsymbol{\pi}^*\|_{1,2;w}$  and  $b := \|\boldsymbol{\pi}^{k+1} - \boldsymbol{\pi}^k\|_{1,2;w}$ . Use Young's inequality in the form

$$\eta L_F a b \leq \frac{\eta\mu}{4} a^2 + \frac{\alpha_{\min}}{4} b^2,$$

which is valid under  $\eta \leq \alpha_{\min}\mu/(4L_F^2)$ , and

$$\eta \|e^k\|_* a \leq \frac{\eta\mu}{4} a^2 + \frac{\eta}{\mu} \|e^k\|_*^2, \quad \eta \|e^k\|_* b \leq \frac{\alpha_{\min}}{4} b^2 + \frac{\eta^2}{\alpha_{\min}} \|e^k\|_*^2.$$

Substituting gives

$$D_{\Psi}(\boldsymbol{\pi}^*, \boldsymbol{\pi}^{k+1}) \leq D_{\Psi}(\boldsymbol{\pi}^*, \boldsymbol{\pi}^k) - \frac{\eta\mu}{2}a^2 + \left(\frac{\eta}{\mu} + \frac{\eta^2}{\alpha_{\min}}\right)\|e^k\|_*^2.$$

Finally, the upper quadratic bound gives  $a^2 \geq 2D_{\Psi}(\boldsymbol{\pi}^*, \boldsymbol{\pi}^k)/L_{\Psi}$ , so

$$D_{\Psi}(\boldsymbol{\pi}^*, \boldsymbol{\pi}^{k+1}) \leq \left(1 - \eta \frac{\mu}{L_{\Psi}}\right)D_{\Psi}(\boldsymbol{\pi}^*, \boldsymbol{\pi}^k) + \left(\frac{\eta}{\mu} + \frac{\eta^2}{\alpha_{\min}}\right)\|e^k\|_*^2,$$

which is the claim. ■

### C.5 Hierarchical mirror dynamics (Thm. 52)

**Theorem 52** (Hierarchical linear convergence). *Let  $\mathbf{z} = (\boldsymbol{\pi}, g)$  be the hierarchical variable with composite divergence  $D_{\Psi}^{\text{hier}}$  (as defined in Appendix B.8). Assume the hierarchical field  $F_{\text{hier}}$  is  $\mu_{\text{hier}}$ -strongly monotone and  $L_{\text{hier}}$ -Lipschitz in a compatible block norm, and that  $D_{\Psi}^{\text{hier}}$  is locally quadratic on the iterates (upper/lower quadratic bounds analogous to Thm. 48 with constants  $\alpha_{\min}^{\text{hier}}$  and  $L_{\Psi}^{\text{hier}}$ ). Then the blockwise KL-mirror step*

$$\mathbf{z}^{k+1} = \arg \min_{\tilde{\mathbf{z}} \in \mathcal{Z}} \left\{ \langle F_{\text{hier}}(\mathbf{z}^k), \tilde{\mathbf{z}} - \mathbf{z}^k \rangle + \frac{1}{\eta} D_{\Psi}^{\text{hier}}(\tilde{\mathbf{z}}, \mathbf{z}^k) \right\}$$

converges linearly:

$$D_{\Psi}^{\text{hier}}(\mathbf{z}^*, \mathbf{z}^{k+1}) \leq \left(1 - \eta \frac{\mu_{\text{hier}}}{L_{\Psi}^{\text{hier}}}\right) D_{\Psi}^{\text{hier}}(\mathbf{z}^*, \mathbf{z}^k),$$

for stepsizes  $\eta$  chosen analogously to Thm. 48.

**Proof** The proof is identical to Thm. 48 after replacing  $(F, \Pi, D_{\Psi}, \|\cdot\|_{1,2;w})$  with the hierarchical counterparts  $(F_{\text{hier}}, \mathcal{Z}, D_{\Psi}^{\text{hier}}, \|\cdot\|_{\text{hier}})$ . Strong monotonicity uses the margin  $\mu_{\text{hier}}$  (Sec. 4.2, Eq. (14)), while Lipschitzness uses the structural coupling bounds (Prop. 16 and Appendix B.10). Local quadratic bounds for the composite KL divergence hold on interior compact subsets, similarly to Remark 49. ■

### C.6 Additional experiment results

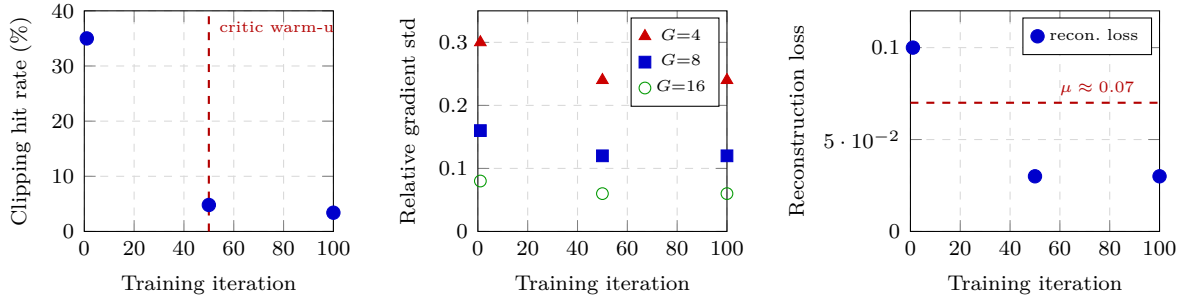
The revised field-error budget isolates the explicit  $G$ -dependence in the sampling term  $\sigma_g^2/G$ . Empirically, the within-group gradient relative standard deviation on Text-Hanabi is approximately 0.24 at  $G=4$ , 0.12 at  $G=8$ , and 0.06 at  $G=16$ , consistent with the expected  $1/\sqrt{G}$  trend. This explains the diminishing returns beyond  $G=8$ : once the sampling term falls below the representation / optimization residuals, further increases in  $G$  produce limited gains while linearly increasing rollout cost.

### C.7 Field-error budget: seed-level analysis

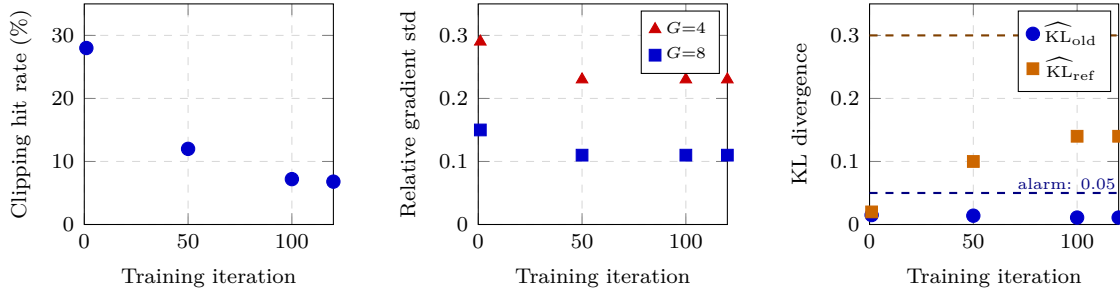
Under the revised theory, the relevant measurable quantities are the components of the field-error budget in Eq. (17) rather than a single scalar  $\delta$ . Across seeds on Text-Hanabi,

Table 16: TravelPlanner full results with selected leaderboard baselines. Delivery Rate measures format compliance; Commonsense and Hard Constraint pass rates (PR) are reported at both micro (Mi, per-constraint) and macro (Ma, per-plan) granularity; Final PR requires all constraints satisfied simultaneously. Best result per column within each setting is **bold**. DICE rows are highlighted.

	Validation (#180)					Test (#1,000)						
	Delivery Rate	Commonsense PR		Hard Constr. PR		Final PR	Delivery Rate	Commonsense PR		Hard Constr. PR		Final PR
		Mi	Ma	Mi	Ma			Mi	Ma	Mi	Ma	
Greedy Search	100	74.4	0	60.8	37.8	0	100	72.0	0	52.4	31.8	0
<i>Two-stage</i>												
Mixtral-8x7B-MoE	49.4	30.0	0	1.2	0.6	0	51.2	32.2	0.2	0.7	0.4	0
Gemini Pro	28.9	18.9	0	0.5	0.6	0	39.1	24.9	0	0.6	0.1	0
GPT-3.5-Turbo	86.7	54.0	0	0	0	0	91.8	57.9	0	0.5	0.6	0
GPT-4-Turbo	89.4	61.1	2.8	15.2	10.6	0.6	93.1	63.3	2.0	10.5	5.5	0.6
GPT-o3	92.8	64.7	4.2	18.9	12.8	1.4	95.6	68.9	5.1	14.3	8.7	1.9
Debate (GPT-4) @3round	95.2	67.3	6.7	22.7	13.1	2.3	97.8	72.4	11.3	17.4	12.1	3.7
MA-Debate (Qwen3-32B)	94.4	65.8	5.1	19.8	11.3	1.7	96.7	70.3	8.2	16.2	9.8	2.8
MA-FT (Qwen3-32B)	97.2	67.9	7.3	23.4	14.6	3.1	98.6	73.1	12.7	21.8	13.2	4.3
Qwen3-235B-Inst	91.1	63.4	3.6	17.3	11.9	1.1	94.3	66.2	3.8	12.7	7.1	1.3
MA-Debate (Qwen3-235B)	96.7	69.8	9.4	27.6	16.8	3.8	98.9	76.7	16.2	24.1	14.9	5.7
DICE (GPT-4)	<b>100</b>	<b>71.4</b>	<b>15.6</b>	<b>32.1</b>	<b>25.7</b>	<b>7.2</b>	<b>100</b>	<b>82.1</b>	<b>26.6</b>	<b>32.4</b>	<b>17.6</b>	<b>9.3</b>
DICE-PC (Qwen3-32B)	98.3	68.2	8.9	26.3	16.7	3.9	99.1	75.8	15.1	24.7	14.3	5.4
DICE-FT (Qwen3-32B)	<b>100</b>	70.1	11.7	29.4	19.8	5.6	<b>100</b>	78.6	18.9	28.1	15.9	7.1
<i>Sole-planning</i>												
DirectGPT-3.5-Turbo	100	60.2	4.4	11.0	2.8	0	100	59.5	2.7	9.5	4.4	0.6
CoTGPT-3.5-Turbo	100	66.3	3.3	11.9	5.0	0	100	64.4	2.3	9.8	3.8	0.4
ReActGPT-3.5-Turbo	82.2	47.6	3.9	11.4	6.7	0.6	81.6	45.9	2.5	10.7	3.1	0.7
ReflexionGPT-3.5-Turbo	93.9	53.8	2.8	11.0	2.8	0	92.1	52.1	2.2	9.9	3.8	0.6
DirectMixtral-8x7B	100	68.1	5.0	3.3	1.1	0	99.3	67.0	3.7	3.9	1.6	0.7
DirectGemini Pro	93.9	65.0	8.3	9.3	4.4	0.6	93.7	64.7	7.9	10.6	4.7	2.1
DirectGPT-4-Turbo	<b>100</b>	80.4	17.2	47.1	22.2	4.4	<b>100</b>	80.6	15.2	44.3	23.1	4.4
DirectGPT-o3	<b>100</b>	82.1	19.7	49.8	24.6	6.1	<b>100</b>	82.9	17.8	46.7	25.3	5.8
Debate (GPT-4) @3round	97.7	78.9	15.6	43.3	20.6	6.7	98.2	79.5	18.8	41.7	22.9	7.1
MA-Debate (Qwen3-32B)	98.9	79.6	16.7	42.7	21.3	7.8	99.3	80.3	18.1	41.2	23.4	8.4
MA-FT (Qwen3-32B)	<b>100</b>	80.8	17.9	45.1	22.8	9.1	<b>100</b>	81.4	19.3	43.8	24.7	9.7
Qwen3-235B-Inst	<b>100</b>	81.3	18.9	48.7	23.9	6.7	<b>100</b>	81.9	17.1	45.9	24.5	6.3
MA-Debate (Qwen3-235B)	99.4	81.7	19.4	48.9	25.1	10.1	99.8	82.6	20.8	47.3	26.7	11.3
DICE-PC (GPT-4)	<b>100</b>	<b>83.3</b>	<b>22.2</b>	<b>51.7</b>	<b>27.8</b>	<b>12.9</b>	<b>100</b>	<b>84.2</b>	<b>23.5</b>	<b>49.8</b>	<b>28.7</b>	<b>15.2</b>
DICE-PC (Qwen3-32B)	<b>100</b>	81.7	18.3	45.8	23.4	8.9	<b>100</b>	82.1	19.7	43.6	24.8	10.3
DICE-FT (Qwen3-32B)	<b>100</b>	82.5	20.1	48.3	25.6	10.6	<b>100</b>	83.4	21.4	46.9	26.5	12.7



(a) Text-Hanabi: clipping boundary hit rate decays from  $\sim 35\%$  to  $< 5\%$  after critic warm-up ( $\sim 50$  iterations), consistent with  $O(L\epsilon^2)$  bias diminishing as policies stabilize. (b) Text-Hanabi: within-group gradient relative std stabilizes at 0.24 ( $G=4$ ), 0.12 ( $G=8$ ), 0.06 ( $G=16$ ), confirming  $O(1/G)$  scaling. (c) Text-Hanabi: reconstruction loss plateaus at  $\sim 0.03$  after 50 iterations, well below the uniqueness margin  $\mu \approx 0.07$  (dashed line).



(d) MATH-500: clipping boundary hit rate decays from  $\sim 28\%$  to  $< 8\%$  after  $\sim 80$  iterations, mirroring the Text-Hanabi trajectory on the full LLM backbone. (e) MATH-500: within-group gradient relative std at  $G=4$  (0.23) and  $G=8$  (0.11), consistent with  $O(1/G)$  scaling and matching Text-Hanabi values. (f) MATH-500:  $\widehat{KL}_{\text{old}}$  remains below 0.02 and  $\widehat{KL}_{\text{ref}}$  below 0.15 throughout training, both well under their respective alarm thresholds (dashed lines).

Figure 9: Empirical error diagnostic time series across training iterations. Row 1: Text-Hanabi (lightweight decision layer, all three error components directly measurable). Row 2: MATH-500 (full LLM backbone, two of three components directly measurable; KL diagnostics serve as indirect evidence for representation error). These time series correspond to the summary statistics reported in Section 5 and provide visual confirmation that the measurable components of the DICE-FT field-error budget remain controlled during training. All plotted points are exact checkpoint measurements, taken at iterations  $\{1, 50, 100\}$  (Text-Hanabi) and  $\{1, 50, 100, 120\}$  (MATH-500). The qualitative trends (decreasing clip-overshoot activity, decreasing gradient variance, stable critic / representation proxy) are consistent with the inexact-mirror regime assumed by Corollary\* 1.

the clip-overshoot term decreases during training, the sampling term exhibits the predicted  $1/G$  behavior, and the critic / representation proxy remains stable after warm-up. We

therefore use these curves as diagnostics of the inexact-mirror regime rather than claiming a universally calibrated neighborhood radius in weighted KL units.

### C.8 Algorithmic details deferred from Section 5

**Heterogeneous temperature specification.** Let  $H_{i,t,\ell}^{\text{ref}}$  denote the entropy of the frozen reference model  $\pi_{\text{ref}}(\cdot | b_i^t, \ell)$  and fix a threshold  $h_0$ ; then

$$\alpha_{i,t,\ell} = \alpha_{\text{hi}} \text{ if } H_{i,t,\ell}^{\text{ref}} \geq h_0, \quad \alpha_{i,t,\ell} = \alpha_{\text{lo}} \text{ otherwise,}$$

with  $0 < \alpha_{\text{lo}} \leq \alpha_{\text{hi}}$ . This schedule is driven only by information available at the time of generation and requires no additional modeling assumptions.

**Group-relative control variate derivation.** For each prompt, we sample a group of  $G$  joint rollouts under  $\pi^{\text{old}}$  and define the group return  $R^{(g)} := \frac{1}{N} \sum_i r_i^{(g)}$ . We compute a leave-one-out standardized return

$$\bar{R}_{-g} := \frac{1}{G-1} \sum_{h \neq g} R^{(h)}, \quad s_{-g} := \sqrt{\frac{1}{G-1} \sum_{h \neq g} (R^{(h)} - \bar{R}_{-g})^2 + \epsilon}, \quad \hat{A}_{\text{grp}}^{(g)} := \frac{R^{(g)} - \bar{R}_{-g}}{s_{-g}}.$$

The group-relative term primarily reduces variance in early training when critic estimates are noisy; the critic-based term dominates for well-trained critics.

**Detailed per-benchmark error diagnostic measurements.** This section provides the full per-benchmark measurements summarized in Section 5.

**Text-Hanabi.** The lightweight decision layer permits direct measurement of all three error components. (a) The fraction of importance ratios hitting the clip boundary ( $|\hat{r} - 1| \geq \epsilon$ ) decreases from  $\sim 35\%$  in early training to  $< 5\%$  after critic warm-up, consistent with  $O(L\epsilon^2)$  clipping bias diminishing as policies stabilize. (b) The within-group gradient variance scales as  $O(1/G)$  empirically ( $G=4$ : relative std 0.24;  $G=8$ : 0.12;  $G=16$ : 0.06), confirming the predicted scaling. (c) The belief encoder’s reconstruction loss (measured as the gap between encoder-based and full-history Q-values on a held-out set of 500 episodes) plateaus at  $\sim 0.03$  after 50 iterations, indicating that representation error is small relative to the uniqueness margin ( $\mu \approx 0.07$ ).

**MATH-500.** The full LLM backbone makes direct Q-value comparisons prohibitive, but two of the three components are directly measurable. The clipping boundary hit rate follows a similar trajectory to Text-Hanabi: starting at  $\sim 28\%$  and declining to  $< 8\%$  after 80 iterations, consistent with the  $O(L\epsilon^2)$  scaling as policies stabilize under the trust region. The within-group gradient variance at  $G=8$  (relative std 0.11) is comparable to the Text-Hanabi measurement at the same group size (0.12), and at  $G=4$  it rises to 0.23, confirming the  $O(1/G)$  scaling on a real LLM backbone. Representation error cannot be measured directly (it would require comparing encoder-based and full-history Q-values through the LLM), but the KL diagnostics ( $\widehat{\text{KL}}_{\text{old}} < 0.02$  and  $\widehat{\text{KL}}_{\text{ref}} < 0.15$  throughout training) provide indirect evidence that the cumulative approximation error remains controlled. Specifically,  $\widehat{\text{KL}}_{\text{old}} < 0.02$  bounds the per-update policy shift, ensuring that importance-ratio-based estimates remain accurate;  $\widehat{\text{KL}}_{\text{ref}} < 0.15$  bounds cumulative drift from the pretrained model, limiting the regime in which representation error could compound.

**Belief encoder architecture details.** For reasoning benchmarks (AIME, MATH-500, ZebraLogic, AutoLogic, PlanBench), we use a two-layer Transformer architecture with 4 attention heads, hidden dimension 256, and  $d_B=256$ , with a causal attention mask that processes the concatenated public stream and private observation tokens. Variable-length histories are handled by truncating to the most recent 2048 tokens and applying a learned positional encoding. For interactive benchmarks with longer horizons (Overcooked-AI, Hanabi, CollabEscape/Capture), the same two-layer Transformer architecture is used with  $d_B$  increased to 512; all other architectural choices (4 heads, causal mask, 2048-token truncation) remain identical. The belief encoder is trained jointly with the critic and mixer using the same Adam optimizer and learning rate schedule (constant lr =  $3 \times 10^{-4}$  for DICE-PC,  $1 \times 10^{-5}$  for DICE-FT). No separate pre-training phase is used. Encoder gradients are derived from the critic regression loss; encoder parameters typically stabilize within the first 30–50 training iterations based on the critic loss plateau.

**Critic regression loss equations.** We train critics by squared error on sampled tokens:

$$\mathcal{L}_{Q_i} := \mathbb{E}_{g,\ell}[(Q_{\psi_i}(b_i^{(g)}, x_{i,\ell+1}^{(g)}, \ell) - G_{i,\ell}^{(g)})^2], \quad \mathcal{L}_{V_i} := \mathbb{E}_{g,\ell}[(V_{\nu_i}^{\text{soft}}(z^{(g)}, b_i^{(g)}, \ell) - G_{i,\ell}^{(g)})^2],$$

with the mixer trained jointly through its dependence on the same targets.

### C.9 Proposition 18: proof sketch and empirical validation

**What is being bounded.** The practical DICE-FT update is analyzed through the field perturbation  $e^k$  in Eq. (15), not through a KL distance to the best-response map. The role of Proposition 18 is to control the conditional second moment of  $\|e^k\|_*$ . Once this is available, Corollary\* 1 follows from Theorem 51.

**Proof sketch for Proposition 18.** Decompose

$$e^k = e_{\text{clip}}^k + e_{\text{samp}}^k + e_{\text{repr}}^k + e_{\text{opt}}^k.$$

By the elementary inequality

$$\|a + b + c + d\|_*^2 \leq 4(\|a\|_*^2 + \|b\|_*^2 + \|c\|_*^2 + \|d\|_*^2),$$

we obtain

$$\mathbb{E}[\|e^k\|_*^2 \mid \mathcal{F}_k] \leq 4 \sum_{u \in \{\text{clip}, \text{samp}, \text{repr}, \text{opt}\}} \mathbb{E}[\|e_u^k\|_*^2 \mid \mathcal{F}_k].$$

For the clipping term, the update perturbation is proportional to the ratio overshoot  $\hat{r} - \text{clip}_\varepsilon(\hat{r})$  multiplied by the bounded update feature  $s(\tau)$ . Thus

$$\mathbb{E}[\|e_{\text{clip}}^k\|_*^2 \mid \mathcal{F}_k] \leq G_{\text{max}}^2 \mathbb{E}[(\hat{r} - \text{clip}_\varepsilon(\hat{r}))^2 \mid \mathcal{F}_k] = G_{\text{max}}^2 \Delta_{\text{clip}}^k.$$

The sampling term is bounded directly by

$$\mathbb{E}[\|e_{\text{samp}}^k\|_*^2 \mid \mathcal{F}_k] \leq \sigma_g^2 / G.$$

The representation term is transferred through the nonnegative monotone mixer. By Appendix Lemma 53, local perturbations of the per-agent critics produce a joint-field perturbation controlled by  $C_{\text{mix}}$ , giving

$$\mathbb{E}[\|e_{\text{repr}}^k\|_*^2 \mid \mathcal{F}_k] \leq C_{\text{mix}}^2 (L_{\text{repr}}^k)^2.$$

The optimization term is controlled by the chosen residual proxy:

$$\mathbb{E}[\|e_{\text{opt}}^k\|_*^2 \mid \mathcal{F}_k] \leq (L_{\text{opt}}^k)^2.$$

Combining the four bounds gives Eq. (17). If ratio overshoots satisfy  $|\hat{r} - \text{clip}_\varepsilon(\hat{r})| \leq c_{\text{ov}}\varepsilon$  on the clipped event, then

$$\Delta_{\text{clip}}^k \leq p_{\text{clip}}^k c_{\text{ov}}^2 \varepsilon^2,$$

which yields the stated  $O(p_{\text{clip}}^k \varepsilon^2)$  scaling.

**Empirical validation.** The revised proposition predicts a controlled inexact-mirror regime when (i) the clip-overshoot term remains small, (ii) the sampling term decays with  $G$ , and (iii) the representation and optimization residuals remain stable after warm-up. The current empirical diagnostics already track the first two directly and track the critic / representation proxy throughout training. We therefore interpret Proposition 18 as a field-error budget rather than as a source of a single universally calibrated neighborhood radius.

### C.10 Representation term: monotone-mixer transfer and architectural interpretation

**Lemma 53** (Monotone mixer transfer). *Let  $Q_{\text{tot}} = f_{\text{mix}}(z, \{Q_i\}_{i=1}^N)$  with  $f_{\text{mix}}$  differentiable in its value inputs. Assume the mixer is monotone,  $\partial f_{\text{mix}} / \partial Q_i \geq 0$  for all  $i$ , and that its local Jacobian satisfies*

$$\|\nabla_Q f_{\text{mix}}(z, \{Q_i\})\|_1 \leq W_{\text{mix}}$$

*on the iterate region. Then for any perturbations  $\{\Delta Q_i\}_{i=1}^N$ ,*

$$|f_{\text{mix}}(z, \{Q_i + \Delta Q_i\}) - f_{\text{mix}}(z, \{Q_i\})| \leq W_{\text{mix}} \max_i |\Delta Q_i|.$$

*Consequently, if the per-agent critic approximation error is bounded by  $L_{\text{repr}}^k$  in sup norm, then the induced joint-value / field perturbation is bounded by a local constant  $C_{\text{mix}} L_{\text{repr}}^k$  with  $C_{\text{mix}}$  proportional to  $W_{\text{mix}}$ .*

**Proof** Apply the mean-value theorem in the value inputs. Because all mixer partial derivatives are nonnegative, the local  $\ell_1$  norm of the Jacobian controls the perturbation without sign cancellation:

$$|f_{\text{mix}}(Q + \Delta Q) - f_{\text{mix}}(Q)| \leq \|\nabla_Q f_{\text{mix}}(\xi)\|_1 \|\Delta Q\|_\infty \leq W_{\text{mix}} \|\Delta Q\|_\infty,$$

for some intermediate point  $\xi$ . ■